The Astrophysical Journal, 774:40 (35pp), 2013 September 1 doi:10.1088/0004-637X/774/1/40

GALAXY CLUSTERS IN THE LINE OF SIGHT TO BACKGROUND QUASARS. III. MULTI-OBJECT SPECTROSCOPY*

H. Andrews[1,2], L. F. Barrientos[1], S. López[3], P. Lira[3], N. Padilla[1], D. G. Gilbank[4], I. Lacerna[1], M. J. Maureira[3], E. Ellingson[5], M. D. Gladders[6,7], and H. K. C. Yee[8]

[1] Instituto de Astrofísica, Pontificia Universidad Católica de Chile, Avenida Vicuña Mackenna 4860, Santiago, Chile; barrientos@astro.puc.cl
[2] Leiden Observatory, Leiden University, P.O. Box 9513, 2300 RA Leiden, Netherlands
[3] Departamento de Astronomía, Universidad de Chile, Casilla 36-D, Santiago, Chile
[4] South African Astronomical Observatory, P.O. Box 9, Observatory 7935, South Africa
[5] Center for Astrophysics and Space Astronomy, University of Colorado at Boulder, Campus Box 389, Boulder, CO 80309-0389, USA
[6] Kavli Institute for Cosmological Physics, University of Chicago, 5640 South Ellis Avenue, Chicago, IL 60637, USA
[7] Department of Astronomy and Astrophysics, University of Chicago, 5640 South Ellis Avenue, Chicago, IL 60637, USA
[8] Department of Astronomy and Astrophysics, University of Toronto, 60 St. George Street, Toronto, Ontario M5S 3H8, Canada
Received 2012 March 30; accepted 2013 June 24; published 2013 August 14

ABSTRACT

We present Gemini/GMOS-S multi-object spectroscopy of 31 galaxy cluster candidates at redshifts between 0.2 and 1.0 and centered on QSO sight lines taken from López et al. The targets were selected based on the presence of an intervening Mg II absorption system at a similar redshift to that of a galaxy cluster candidate lying at a projected distance $<2\ h_{71}^{-1}$ Mpc from the QSO sight line (a "photometric hit"). The absorption systems span rest-frame equivalent widths between 0.015 and 2.028 Å. Our aim was three-fold: (1) to identify the absorbing galaxies and determine their impact parameters, (2) to confirm the galaxy cluster candidates in the vicinity of each quasar sightline, and (3) to determine whether the absorbing galaxies reside in galaxy clusters. In this way, we are able to characterize the absorption systems associated with cluster members. Our main findings are as follows. (1) We identified 10 out of 24 absorbing galaxies with redshifts between $0.2509 \leqslant z_{\rm gal} \leqslant 1.0955$, up to an impact parameter of $142\ h_{71}^{-1}$ kpc and a maximum velocity difference of 280 km s^{-1}. (2) We spectroscopically confirmed 20 out of 31 cluster/group candidates, with most of the confirmed clusters/groups at $z < 0.7$. This relatively low efficiency results from the fact that we centered our observations on the QSO location, and thus occasionally some of the cluster centers were outside the instrument field of view. (3) Following from the results above, we spectroscopically confirmed of 10 out of 14 photometric hits within ∼650 km s^{-1} from galaxy clusters/groups, in addition to two new ones related to galaxy group environments. These numbers imply efficiencies of 71% in finding such systems with MOS spectroscopy. This is a remarkable result since we defined a photometric hit as those cluster–absorber pairs having a redshift difference $\Delta z = 0.1$. The general population of our confirmed absorbing galaxies have luminosities $L_B \sim L_B^*$ and mean rest-frame colors $(R_c - z')$ typical of S_{cd} galaxies. From this sample, absorbing cluster galaxies hosting weak absorbers are consistent with lower star formation activity than the rest, which produce strong absorption and agree with typical Mg II absorbing galaxies found in the literature. Our spectroscopic confirmations lend support to the selection of photometric hits made in López et al.

Key words: cosmology: observations – intergalactic medium – quasars: absorption lines

1. INTRODUCTION

Galaxies hosting Mg II absorption systems seen in the spectra of background QSOs (hereafter Mg II *absorbing galaxies*) appear to be a quite heterogeneous sample at $z \lesssim 1$. They span a rather broad range of spectral types and brightness, but concentrate on high luminosities ($L \sim L_B^*$) with colors and spectral features typical of S_b or S_c spiral field galaxies (e.g., Zibetti et al. 2007), lying at impact parameters ∼40–100 h_{71}^{-1} kpc from the quasar sight line (Steidel et al. 1994; Lindner et al. 1996; Churchill et al. 2005; Kacprzak et al. 2005, 2007; Chen et al. 2010).

Models assuming that absorbing gas resides within galactic halos are in general agreement with observable data available for Mg II absorbers (Steidel et al. 2002; Lin & Zou 2001). However, the very origin of these absorption systems (e.g., whether the absorptions are specifically produced in the disk or halo by Type II supernova ejecta, gas accretion, stripped gas, stellar outflows, etc.) has not yet been well established.

Correlations between Mg II absorption strength and galactic halo masses (Bouché et al. 2006; Gauthier et al. 2009) or galaxy type (Zibetti et al. 2007; Rubin et al. 2010; Ménard et al. 2011) have been thoroughly studied, and suggest a link between Mg II absorber intensities and the star formation in their host galaxies. However, such studies have mostly considered strong Mg II absorbers ($W_0^{2796} > 1.0$ Å). Thus, we are still lacking larger galaxy surveys that include weak Mg II absorption systems (i.e., $W_0^{2796} < 0.3$ Å).

Furthermore, despite some Mg II systems having been found to populate galaxy group or cluster environments (Bechtold & Ellingson 1992; Steidel & Dickinson 1992; Bowen et al. 1995; Churchill & Charlton 1998; Chen et al. 2010; Gauthier 2013), no studies have searched for galaxy group environments in a systematic fashion.

The Quasars behind Clusters project (López et al. 2008, hereafter Paper I) is the first Mg II survey designed to specifically

* Based on observations obtained at the Gemini Observatory, which is operated by the Association of Universities for Research in Astronomy, Inc., under a cooperative agreement with the NSF on behalf of the Gemini partnership: the National Science Foundation (United States), the Science and Technology Facilities Council (United Kingdom), the National Research Council (Canada), CONICYT (Chile), the Australian Research Council (Australia), Ministério da Ciência e Tecnologia (Brazil), and Ministerio de Ciencia, Tecnología e Innovación Productiva (Argentina).

target galaxy cluster/group environments; Mg II systems are sought in lines of sight (LOSs) toward quasars known to intersect galaxy cluster/group candidates at photometric redshifts $z_{\rm clus}^{\rm phot} \sim 0.2$–$0.9$ drawn from the Red-Sequence Cluster Survey 1 (RCS1; Gladders & Yee 2000). Using a sample of ∼400 QSO–cluster pairs at clustercentric-projected distances $d < 2\ h_{71}^{-1}$ Mpc, López et al. (2008) detected differences between the number density of absorbers most probably located in galaxy cluster/group environments and those related to the field. While the strongest Mg II systems ($W_0^{2796} > 2$ Å) were found to be up to 10 times more abundant in clusters than those produced in the field, weak Mg II systems ($W_0^{2796} < 0.3$ Å) did not show a similar excess. The proposed explanation for this signal was that weak systems should occur in galactic halos that have been truncated due to environmental effects, i.e., galaxy harassment or ram pressure stripping. This interpretation was later used by Padilla et al. (2009, Paper II) to put constraints on the sizes of baryonic halos around cluster galaxies.

The association between Mg II absorption and galaxy cluster/group candidates in Paper I is subject to uncertainties in the photometric redshifts of cluster/group candidates, from which the cluster redshift path of the survey $\Delta z_{\rm cluster}$ was derived. Therefore, it becomes necessary to reduce the photometric redshift uncertainties of the clusters, in order to establish a better relation between absorbers and their environment.

The work presented here is based on Gemini/GMOS-S MOS observations of 31 cluster candidates drawn from Paper I. Our aim is three-fold: (1) to find the Mg II absorbing galaxies and calculate their LOS impact parameters, (2) to verify the overabundance of galaxies in the vicinity of each quasar sight line due to the presence of clusters of galaxies, and (3) to determine whether or not the absorbing galaxies reside in galaxy clusters.

This paper is organized as follows. In Section 2, we describe our data and the details of the spectroscopic observations and reduction steps for a sample of 23 Mg II systems. Results are given in Section 3, specifically the detection of absorbing galaxies, and a general view of their properties is presented in Section 3.1; the spectroscopic confirmation of cluster/group candidates is detailed in Section 3.2 (with the caveat that having a QSO in the middle of the field limits the ability of confirming clusters); the confirmation of spectroscopic hits is presented in Section 3.3. A discussion of our results and their implications is given in Section 4. Our concluding remarks are outlined in Section 5. The cosmological parameters adopted in this study are $\Omega_m = 0.27$, $\Omega_\Lambda = 0.73$, and $H_0 = 71\ h_{71}$ km s^{-1} Mpc^{-1}.

2. DATA

In Paper I, the matching of an Mg II system to the presence of a galaxy cluster candidate was termed a *photometric hit*. Explicitly, for an Mg II absorbing system at $z_{\rm abs}$, a photometric hit was defined as $z_{\rm abs} \in [z_{\rm min}, z_{\rm max}]$, where $z_{\rm min} = z_{\rm clus}^{\rm phot} - \delta z_{\rm clus}^{\rm phot}$ and $z_{\rm max} = z_{\rm clus}^{\rm phot} + \delta z_{\rm clus}^{\rm phot}$, with $z_{\rm clus}^{\rm phot}$ being the photometric redshift of an RCS1 cluster/group candidate with a redshift uncertainty $\delta z_{\rm clus}^{\rm phot}$. We set $\delta z_{\rm clus}^{\rm phot} = 0.1$, except where $z_{\rm clus}^{\rm phot} - \delta z_{\rm clus}^{\rm phot} < z_{\rm EW}$. $z_{\rm EW}$ is the minimum redshift at which a system with $W_0^{2796} = 0.05$ Å could be detected as a 3σ detection; in these cases, $z_{\rm min}$ was set to $z_{\rm EW}$.

The spectroscopic confirmation of RCS1 cluster/group candidates leads to a new definition of a *spectroscopic hit*. By definition, a spectroscopic hit corresponds to an Mg II absorption (assumed to originate in a galactic halo) located in the environment of a spectroscopically confirmed galaxy cluster.

2.1. Region Selection

Our data consist of multi-object spectroscopy covering nine fields centered on different quasar sight lines, each one presenting one or more photometric hits.

These LOSs were drawn from a list of photometric hits presented in Paper I, detected in high-resolution spectroscopic data using the MIKE echelle spectrograph mounted on the 6.5 m Magellan Telescope at the Las Campanas Observatory. In this sample, Mg II absorption systems were detected at a $>3\sigma$ detection level in both doublet lines and have an uncertainty $\delta z_{\rm abs} \sim 10^{-4}$ (see Paper I for further details). Spanning a wide range of absorption redshifts ($0.2507 \leqslant z_{\rm abs} \leqslant 1.0951$) and rest-frame equivalent widths ($0.015 \leqslant W_0^{2796} \leqslant 2.028$ Å), they are representative of the high-resolution sample in Paper I.

The sample of galaxy cluster/group candidates lying at clustercentric-projected distances $d < 2\ h_{71}^{-1}$ Mpc from the quasar sight lines consists of 31 candidates with photometric redshifts between $0.173 \leqslant z_{\rm clus}^{\rm phot} \leqslant 1.032$ and richness parameters $B_{gc} < 1037$ (with a mean value $\overline{B_{gc}} = 346$; see Section 3.2 for more details). These fields were available for observations during the second semester of 2008.

Table 1 shows the Mg II absorption systems and the number of RCS1 cluster/group candidates lying at a clustercentric impact parameter $d < 2\ h_{71}^{-1}$ Mpc from each LOS studied in this work. The LOS to the quasar HE2149−2745A, also included in the analysis presented in Paper I, was taken from the literature and is outside the field covered by the RCS1 and Sloan Digital Sky Survey (SDSS; Williams et al. 2006, hereafter W06; Momcheva et al. 2006, hereafter M06). Absorption line redshifts were redefined with respect to Paper I to match the strongest Mg II velocity component.

Our analysis makes use of photometric data from both the RCS1 galaxy cluster and object catalogs, where the latter provided $(R_c - z')$ and z' magnitudes for all extended sources in our fields down to limiting magnitudes $R_c = 24.1$ and $z' = 23.1$ (Gladders & Yee 2000; Yee 1991).

In the following, all apparent magnitudes are given in the AB system and are corrected for galactic extinction according to the dust maps of Schlegel et al. (1998).

2.2. MOS Observations

Our spectroscopic data were obtained with the Gemini Multi-Object Spectrograph (GMOS) at the Gemini South Telescope in Cerro Pachón, Chile. The GMOS field of view (5.′5 × 5.′5) is wide enough to probe megaparsec-scale-projected distances at various redshifts. This is necessary since we consider cluster/group candidates at clustercentric impact parameters $d < 2\ h_{71}^{-1}$ Mpc from the LOS at photometric redshifts $z_{\rm clus}^{\rm phot} \sim 0.2$–$1$ (which translate into angular separations of ∼10′–4′, respectively). The spectroscopic data were acquired in queue mode between 2008 July and 2008 December (program ID: GS-2008A-Q-10; PI: S. López). In order to obtain a good signal-to-noise ratio (S/N) of the spectra and to maximize spectroscopic completeness, two masks per field were designed: for faint targets ($R_c \gtrsim 21$) an exposure time of 2 × 3000 s was chosen, whereas for brighter ones ($R_c < 21$) the exposure time was 2 × 1800 s.

Table 1
Fields Studied in This Work

The Sample							
LOS	z_{em} [a]	N_{clus} [b]	z_{abs} [c]	W_0^{2796} [d] (Å)	$\sigma_{W_0^{2796}}$ (Å)	Photo-hit[e]	Photo-hit I[f]
022300.41 + 005250.0	1.248	2	0.9500	0.043	0.010	Yes	No
022441.09 + 001547.9	1.201	5	0.2507	0.732	0.037	Yes	Yes
			0.3791	1.181	0.043	Yes	Yes
			0.6152	0.181	0.016	No	No
			0.9402	0.080	0.020	No	No
			1.0560	0.881	0.036	No	No
022553.59 + 005130.9	1.815	5	0.6821	0.333	0.019	Yes	Yes
			0.7500	0.159	0.015	Yes	Yes
			1.0951	1.685	0.065	No	No
			1.2258	0.177	0.032	No	No
022839.32 + 004623.0	1.288	5	0.6548	0.597	0.016	Yes	Yes
HE2149−2745A	2.030	1	0.4090	0.228	0.008	No	No
			0.4464	0.016	0.005	Yes*	No
			0.5144	0.028	0.003	No	No
			0.6012	0.175	0.006	Yes	Yes
			0.6032	0.015	0.004	Yes	No
			1.0189	0.219	0.013	No	No
231500.81−001831.2	1.324	6	0.5043	0.148	0.009	Yes	Yes
			0.5072	0.063	0.009	Yes	Yes
231509.34 + 001026.2	0.848	1	0.4473	1.758	0.009	Yes	Yes
231759.63−000733.2	1.148	1	0.6013	0.109	0.016	Yes	Yes
231958.70−002449.3	1.891	5	0.4071	0.151	0.017	No	No
			0.4158	0.192	0.021	No	No
			0.8463	2.028	0.024	Yes	Yes

Notes.
[a] Redshift of the QSO.
[b] The number of RCS1 cluster/group candidates lying at $d < 2\ h_{71}^{-1}$ Mpc from the LOS.
[c] Absorption redshift with $\delta z_{abs} \sim 10^{-4}$.
[d] Rest-frame equivalent width determined in Paper I.
[e] Absorption system that is considered as a photometric hit or not according to Tables 2 and 3 from Paper I, except for * which corresponds to a new photo-hit. These are used in the analysis of the present work.
[f] Absorption system that is considered as a photometric hit used in the analysis of Paper I, that is, those having $z < 0.9$ and $W_0^{2796} > 0.05$ Å.

Since the goals of the MOS observations were to identify Mg II absorbing galaxies and to confirm galaxy clusters, the masks were centered on QSO LOSs and position angles chosen to maximize the number of cluster candidates (i.e., their cluster centers) within the field of view.

The 400 line mm^{-1} grating (R400_G5325) was chosen and two central wavelengths were used (670 nm and 695 nm)—one for each of the two sets of exposures—in order to combine two spectra of the same object, avoiding the loss of information falling into the gaps between the three CCDs of the Gemini mosaic detector. The slit width for all targets was set to 1″, while the slit length varied from 7″ to 10″ to ensure sufficient sky counts for good sky subtraction.

Target selection for each mask focused mainly on sources near the LOSs of the background quasars, with the purpose of detecting absorbing galaxies. More specifically, galaxies at an impact parameter $\rho < 150\ h_{71}^{-1}$ kpc from the LOS (measured at the absorption redshift z_{abs}) were categorized as first priority targets in the selection algorithm. This limit permits comparison with impact parameters found in studies of the halo cross sections of Mg II absorbing galaxies in the field (Churchill et al. 2005 and references therein; Chen et al. 2010). In this study, we emphasize that ρ (h_{71}^{-1} kpc) refers to galaxy impact parameters to the LOS, while d (h_{71}^{-1} Mpc) refers to clustercentric impact parameters to the LOS.

Based on the R_c and z' color–magnitude diagram for galaxy-type objects around the cluster/group candidate coordinates (Gladders & Yee 2005), in addition to already known color–magnitude relations derived from composite clusters of galaxies (Gilbank et al. 2008), we selected objects of second priority in order to detect potential brightest cluster members. Second priority objects with an impact parameter $\rho < 150\ h_{71}^{-1}$ kpc from the LOS (at z_{abs}) were re-categorized as first priority objects.

Finally, third priority targets were chosen by performing a visual inspection of objects not selected as potential cluster members. The bias in this category toward bright/bluer galaxies permits the selection of galaxies in the outer regions of the clusters potentially exhibiting bluer colors.

The total number of selected targets was 440. Table 2 lists the number of spectroscopic sources selected in each field (N_{tot}) and those at an impact parameter $\rho < 150\ h_{71}^{-1}$ kpc from the respective LOSs ($N_{\rho < 150\,h_{71}^{-1}\,kpc}$) with a magnitude $R_c \leqslant R_{faint}$, where R_{faint} is the magnitude of the faintest object inside this region.

2.3. MOS Data Reduction

Data reduction was performed using the GEMINI IRAF package version 1.9, following standard IRAF v2.14 reduction procedures. The dispersion solution was found using 40–45

Table 2
Spectroscopic Targets Observed with GMOS

The Sample			
LOS	$N_{\rm tot}$ [a]	$N_{\rho < 150\,h_{71}^{-1}\,{\rm kpc}}$ [b]	$R_{\rm faint}$ [c]
022300.41 + 005250.0	43	3	24.75
022441.09 + 001547.9	51	8	23.64
022553.59 + 005130.9	48	2	22.30
022839.32 + 004623.0	50	3	23.00
HE2149−2745A	49	4	...
231500.81−001831.2	55	7	22.67
231509.34 + 001026.2	49	6	22.91
231759.63−000733.2	49	2	21.96
231958.70−002449.3	46	4	25.73

Notes.
[a] The number of GMOS targets per field. A total of 440 slits (439 objects) were observed with GMOS.
[b] The number of GMOS targets at an impact parameter $\rho < 150\,h_{71}^{-1}$ kpc from the LOS.
[c] Magnitude of the faintest target at an impact parameter $\rho < 150\,h_{71}^{-1}$ kpc from the LOS.

spectral lines of the CuAr arc lamp distributed among the whole wavelength range. A fourth- or fifth-order Chebyshev polynomial was fitted to the data and the resulting rms of the fits ranged between 0.15 and 0.22 Å. The resulting wavelength interval starts at ∼4000–4500 Å for some spectra, ending at ∼8500–9000 Å in others; the exact wavelength range depends on the position of the slit in the pre-image. The final data had a dispersion of ∼1.365 Å pixel^{-1} with a resolution element of FWHM ∼ 7 Å ($R \sim 1000$) equivalent to ∼350 km s^{-1} at $\lambda = 6000$ Å.

The final S/N of our spectra ranged between 5 and 20 pixel^{-1} at 6000 Å. Flux spectra were not calibrated as we were interested only in obtaining galaxy redshifts. We were able to use ∼88% of the reduced spectra, while the rest suffered from low S/N, artifacts, or fringing.

We measured redshifts by fitting Gaussian profiles to the spectral features (using the task rvidlines in the NOAO.RV IRAF package) and through a visual inspection of the two-dimensional spectra whenever necessary. Air-to-vacuum and heliocentric corrections were applied to each spectrum.

For early-type galaxies, redshifts were measured primarily with the lines Ca II H, Ca II K, and the *G*-band absorption lines. For late-type galaxies, the H_β, [O III] λ4959, and/or [O III] λ5007 were used. Whenever possible, [N II] λ6548, H_α λ6563, [N II] λ6583, [S II] λ6716, and/or [S II] λ6731 emission features were also considered. Nearly 55% of the galaxies show spectral features typical of early-type galaxies, of which ∼63% also show the [O II] λ3727 emission. Galaxies that show late-type features comprise 45% of the entire sample.

The mean redshift uncertainty of our galaxy catalog was ∼0.0005, equivalent to $\lesssim$100 km s^{-1} at $z = 0.55$. All redshifts were classified as type 1, type 2, or type 3 according to the reliability of our measurements, with type 1 being the most reliable and type 3 the least reliable. Galaxies with type 1 redshifts have spectra with two or more clear spectral features that could be modeled using Gaussian profiles. Type 2 redshifts were measured using only one or two detectable spectral lines alongside the possible presence of weaker ones, in such a way that those redshifts are still dependable. Those redshifts obtained by using only one (predominantly [O II] λ3727) or two spectral lines of poor signal-to-noise were classified as type 3. In total, 55% of our galaxies were assigned type 1 redshifts, 23% type 2 redshifts, and the remaining 22% type 3 redshifts.

In order to increase the total number of galaxies with spectroscopic redshifts, a search for luminous red galaxies and spectroscopic targets from the DR7 SDSS was performed, increasing our spectroscopic sample by 47 and adding an average of one and three galaxies per field, respectively (without considering HE2149−2745A that is outside the SDSS area). Of these, approximately 10% had spectroscopy from both our Gemini data and the SDSS database yielding redshift agreements of $\sim 10^{-4}$ even for our less reliable type 3 redshifts. We also searched for objects in the NASA/IPAC Extragalactic Database (NED), adding 420 more redshifts to our data. The total number of galaxies with redshifts from all available sources is 43 from SDSS, 420 from NED, and 383 from our Gemini survey.

In the odd-numbered figures from 1–17, we show a snapshot of each 5.′5 × 5.′5 pre-image field observed with GMOS. Targets have been marked with a circle and are identified with a number. Moreover, a small snapshot of each field is shown in the lower parts of these figures, indicating the center positions of the galaxy cluster/group candidates lying at $d < 2\,h_{71}^{-1}$ Mpc from the quasar sight lines. Their center positions are shown in circles indicating a physical radius of $0.5\,h_{71}^{-1}$ Mpc from the cluster center positions. The redshift histograms (even-numbered Figures 2–18) show all available redshifts for each field (see Section 3.2 for more details). The vertical lines in these plots indicate the absorption redshifts $z_{\rm abs}$ and the photometric redshifts of galaxy cluster/group candidates present in the fields. Tables 3–11 specify the number and redshift of each target, the redshift reliability classifier, and magnitudes.

3. RESULTS

3.1. Mg II Absorbing Galaxies

We define an absorbing galaxy as the closest galaxy to the LOS, observed with GMOS as having a redshift within typical galactic stellar velocity dispersions (<300 km s^{-1}) from an Mg II absorption system (see, e.g., Steidel et al. 1994; Le Brun et al. 1997). Previous surveys have found absorption galaxies at a few times 10 kpc. Our selection of targets for spectroscopic observations primarily focused on galaxies residing at impact parameters $\rho < 150\,h_{71}^{-1}$ kpc from the LOS and having R_c-band magnitudes brighter than ∼23.5 in GMOS pre-images.

The exposure time (see Section 2.2) and bright wings of the quasar spatial profile restricted the search for Mg II absorbing galaxies to objects typically brighter than $M_{R_c} \sim -20$ (at $z \sim 0.6$) and at impact parameters $\rho \gtrsim 2''$ equivalent to $\sim 8\,h_{71}^{-1}$ kpc at $z = 0.25$ and $16\,h_{71}^{-1}$ kpc from the LOS at $z = 1$.

Table 12 summarizes the Mg II absorbing galaxies detected in our sample. The table lists the absorption systems of each LOS: their rest-frame equivalent widths W_0^{2796} (Å) and errors $\sigma_{W_0^{2796}}$ (Å), the redshift at which the Mg II absorbing galaxy was found $z_{\rm gal}$, its impact parameter to the LOS ρ (h_{71}^{-1} kpc), if the absorption was considered a photometric hit in this work, the spectral features used to determine its redshift, and the absolute magnitude M_{R_c} corrected for *k* dimming according to Fukugita et al. (1995). These *k* corrections have been computed by matching the observed galaxy colors and those for a wide range of galaxies' spectral energy distribution at the measured redshift. Absorbing galaxies in the field centered on HE2149−2745A

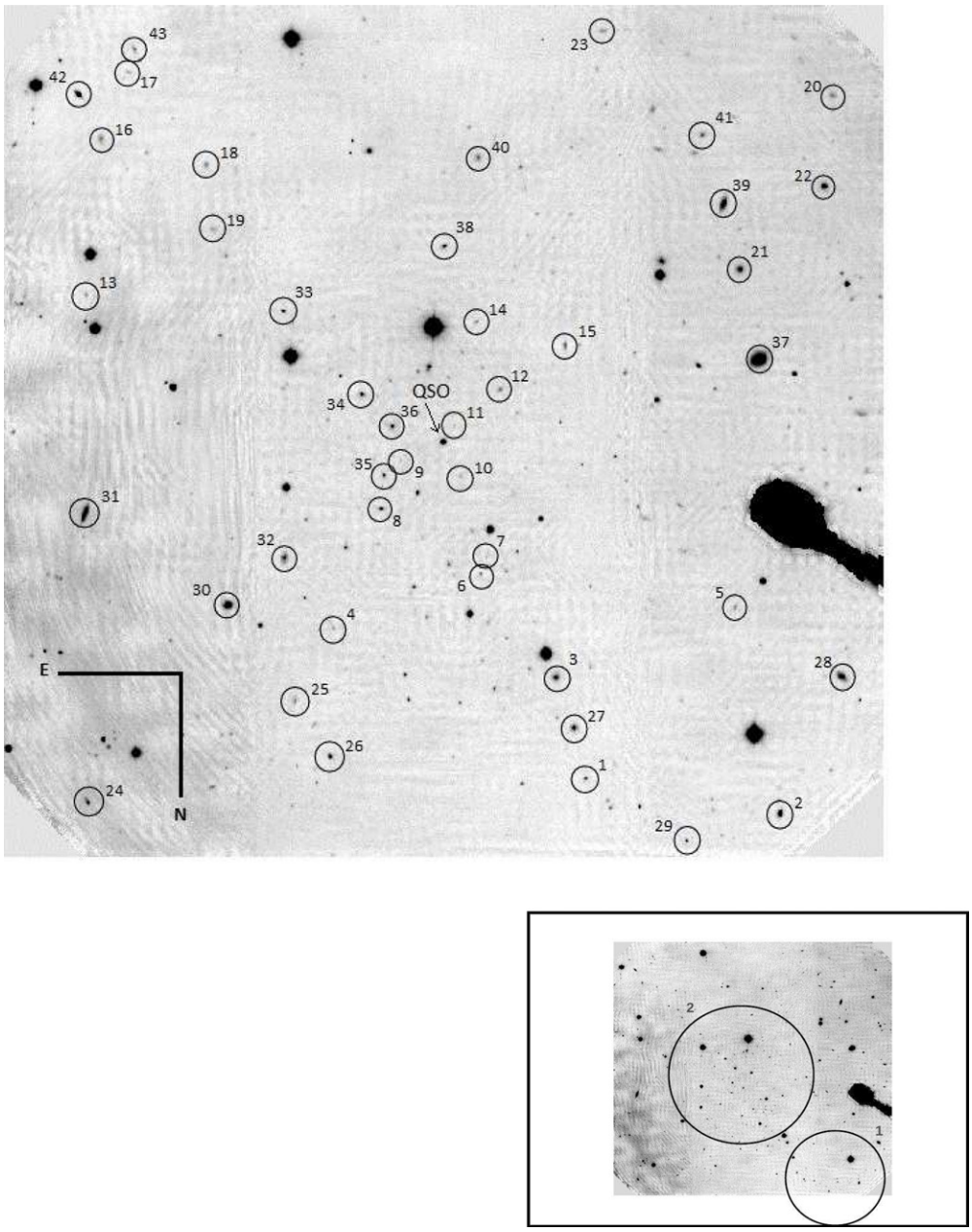

Figure 1. Top: 5′.5 × 5′.5 image of the field centered on the SDSS quasar 022300.41 + 005250.0. Galaxies are labeled according to the identification number given in Table 3. Bottom: a zoom-out of the image shown at the top. Center coordinates of each RCS1 cluster/group candidate are shown in circles. Each cluster is labeled according to their identification numbers given in the redshift histogram of Figure 2.

lack RCS1 and SDSS photometry, and as such no absolute magnitudes can be determined for them.

Out of a total of 24 absorption systems, Mg II absorbing galaxies were identified in 10 cases: 9 with our spectroscopic search and 1 from the literature, leading to a success rate of 41.7%. These galaxies have redshifts between $0.2509 \leqslant z_{\rm gal} \leqslant 1.0955$ ($\bar{z} = 0.55$). Detection of galaxies at $z > 1$ was unlikely because the typical [O II] λ3727 emission feature reaches $\lambda > 7500$ Å, a region of the spectra contaminated by fringing. The one high-z absorbing galaxy that we detected, a very bright source with $M_{R_c} = -20.21$ (see Figures 19 and 5), shows a clear [O II] λ3727 emission feature in its spectrum. The characterization of these absorbing galaxies is detailed in Section 3.4.

The median velocity difference $\delta v_{\rm gal} \equiv c(z_{\rm gal} - z_{\rm abs})/(1+z)$ is ~ -50 km s^{-1}, spanning a range between ~ -280 and 57 km s^{-1} and being consistent with galactic kinematics (e.g., Steidel et al. 2002). Despite these small velocity differences indicating genuine matches, we cannot exclude absorption from galaxies below our detection limit.

The low success rate results from observational design. Slit lengths are an important constraint when trying to observe all objects within a certain region using multi-object spectrographs. This, combined with low S/N sources and fringing, did not allow us to obtain redshifts for all objects within 150 h_{71}^{-1} kpc from the LOS. Consequently, the missing absorbing galaxies may lie at lower impact parameters to the LOS, may be hidden behind bright/large foreground objects within the region

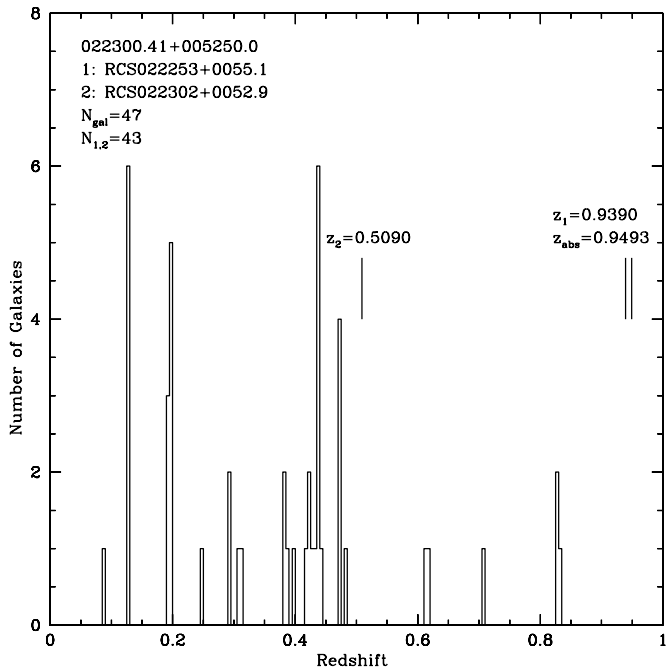

Figure 2. Redshift histogram of the field centered on the SDSS quasar 022300.41 + 005250.0. The bin size is of 0.005 in redshift space, which translates into $\Delta v \sim 1000$ km s^{-1} at $z = 0.5$. The total number of redshifts available for this field is given by $N_{\rm gal}$, from which $N_{1,2}$ is the number of redshifts classified with reliability flag 1 or 2.

(see, for example, Figures 3 and 7), or are too faint for reliable detection. Further and deeper spectroscopic observations must be planned to identify more absorbing systems and improve the number of matches to galaxy counterparts.

Figure 20 presents the R_c-band absolute magnitude versus redshift for our absorbing galaxies and interlopers, i.e., galaxies near the LOS that do not produce any Mg II absorption detectable in the quasar spectra. The survey is complete down to M^* ($z = 0$) for galaxies to $z < 0.7$.

Our absorbing galaxies have absolute magnitudes spanning a range between $M_{R_c} - 5\log h_{71} = -18.78$ ($z_{\rm gal} = 0.2509$, $W_0^{2796} = 0.732$ Å) and -22.07 ($z_{\rm gal} = 0.3793$, $W_0^{2796} = 1.181$ Å), with a median value of $M_{R_c} = -20.21$ comparable to M^* of present-day galaxies (Blanton et al. 2001). Moreover, interlopers show similar magnitude ranges and are also comparable to M^* galaxies. Thus, no difference in brightness can be distinguished between Mg II absorbing galaxies and interlopers. The median impact parameter of our 10 absorbing galaxies is 63.5 h_{71}^{-1} kpc. The highest redshift Mg II absorbing galaxy in our sample ($z_{\rm gal} = 1.0955$, $W_0^{2796} = 1.685$ Å) has an impact parameter at the minimum distance probed by our spectroscopic campaign (16.4 h_{71}^{-1} kpc), while the largest impact parameter, 142.7 h_{71}^{-1} kpc ($z_{\rm gal} = 0.4092$, $W_0^{2796} = 0.228$ Å), is approximately 43 km s^{-1} away from the absorption redshift.

Spectra of the absorbing galaxies are shown in Figure 19. We do not show the galaxy at $z_{\rm gal} = 0.6030$ responsible for the weak absorption of $W_0^{2796} = 0.015$ Å seen in the spectrum of the gravitationally lensed quasar HE2149−2745A (Wisotzki et al. 1996). This galaxy, taken from the literature, appears to be the lensing galaxy of the system as published in Eigenbrod et al. (2007). Despite the fact that no Mg II absorption was reported in that case, Paper I did detect an absorption with $W_0^{2796} = 0.015$ Å (the weakest in our sample) by analyzing a high resolution spectrum of the QSO.

Three out of the 10 galaxies show only emission lines, and more than half have Ca II K-, Ca II H-, and G-band absorption transitions among their spectral features. With the exception of the lensing galaxy, a common feature within our absorbing galaxies is the presence of the [O II] λ3727 emission line, denoting some level of recent star formation activity (see Table 12). Complementary to this, the mean $(R_c - z')$ color of our galaxies is 0.57, typical of S_{bc}–S_{cd} galaxies at $\bar{z} = 0.55$ (Fukugita et al. 1995).

3.2. Galaxy Clusters

The second goal of this work is to reduce the photometric redshift uncertainty of RCS1 cluster group/candidates ($\delta z_{\rm clus}^{\rm phot} = 0.1$) by confirming them spectroscopically. This will allow us to properly establish the possible connection between Mg II absorbers and galaxy overdensities.

As mentioned before, the sample contains 31 galaxy cluster/group candidates, of which 30 are from the RCS1 and 1 is taken from the literature. The RCS1 galaxy cluster/group candidates were detected with a significance $> 3\sigma_{\rm RCS}$ and are mostly poor: 27 have richness parameters $B_{gc} < 800$ and only 3 have $800 < B_{gc} < 1100$ (Yee & López-Cruz 1999), corresponding to clusters with A0–1 richness classes (Yee & López-Cruz 1999).

The confirmation algorithm we adopted is divided into three steps: (1) to detect overdensities in redshift space, (2) to associate galaxy cluster candidates (i.e., those without spectroscopic redshifts) with observed redshift overdensities, and (3) to define cluster membership to estimate cluster redshifts $z_{\rm clus}^{\rm spec}$ and rest-frame velocity dispersions σ_v (km s^{-1}).

We detect redshift overdensities by looking at redshift histograms for each field. Even-numbered Figures 2–18 show redshift histograms, using all redshift classes, with a bin size of 0.005. At $z = 0.173$ and $z = 1.032$ (the minimum and maximum photometric redshifts of our cluster/group candidate sample), this bin translates into velocity bin widths of ∼1280 and 740 km s^{-1}, respectively.

To define the extent of the redshift overdensities, we focus on ±1000 km s^{-1}, centered on each redshift peak identified in the redshift histograms, with a rest-frame bin width of 250 km s^{-1}. We concentrated specifically on peaks near the photometric redshifts of RCS1 cluster/group candidates. Since our survey strategy was designed to spectroscopically confirm an average of ∼3 clusters per field, and—as a result of the spectroscopic mask design procedure—we observed ∼50 objects per field, then a more conservative approach had to be adopted when stating the considerable number of members to obtain a reliable estimate of $z_{\rm clus}^{\rm spec}$. Consequently, peaks of more than 15 members were considered sufficient to identify a cluster of galaxies.

The association of cluster/group candidates with observed redshift overdensities was established once the redshift of central galaxies was obtained, i.e., (1) early-type galaxies located at projected distances $d_{\rm clus} < 500\ h_{71}^{-1}$ kpc from the cluster/group candidate center coordinates given by the RCS1, (2) with similar redshifts ($|\delta v| < 1000$ km s^{-1}) to the galaxy cluster/group candidate photometric redshifts and within their photometric redshift uncertainty ($\delta z_{\rm clus}^{\rm phot} = 0.1$), and (3) showing colors and magnitudes following a red sequence in $(R_c - z')$ versus z', built by including all extended sources at $d_{\rm clus} < 500\ h_{71}^{-1}$ kpc from the cluster center as defined by the RCS1 photometric object catalog (Gladders & Yee 2000). To obtain these color–magnitude relations, we performed rough color cuts in the color–magnitude diagrams, fitted a linear regression

Table 3
Spectroscopic Targets of Field Centered on 022300.41 + 005250.0

No.	R.A. (J2000)	Decl. (J2000)	z_{gal}	$\sigma_{z_{gal}}$	Flag[a]	z'	$R_c - z'$	Comments
1	02 22 56.77	+00 54 57.56	0.43834	0.00007	1	20.26	0.81	Ca II H, Ca II K
2	02 22 51.75	+00 55 10.67	0.19624	0.00057	3	18.72	0.63	Mg I 5176, Na D 5892
3	02 22 57.55	+00 54 19.48	0.47211	0.00010	1	19.00	0.55	[O II] 3727, Ca II H, Ca II K, H_β
4	02 23 03.31	+00 54 01.04	0.41877	0.00012	2	21.72	0.50	[O II] 3727, H_β, [O III] 5007
5	02 22 52.92	+00 53 53.23	0.29379	0.00005	1	21.28	0.24	H_γ, H_β, [O III] 4959, [O III] 5007
6	02 22 59.48	+00 53 40.52	...	...	0	20.72	1.84	...
7	02 22 59.34	+00 53 34.01	...	...	0	21.51	1.54	...
8	02 23 02.07	+00 53 15.97	0.43740	0.00007	1	20.18	0.83	Ca II H, Ca II K
9	02 23 01.56	+00 52 57.65	...	...	0	23.29	1.20	...
10	02 23 00.02	+00 53 03.73	0.83062	0.00080	3	22.17	1.29	[O II] 3727
11	02 23 00.18	+00 52 44.47	...	...	0	22.76	0.49	...
12	02 22 58.99	+00 52 30.83	...	...	0	20.16	1.46	...
13	02 23 09.71	+00 51 55.22	0.70911	0.00012	1	21.21	1.00	[O II] 3727, Ca II H, Ca II K
14	02 22 59.61	+00 52 05.38	0.24733	0.00005	1	21.63	0.15	H_β, [O III] 4959, [O III] 5007, H_α
15	02 22 57.32	+00 52 14.20	0.48234	0.00010	1	20.41	0.64	[O II] 3727, Ca II H, H_β, [O III] 5007
16	02 23 09.31	+00 50 56.22	0.30679	0.00010	1	20.19	0.32	Ca II H, H_β, [O III] 4959, [O III] 5007
17	02 23 08.63	+00 50 31.06	0.82949	0.00085	2	20.80	1.28	[O II] 3727, Ca II H
18	02 23 06.60	+00 51 06.01	0.31065	0.00010	1	20.87	0.37	[O II] 3727, [S II] 4068, [O III] 4959, [O III] 5007
19	02 23 06.42	+00 51 30.28	0.19584	0.00012	2	21.02	0.42	H_β, [O III] 4959, [O III] 5007
20	02 22 50.39	+00 50 39.98	0.19500	0.00007	1	20.81	0.31	H_β, [O III] 5007
21	02 22 52.79	+00 51 45.54	0.61172	0.00021	3	19.00	0.46	H_β, [O III] 4959
22	02 22 50.60	+00 51 14.26	0.08511	0.00004	1	19.14	0.24	He I 5875, [N II] 6548, H_α, [N II] 6583, [S II] 6716, [S II] 6730
23	02 22 56.34	+00 50 15.50	0.19658	0.00006	1	20.88	0.29	H_β, [O III] 5007, H_α
24	02 23 09.66	+00 55 06.56	0.42789	0.00006	1	19.52	0.69	Ca II H, Ca II K, *G* band
25	02 23 04.30	+00 54 28.26	0.42024	0.00012	1	20.46	0.41	[O II] 3727, [O III] 4959, [O III] 5007
26	02 23 03.39	+00 54 49.18	0.47211	0.00009	1	19.79	0.79	[O II] 3727, Ca II H, Ca II K, H_δ, *G* band
27	02 22 57.08	+00 54 38.34	0.44022	0.00009	1	18.92	0.64	[O II] 3727, Ca II H, Ca II K, H_β, [O III] 5007
28	02 22 50.15	+00 54 19.26	0.19301	0.00042	2	18.37	0.59	Mg I 5176, Na D 5892
29	02 22 54.17	+00 55 21.11	0.38917	0.00012	1	20.20	0.64	Ca II H, Ca II K, *G* band
30	02 23 06.04	+00 53 52.08	0.12877	0.00003	1	17.93	0.58	[N II] 6548, [N II] 6583, H_α, [S II] 6716
31	02 23 09.74	+00 53 17.81	0.12794	0.00004	1	18.35	0.58	[O II] 3727, H_β, [O III] 5007, [N II] 6548, H_α, [N II] 6583, [S II] 6716
32	02 23 04.57	+00 53 34.40	0.42039	0.00014	2	19.12	0.60	[O II] 3727, Ca II K
33	02 23 04.60	+00 52 01.31	0.47146	0.00006	1	20.32	0.87	Ca II H, Ca II K, *G* band
34	02 23 02.57	+00 52 32.66	0.43393	0.00012	1	19.65	0.81	Ca II H, Ca II K, *G* band
35	02 23 02.00	+00 53 03.30	0.43615	0.00012	1	19.97	0.81	Ca II H, Ca II K, *G* band
36	02 23 01.78	+00 52 44.69	0.43908	0.00012	1	19.16	0.87	Ca II H, Ca II K, *G* band
37	02 22 52.30	+00 52 19.52	0.12706	0.00057	2	16.44	0.59	Mg I 5176, Na D 5892
38	02 23 00.43	+00 51 36.79	0.43924	0.00012	1	19.83	0.85	Ca II H, Ca II K, *G* band
39	02 22 53.21	+00 51 20.84	0.19601	0.00049	3	18.33	0.61	Mg I 5176, Na D 5892
40	02 22 59.56	+00 51 03.46	0.43909	0.00005	1	20.19	0.61	[O II] 3727, Ca II H, Ca II K, H_β
41	02 22 53.76	+00 50 54.85	0.61774	0.00040	2	20.11	0.80	[O II] 3727, Ca II H, Ca II K
42	02 23 09.89	+00 50 39.52	0.19435	0.00007	1	18.60	0.66	Ca II H, Ca II K
43	02 23 08.45	+00 50 22.31	0.47197	0.00007	2	20.47	0.82	[O II] 3727, Ca II K

Notes. Whenever information could not be obtained for a specific target, a "..." symbol is used. Stars found in our data have zero redshift.
[a] Redshift reliability classifier.

$(R_c - z') = a_0 z' + a_1$, and obtained the standard uncertainties of the constants σ_{a_0} and σ_{a_1}.

The conditions described above are satisfied in most cases where RCS1 cluster/group centers reside within the pre-image field of view. However, as ∼32% of our cluster/group candidate centers fall outside, a different approach had to be applied in order to establish the association between the RCS1 candidates and the redshift overdensities. For these cases, at least two of the following conditions had to be fulfilled: (1) galaxies residing at a clustercentric-projected distance $d_{clus} < 2\ h_{71}^{-1}$ Mpc, (2) having similar redshifts ($|\delta v| < 1000$ km s^{-1}) near the galaxy cluster/group candidate photometric redshifts and within their photometric redshift uncertainty ($\delta z_{clus}^{phot} = 0.1$), and/or (3) falling at less than $\pm 3\sigma_{a_1}$ from the color–magnitude relation that includes all photometric-extended sources at $d_{clus} < 500\ h_{71}^{-1}$ kpc from the cluster/group candidate center, taking into account, at large clustercentric distances, that galaxies tend to be morphologically different and have bluer colors (Dressler 1980). In the last criterion, to mitigate against foreground and background contamination, we additionally require that the first two conditions also be satisfied.

One special case is the field centered on HE2149−2745A. Here, the overdensity found at $z \sim 0.6$ (see the histogram in Figure 10) is consistent with the galaxy cluster detection of M06 and W06, who detected a red sequence at a photometric redshift $z_{clus}^{phot} = 0.590$ and that was then spectroscopically confirmed at $z_{clus}^{spec} = 0.6030$. Additionally, we find two more overdensities in the field at $z \sim 0.2768$ and $z \sim 0.7395$. While the former has already been identified by M06, the latter is reported here for the first time due to the depth of our observations.

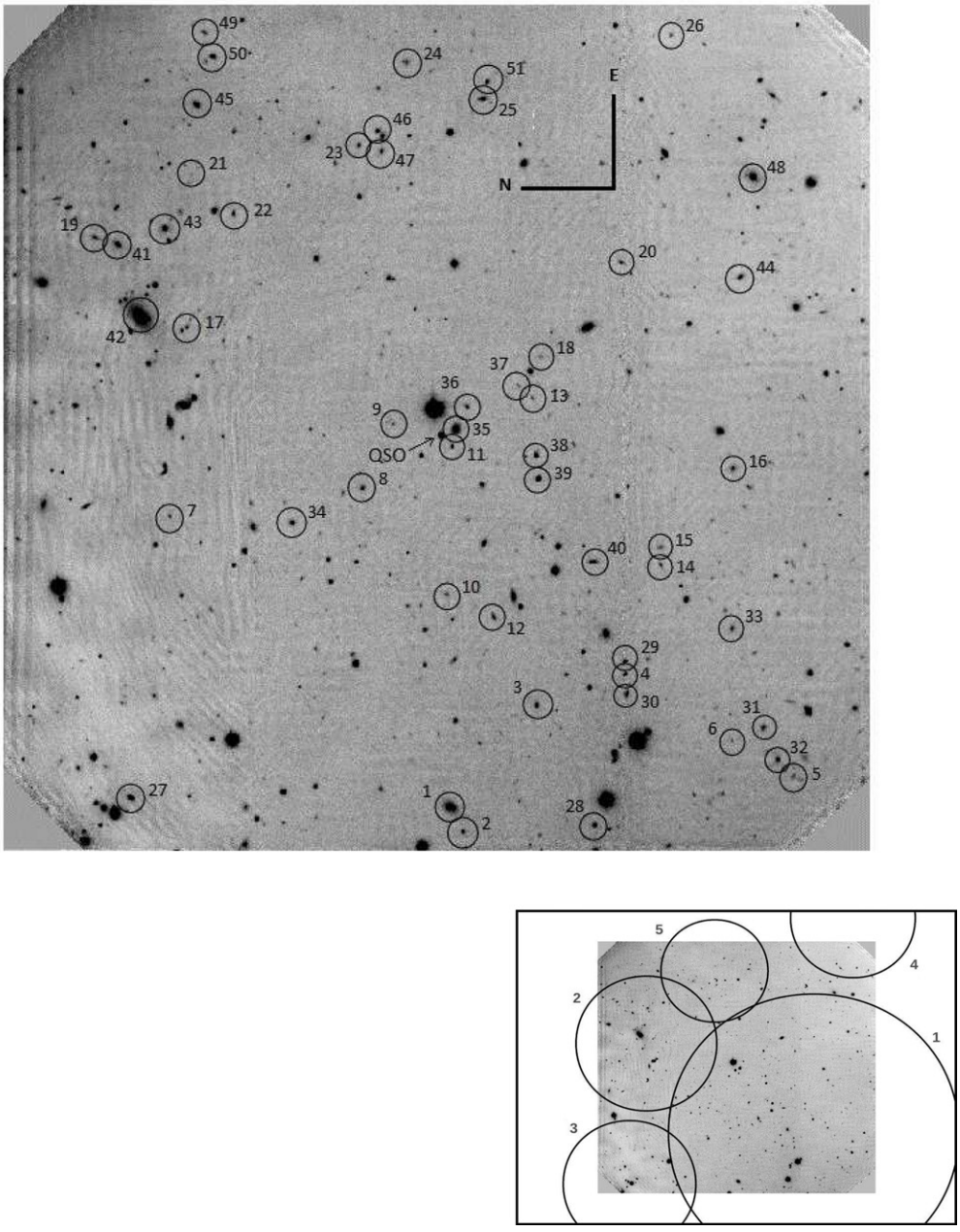

Figure 3. Top: 5.′5 × 5.′5 image of the field centered on the SDSS quasar 022441.09 + 001547.9. Galaxies are labeled according to the identification number given in Table 4. Bottom: a zoom-out of the image shown at the top. Center coordinates of each RCS1 cluster/group candidate are shown in circles. Each cluster is labeled according to their identification numbers given in the redshift histogram of Figure 4.

To assign cluster members, we followed the procedure of Fadda et al. (1996) and Blindert (2006), where galaxies at $|\delta v| \leqslant 4000$ km s^{-1} from each redshift peak (for all redshift flags) are subjected to an interloper rejection scheme using both galaxy angular position and clustercentric radial velocity. More specifically, this technique utilizes overlapping and shifting clustercentric distance bins of size $r_{\rm gap}$ (or larger) so that each bin contains at least $n_{\rm bin}$ galaxies. For each bin, a velocity-fixed-gap-rejection scheme is applied to discard galaxies at $\geqslant v_{\rm gap}$ km s^{-1} from their neighbors. Here, the values of $n_{\rm bin}$, $r_{\rm gap}$, and $v_{\rm gap}$ were chosen to be 10, 0.5 h_{71}^{-1} Mpc, and 1000 km s^{-1}, respectively, motivated by the small number of input redshifts per cluster and the small range of cluster richness.

Cluster redshifts, $z_{\rm clus}^{\rm spec}$, and velocity dispersions, σ_v (km s^{-1}), were determined with bi-weight estimators of location and scale from Beers et al. (1990). Uncertainties in σ_v were obtained using the jackknife method and were corrected to the rest frame.

Table 13 provides a summary of the results concerning the confirmation of RCS1 cluster/group candidates in our sample. All 31 cluster/group candidates lying at an impact parameter $d < 2\ h_{71}^{-1}$ Mpc from each LOS are listed, as well as their photometric redshifts $z_{\rm clus}^{\rm phot}$, spectroscopic redshifts $z_{\rm clus}^{\rm spec}$, and rest-frame velocity dispersion estimates σ_v (km s^{-1}) (both measured irrespective of redshift reliability flag). The final column includes comments about each galaxy cluster confirmation.

From a total of 31 cluster/group candidates, 20 were spectroscopically confirmed, spanning a redshift range $0.2659 \leqslant z_{\rm clus}^{\rm spec} \leqslant 1.0152$. Of these, 10 have a significant number of members ($N \geqslant 15$). Among clusters confirmed with fewer

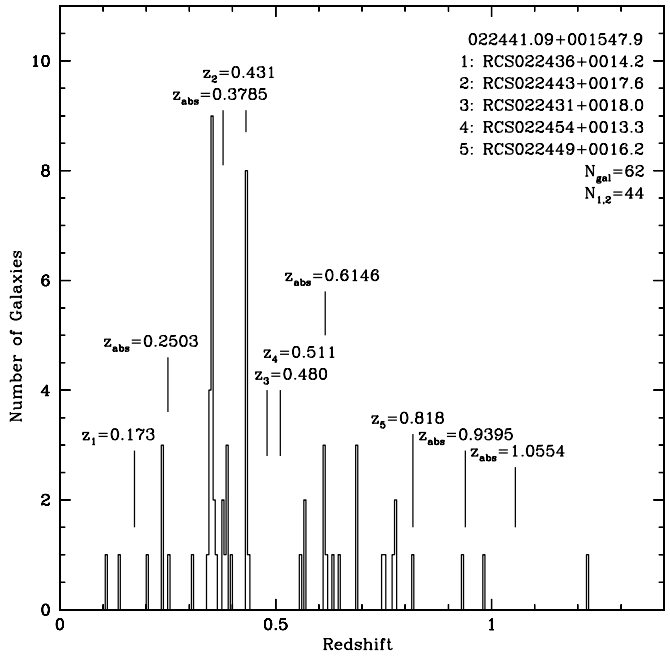

Figure 4. Redshift histogram of the field centered on the SDSS quasar 022441.09 + 001547.9. The bin size is of 0.005 in redshift space, which translates into $\Delta v \sim 1000$ km s^{-1} at $z = 0.5$. The total number of redshifts available for this field is given by $N_{\rm gal}$, from which $N_{1,2}$ is the number of redshifts classified with reliability flag 1 or 2.

members, seven are based on the detection of central galaxies (see comments in Table 13). For these, cluster redshift estimates are considered to be quantitatively reliable, while velocity dispersions should be considered as qualitative estimates only. Out of the final three confirmed clusters, two (in the field 231500.8−001831.2) were considered blended at the same redshift as it is not possible to separate them in photometric redshift and distance to the QSO LOS (see below). The remainder has a significant number of member galaxies, but the center lies out of the field.

Our spectroscopic survey proved more effective in detecting galaxies (and hence, galaxy overdensities) at $z \lesssim 0.7$. Out of 21 low-z galaxy cluster/group candidates ($z^{\rm phot}_{\rm clus} \lesssim 0.7$), we recovered 18, while from a total of 10 high-z galaxy cluster/group candidates, we were able to confirm only 2 thanks to the redshifts retrieved from NED.

The redshifts of the confirmed clusters can be compared with those estimated photometrically, as shown in Figure 21. Also shown are the RCS1 galaxy cluster redshifts calculated in Barrientos et al. (2004), Blindert (2006), Gilbank et al. (2007), and Gladders et al. (2002). We exclude all cluster redshifts found in the field 231500.81−001831.2 because we were unable to confirm the different cluster candidates individually. The resulting redshift differences $\delta z = |z^{\rm phot}_{\rm clus} - z^{\rm spec}_{\rm clus}|$ range between $0.004 \lesssim \delta z \leqslant 0.079$ for our confirmed clusters with $N \geqslant 15$ members, and $\delta z \lesssim 0.070$ for those with $N < 15$; both follow the one-to-one relation (dotted line) and are within typical δz values obtained in studies at similar redshift ranges (Blindert 2006; Gladders et al. 2002).

Taking into account past investigations shown in Figure 21 and data that we present here (including our confirmations), we find an average redshift offset of $\delta z/(1 + z^{\rm spec}_{\rm clus}) = 0.036 \pm 0.032$ (Wittman et al. 2001; Gilbank et al. 2007). This estimate implies $\delta z \sim 0.06$ at $z = 0.5$–0.7, reinforcing the empirical difficulty in confirming the overlapping clusters in the LOS 231500.81−001831.2 and 231958.70−002449.3 fields.

We also estimate cluster masses M_{200} and radii r_{200} by using the virial theorem (Carlberg et al. 1997). The mean virial radius r_{200} of our clusters confirmed with $N \geqslant 15$ members is $\overline{r_{200}} = 1.57 \pm 0.58\ h_{71}^{-1}$ Mpc and the mass enclosed within it is $\overline{M_{200}} = 6.92 \pm 4.15 \times 10^{14}\ h_{71}^{-1}\ M_{\odot}$. These values should be considered qualitatively. Thus, our sample of confirmed clusters appears to have mean masses consistent with $\overline{B_{gc}}$ typical of clusters of low-intermediate mass (Yee & Ellingson 2003).

Comments on the individual cluster detections can be found in the Appendix.

3.3. Spectroscopic Hits

Combining the results from Sections 3.1 and 3.2, we are now able to correlate Mg II absorbers with cluster/group environments, i.e., to confirm photometric hits.

According to our definition in Section 1, a spectroscopic hit is detected whenever either an Mg II absorption or an absorbing galaxy is found to reside in a spectroscopically confirmed galaxy cluster/group environment. More specifically, when $z_{\rm abs}$ (or $z_{\rm gal}$, if possible) falls within ± 1000 km s^{-1} of $z^{\rm spec}_{\rm clus}$, the confirmed cluster/group redshift.

Despite in some cases either being unable to confirm RCS1 cluster/group candidates or not expecting to find any, we did detect an agglomeration of few galaxies ($N < 10$) with similar redshifts ($|\delta v| \lesssim 1000$ km s^{-1}) separated at projected distances $\lesssim 0.5\ h_{71}^{-1}$ Mpc from each other. We consider these kinds of systems as groups of galaxies; absorbers inhabiting such redshifts and closeness in space are identified as group absorbers: spectroscopic hits associated with groups instead of clusters of galaxies.

We emphasize this distinction between group and cluster absorbers since galaxies in clusters may be affected by a history of extreme events, while the halos of galaxies in our newly defined groups of galaxies may experience less aggressive (ongoing) interactions. Thus, it is important to distinguish them from those galaxies that, according to our follow-up, appear completely isolated.

All spectroscopic hits detected in our sample are listed in Table 14. The table shows the cluster/group redshift $z^{\rm spec}_{\rm clus}$, rest-frame velocity dispersion σ_v (km s^{-1}), rest-frame velocity difference $\delta v_{\rm gal}$ (km s^{-1}) (between the redshift of the Mg II absorbing galaxy $z_{\rm gal}$ and the absorption redshift $z_{\rm abs}$), and the rest-frame velocity difference $\delta v_{\rm clus}$ (km s^{-1}) (between the cluster redshift $z^{\rm spec}_{\rm clus}$ and the absorber at $z_{\rm abs}$ or absorbing galaxy at $z_{\rm gal}$, if found).

From a total of 24 absorption systems, only 14 are considered as photo-hits. From these 14 Mg II–cluster pair candidates, 8 are confirmed as spectroscopic hits associated with galaxy clusters, and 2 with galaxy groups. This makes a total of 10 confirmations out of 14, corresponding to a ∼71% success rate in spectroscopically confirming photometric hits as Mg II absorbers in clusters/groups of galaxies. Additionally, two new spectroscopic hits were not classified as photometric hits as they were not matched to RCS1 clusters near $z_{\rm abs}$. Based on our spectroscopic survey of galaxies, we hypothesize that they are likely related to galaxy groups. Of the 12 absorption systems associated with galaxy clusters/groups, 10 are found at $z < 0.7$.

Table 4
Spectroscopic Targets of Field Centered on 022441.09 + 001547.9

No.	R.A. (J2000)	Decl. (J2000)	$z_{\rm gal}$	$\sigma_{z_{\rm gal}}$	Flag[a]	z'	$R_c - z'$	Comments
1	02 24 31.66	+00 15 45.32	0.35485	0.00005	2	18.63	0.70	Ca II H, Ca II K, *G* band, H_γ
2	02 24 31.02	+00 15 40.36	0.35510	0.00022	3	20.78	0.70	Ca II H, Ca II K, *G* band
3	02 24 34.25	+00 15 11.77	0.64546	0.00010	1	20.72	0.66	[O II] 3727, Ca II H, Ca II K, H_δ
4	02 24 35.04	+00 14 37.57	0.38374	0.00010	1	20.94	0.54	H_β, [O III] 5007, H_α, [N II] 6583
5	02 24 32.44	+00 13 32.30	0.63028	0.00033	3	23.40	0.25	[O II] 3727, [O III] 5007
6	02 24 33.33	+00 13 55.92	0.35481	0.00012	1	21.67	0.51	H_β, [O III] 4959, [O III] 5007
7	02 24 39.05	+00 17 33.97	0.56784	0.00021	3	22.39	0.63	[O II] 3727, Ca II H
8	02 24 39.78	+00 16 19.31	0.81839	0.00016	2	20.35	1.66	Ca II H, Ca II K
9	02 24 41.41	+00 16 07.39	0.93172	0.00080	3	23.41	0.17	[O II] 3727
10	02 24 37.07	+00 15 46.76	0.35191	0.00022	3	21.72	0.47	[O II] 3727, Ca II H, Ca II K, H_β, [O III] 5007
11	02 24 40.83	+00 15 44.68	0.25088	0.00011	1	21.23	0.50	[O II] 3727, H_γ, H_β, [O III] 4959, [O III] 5007, H_α, [N II] 6583
12	02 24 36.50	+00 15 28.44	0.35217	0.00009	1	20.35	0.65	[O II] 3727, Ca II H, Ca II K, H_β, [O III] 5007
13	02 24 42.07	+00 15 13.46	0.68534	0.00005	2	22.06	0.67	Ca II H, Ca II K, [O II] 3727, H_δ
14	02 24 37.82	+00 14 23.68	0.43117	0.00002	1	21.35	0.42	[O II] 3727, Ca II H, Ca II K, H_β, [O III] 5007
15	02 24 38.27	+00 14 23.75	0.77796	0.00080	2	21.18	0.45	[O II] 3727
16	02 24 40.27	+00 13 55.70	...	...	0	20.47	0.51	...
17	02 24 43.87	+00 17 27.38	...	...	0	21.72	0.49	...
18	02 24 43.13	+00 15 10.01	0.98009	0.00080	2	22.12	0.90	[O II] 3727
19	02 24 46.16	+00 18 03.06	0.10770	0.00012	1	21.31	0.13	H_β, [O III] 5007, H_α
20	02 24 45.53	+00 14 38.94	0.36228	0.00003	1	20.99	0.31	H_γ, H_β, [O III] 4959, [O III] 5007
21	02 24 47.76	+00 17 25.66	1.22330	0.00018	1	23.67	0.16	Fe II 2374−2382, Mn II 2576, Fe II 2586, Mn II 2594, Fe II 2600
22	02 24 46.76	+00 17 09.28	0.34656	0.00013	1	20.83	0.62	[O II] 3727, Ca II H, Ca II K, H_β, [O III] 5007
23	02 24 48.50	+00 16 20.78	0.37887	0.00006	1	21.28	0.31	[O II] 3727, Ca II H, Ca II K, H_β, [O III] 5007, H_γ
24	02 24 50.62	+00 16 02.06	0.61225	0.00080	2	20.82	0.80	[O II] 3727
25	02 24 49.69	+00 15 32.40	0.30797	0.00012	1	20.41	0.37	[O II] 3727, Ca II K, H_β, [O III] 5007
26	02 24 51.31	+00 14 19.57	0.38888	0.00006	1	21.97	0.49	H_β, [O III] 5007, H_α
27	02 24 31.89	+00 17 49.09	0.43430	0.00021	2	19.19	0.83	Ca II H, Ca II K
28	02 24 31.19	+00 14 49.38	0.39753	0.00007	1	20.76	0.56	[O II] 3727, [O III] 5007
29	02 24 35.35	+00 14 37.57	0.20110	0.00042	3	20.94	0.54	[O III] 4959, [O III] 5007
30	02 24 34.54	+00 14 36.78	0.34920	0.00020	3	20.46	0.75	Ca II H, Ca II K
31	02 24 33.68	+00 13 43.86	0.74531	0.00060	3	20.72	0.80	[O II] 3727
32	02 24 32.86	+00 13 38.35	0.75270	0.00014	3	20.35	1.51	[O II] 3727, Ca II H
33	02 24 36.21	+00 13 56.06	0.77845	0.00080	3	20.66	0.95	[O II] 3727
34	02 24 38.89	+00 16 46.52	0.35460	0.00035	3	19.77	0.69	Ca II H, Ca II K, *G* band
35	02 24 41.29	+00 15 43.09	0.37929	0.00012	1	19.00	0.51	[O II] 3727, H_β, H_δ
36	02 24 41.85	+00 15 38.81	0.61516	0.00080	3	21.42	0.52	[O II] 3727
37	02 24 42.38	+00 15 18.94	0.68548	0.00080	3	21.86	0.80	[O II] 3727
38	02 24 40.62	+00 15 12.02	0.55876	0.00010	1	20.46	0.59	[O II] 3727, Ca II H, Ca II K
39	02 24 40.01	+00 15 11.20	0.35013	0.00015	1	19.84	0.78	Ca II H, Ca II K, *G* band, H_γ
40	02 24 37.90	+00 14 49.70	0.35554	0.00012	3	20.19	0.53	H_β, [O III] 4959, [O III] 5007
41	02 24 45.98	+00 17 54.02	0.35270	0.00023	2	19.49	0.73	Ca II H, Ca II K, *G* band
42	02 24 44.13	+00 17 45.60	0.35144	0.00004	1	16.68	0.75	Ca II H, Ca II K, H_δ, *G* band, H_β, Mg I 5175
43	02 24 46.39	+00 17 35.77	0.68621	0.00023	2	19.54	1.30	Ca II H, Ca II K
44	02 24 49.54	+00 17 23.53	0.34470	0.00042	3	19.61	0.69	Ca II K, *G* band
45	02 24 45.15	+00 13 52.86	...	...	0	20.26	0.77	...
46	02 24 48.87	+00 16 13.44	0.61090	0.00076	2	20.51	1.25	Ca II H, Ca II K, *G* band
47	02 24 48.36	+00 16 11.89	0.61190	0.00080	3	20.20	1.35	Ca II K
48	02 24 47.70	+00 13 47.78	0.43289	0.00013	1	18.75	0.62	Ca II H, Ca II K, *G* band, H_δ, H_β
49	02 24 51.37	+00 17 20.54	0.77240	0.00064	3	23.75	0.92	[O II] 3727, H_γ
50	02 24 50.76	+00 17 17.38	0.43410	0.00030	3	20.35	0.56	[O II] 3727, H_β
51	02 24 50.11	+00 15 31.00	0.43202	0.00006	1	21.07	0.38	[O II] 3727, H_β, [O III] 5007

Notes. Whenever information could not be obtained for a specific target, a "..." symbol is used. Stars found in our data have zero redshift.
[a] Redshift reliability classifier.

From the four photo-hits that could not be confirmed, we find two of those are at the redshift boundaries of the survey, one at $z = 0.2507$ and the other one at $z = 0.95$ (where the RCS1 cluster catalog is incomplete). The other two remaining could not be assigned clusters. If we considered these last two absorbers as contaminants in our Mg II–cluster pair study, then we have a contamination of 29% (or 43% if the group absorbers are not considered as spectroscopic hits). Similarly, if we exclude the photo-hits in redshift boundaries where RCS1 is highly incomplete, then the contamination is only 17% (33% if the group absorbers are not considered hits).

The median redshift of Mg II absorbers associated with galaxy cluster environments was $z_{\rm med} = 0.60$, and for those in galaxy group environments $z_{\rm med} = 0.62$. The mean velocity difference of the whole sample of spectroscopic hits $\delta v_{\rm clus}$ is -22.46 km s^{-1} and spans a range between $+468.16$ and -656.25 km s^{-1}, consistent with typical cluster velocity dispersions.

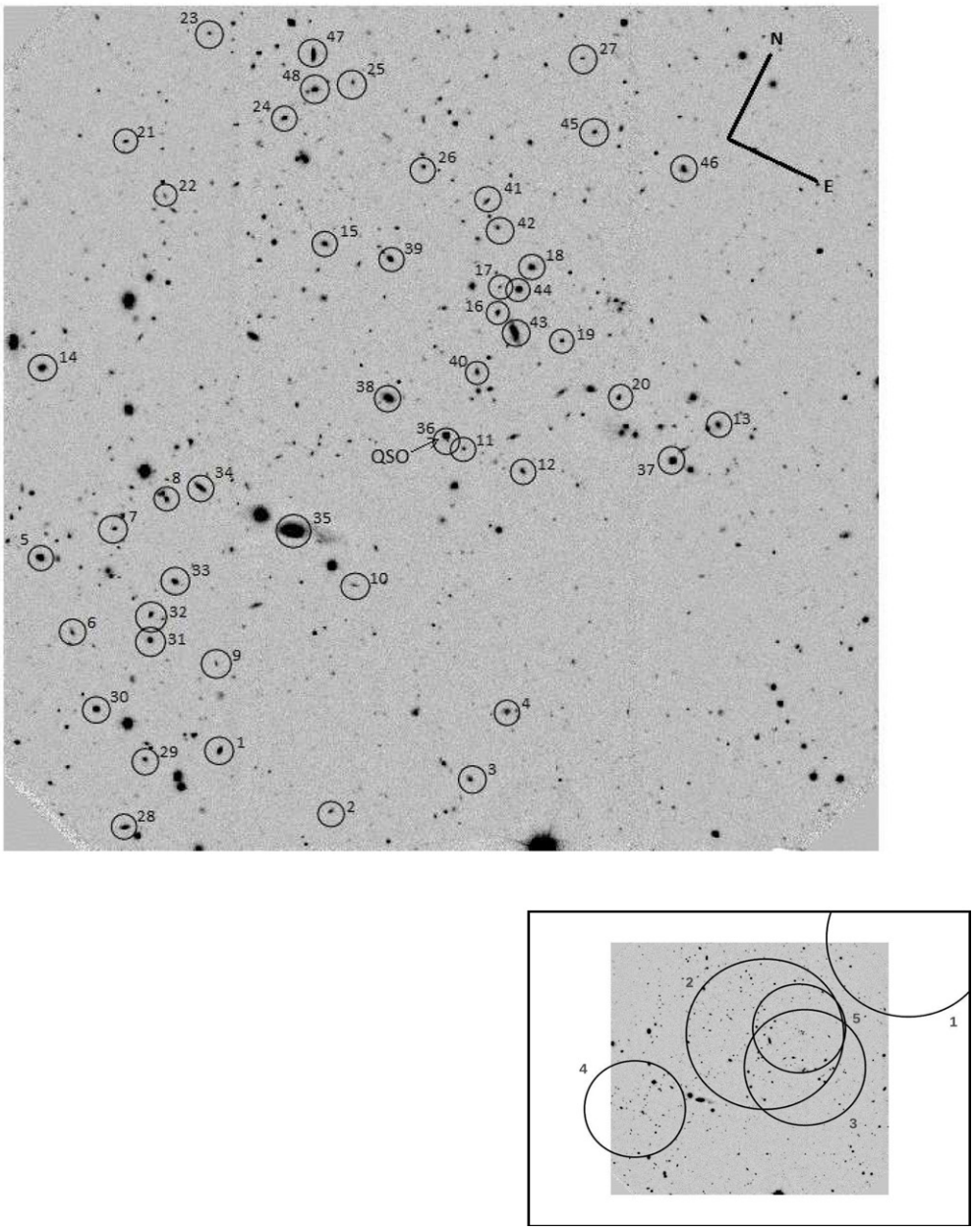

Figure 5. Top: 5′.5 × 5′.5 image of the field centered on the SDSS quasar 022553.59 + 005130.9. Galaxies are labeled according to the identification number given in Table 5. Bottom: a zoom-out of the image shown at the top. Center coordinates of each RCS1 cluster/group candidate are shown in circles. Each cluster is labeled according to their identification numbers given in the redshift histogram of Figure 6.

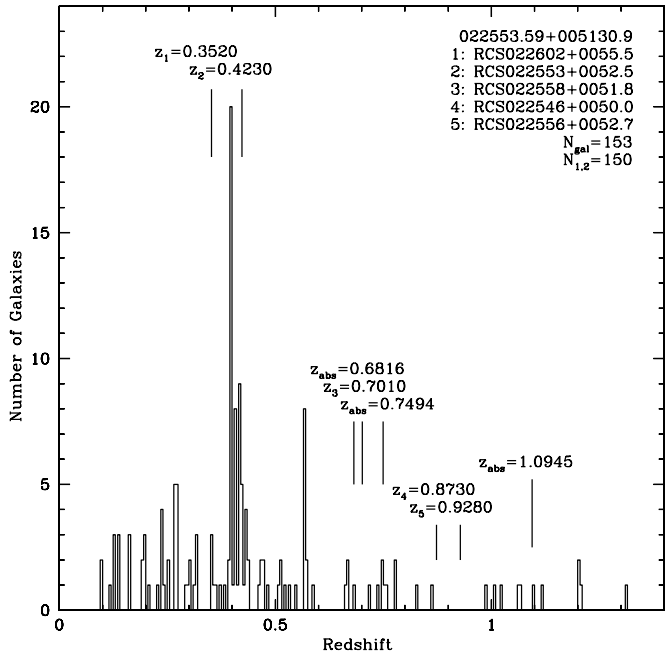

Figure 6. Redshift histogram of the field centered on the SDSS quasar 022553.59 + 005130.9. The bin size is of 0.005 in redshift space, which translates into $\Delta v \sim 1000$ km s^{-1} at $z = 0.5$. The total number of redshifts available for this field is given by $N_{\rm gal}$, from which $N_{1,2}$ is the number of redshifts classified with reliability flag 1 or 2.

The 10 absorbers in Table 14 that are not considered as photometric hits exhibit a wide redshift distribution, with four at $z > 1$, where the RCS1 cluster catalog is highly incomplete, and assignment therefore unreliable.

3.4. Characterization of Mg II Absorbers Associated with Cluster Galaxies

Several studies have investigated the so-called standard model of absorbers established by the work of Steidel (1995). According to this model, the gaseous extent of a galaxy can be described by a Holmberg luminosity scaling relation of the form $R(L) = R^*(L/L^*)^\beta$. In the sample of Steidel (1995), all Mg II absorbing galaxies fell below the relation, while non-absorbing galaxies fell above the relation. This result led Steidel (1995) to conclude that all normal galaxies with luminosities $L > 0.05\ L_K^*$ should have Mg II gaseous halos. However, other studies (Churchill et al. 2005) have found otherwise, due to the presence of interlopers and misidentified absorbing galaxies within the original sample used by Steidel (1995).

Figure 22 shows the observed impact parameter versus B-band luminosity for our absorbing galaxies (enclosed in a large open circle) and interlopers, associated with the field (filled triangles), galaxy groups (open circles), and galaxy clusters (filled circles). B-band magnitudes were obtained by converting SDSS photometry using the transformation given in Windhorst et al. (1991). We show only seven absorbing galaxies because we do not have photometry for the three absorbing galaxies found in the field centered on the LOS to HE2149−2745A.

We adopted the Holmberg relation determined by Chen & Tinker (2008) with $R^* \sim 89\ h_{71}^{-1}$ kpc and $\beta = 0.35$ for absorbing field galaxies. Figure 22 shows that bright galaxies generally tend to have larger Mg II halo sizes than fainter ones. Our data (regardless of environment) do not follow the standard model since there are seven interlopers lying below the line indicating that the covering factor of Mg II halos is less than unity, which can also be deduced from the large number of interlopers seen in our sample (see also Figure 20). However, in general, most absorbing galaxies confirmed in this work lie below the Holmberg relation derived in Chen & Tinker (2008), with interlopers falling above the line. Most importantly, all our absorbing galaxies confirmed in the field lie below the relation and most field interlopers lie above it. That our two absorbing cluster galaxies lie above the relation may indicate that the environment modifies the relation between galaxy luminosity and Mg II halo sizes.

Given the aforementioned contamination of the Steidel (1995) data and the lack of additional information about their assignment to groups or clusters, it would be interesting to test the standard model with a larger sample of confirmed Mg II absorbers and interlopers inhabiting cluster/group/field environments.

Figure 23 (left panel) shows the rest-frame equivalent width of the Mg II absorptions against the impact parameter to the LOS of our absorbing galaxies (enclosed in a large open circle) confirmed in the field, groups of galaxies, and clusters of galaxies (the symbols are the same as shown in Figure 22). We also plot the sample of absorbing field galaxies published in the work of Chen et al. (2010) as a reference. From this figure, we can see that regardless of their environment, our sample of absorbing galaxies appears to follow the anti-correlation tendency found for absorbing galaxies in the field (e.g., Chen et al. 2010).

Chen et al. (2010) found that the large scatter in this anti-correlation could be diminished when parameterizing the galaxy impact parameter ρ and the B-band luminosity of absorbing field galaxies in a scaling relation ($D = \rho \times (L_B/L_{B^*})^{-0.35}$ h_{71}^{-1} kpc). The right panel of Figure 23 shows the absorption rest-frame equivalent width W_0^{2796} (Å) versus the luminosity-weighted impact parameter D (h_{71}^{-1} kpc). This plot shows our data (enclosed by a large open circle) compared to that of Chen et al. (2010). The symbols are the same as shown in the left panel. Of our three field points (filled triangles), one falls at $>3\sigma$ from the anti-correlation found by Chen et al. (2010; solid line). This outlier from the 231509.34 + 001026.2 field is the second strongest absorber in our sample ($W_0^{2796} = 1.758$ Å), situated $61.19\ h_{71}^{-1}$ kpc from the LOS, and appears to be the closest galaxy to the quasar sight line up to the RCS1 limiting magnitude.

Our small sample of absorbing galaxies does not allow us to determine if a tight anti-correlation is valid for absorbing galaxies in clusters or groups of galaxies. When neglecting the environment, they appear to follow the anti-correlation found for absorbing galaxies in the field (solid line). However, a maximum likelihood method applied to a larger catalog of absorbers would be useful to establish a specific scaling relation between ρ (h_{71}^{-1} kpc) and galaxy luminosity for absorbing cluster/group galaxies; the scaling relation found for absorbing field galaxies ($D = \rho \times (L_B/L_{B^*})^{-0.35}$ (h_{71}^{-1} kpc)) does not necessarily hold for galaxies in clusters/groups. Applying this scaling relation could therefore be misleading when trying to define an analogous anti-correlation for absorbing cluster/group galaxies.

Until a large sample of absorbing cluster/group galaxies is available, the linear relation between both variables remains valid for isolated Mg II absorbing galaxies, yet remains unknown for those in clusters/groups.

4. DISCUSSION

In our search for Mg II absorbers inhabiting dense environments, we detected eight in clusters of galaxies and two in

Table 5
Spectroscopic Targets of Field Centered on 022553.59 + 005130.9

No.	R.A. (J2000)	Decl. (J2000)	$z_{\rm gal}$	$\sigma_{z_{\rm gal}}$	Flag[a]	z'	$R_c - z'$	Comments
1	02 25 50.89	+00 49 08.83	0.40633	0.00011	1	20.36	0.53	[O II] 3727, Ca II K, H_β, [O III] 5007
2	02 25 54.06	+00 49 01.42	0.39400	0.00008	1	21.80	0.26	[O II] 3727, H_β, [O III] 4959, [O III] 5007
3	02 25 57.11	+00 49 30.68	0.27039	0.00007	1	21.13	0.27	[O II] 3727, H_β, [O III] 4959, [O III] 5007
4	02 25 57.42	+00 49 59.84	0.51153	0.00007	1	21.96	1.00	[O II] 3727, H_γ, H_β, [O III] 5007
5	02 25 44.97	+00 49 54.80	0.09798	0.00004	1	19.52	0.21	[O II] 3727, H_β, [O III] 4959, [O III] 5007, H_α, [N II] 6583, [S II] 6716, [S II] 6730
6	02 25 46.36	+00 49 32.16	0.43080	0.00045	3	21.40	0.75	Ca II H, Ca II K
7	02 25 46.48	+00 50 14.71	0.19232	0.00011	1	21.05	0.13	[O II] 3727, H_β, [O III] 4959, [O III] 5007
8	02 25 47.47	+00 50 31.96	0.58654	0.00018	1	20.31	1.15	[O II] 3727, Ca II H, Ca II K
9	02 25 50.06	+00 49 39.65	0.09824	0.00022	1	22.39	0.33	H_β, [O III] 4959, [O III] 5007
10	02 25 52.69	+00 50 25.22	0.74548	0.00080	2	21.51	0.80	[O II] 3727
11	02 25 54.12	+00 51 28.22	0.57103	0.00035	1	21.01	1.01	Ca II H, Ca II K
12	02 25 55.72	+00 51 27.58	0.68241	0.00012	1	20.68	0.63	[O II] 3727, Ca II H, Ca II K
13	02 25 59.99	+00 52 09.52	0.39532	0.00003	1	20.27	0.37	H_γ, H_β, [O III] 4959, [O III] 5007
14	02 25 43.39	+00 51 03.13	0.40418	0.00008	1	19.58	0.55	[O II] 3727, Ca II H, Ca II K, H_δ
15	02 25 49.06	+00 52 23.74	0.19824	0.00006	1	20.48	0.24	[O II] 3727, H_β, [O III] 4959, [O III] 5007
16	02 25 53.77	+00 52 21.36	0.39449	0.00005	1	20.09	0.71	[O II] 3727, H_β, [O III] 4959, [O III] 5007
17	02 25 53.60	+00 52 30.86	0.74775	0.00080	3	21.79	0.91	[O II] 3727
18	02 25 54.17	+00 52 41.99	0.53291	0.00006	1	19.72	0.79	[O II] 3727, Ca II H, Ca II K, H_γ
19	02 25 55.54	+00 52 19.49	0.23591	0.00006	1	20.93	0.32	H_γ, H_β, [O III] 4959, [O III] 5007, H_α, [N II] 6583
20	02 25 57.39	+00 52 06.49	0.39743	0.00013	1	20.29	0.59	Ca II H, Ca II K, H_δ, *G* band
21	02 25 43.42	+00 52 34.86	0.40693	0.00012	1	21.02	0.59	[O II] 3727, H_β, [O III] 5007
22	02 25 44.82	+00 52 20.71	0.42169	0.00008	1	21.91	−0.21	[O II] 3727, H_γ, H_β, [O III] 4959, [O III] 5007
23	02 25 44.49	+00 53 24.58	0.13893	0.00004	1	21.86	0.59	H_β, [O III] 4959, [O III] 5007, H_α
24	02 25 47.02	+00 53 03.62	0.40838	0.00034	1	20.62	0.68	[O II] 3727, H_δ, H_γ, H_β, [O III] 5007
25	02 25 48.33	+00 53 25.15	0.12931	0.00005	1	21.27	0.53	H_γ, H_β, [O III] 4959, [O III] 5007, H_α
26	02 25 50.75	+00 53 03.98	0.73801	0.00023	1	20.94	1.45	[O II] 3727, Ca II H, Ca II K
27	02 25 53.60	+00 54 03.31	0.66596	0.00004	1	24.94	−0.30	[O II] 3727, H_γ, H_β, [O III] 4959
28	02 25 49.29	+00 48 29.16	0.29930	0.00085	2	19.98	0.82	Ca II K, *G* band
29	02 25 49.18	+00 48 56.09	0.75676	0.00025	3	21.16	1.12	[O II] 3727, Ca II K
30	02 25 47.58	+00 49 07.97	0.56685	0.00010	1	20.22	0.34	[O II] 3727, Ca II H, Ca II K
31	02 25 48.28	+00 49 39.54	0.31383	0.00012	1	19.83	0.64	Ca II H, Ca II K, *G* band
32	02 25 48.09	+00 49 48.61	0.40926	0.00019	1	20.61	0.73	[O II] 3727, Ca II H, Ca II K, H_δ, H_β
33	02 25 48.37	+00 50 03.44	0.41511	0.00009	1	20.02	0.67	[O II] 3727, Ca II H, Ca II K, H_δ, H_β
34	02 25 48.18	+00 50 40.42	0.41906	0.00022	1	19.62	0.74	[O II] 3727, Ca II H, Ca II K
35	02 25 50.78	+00 50 36.74	0.16005	0.00013	1	16.95	0.54	[O II] 3727, Ca II H, Ca II K, H_δ, H_β, [O III] 5007
36	02 25 53.67	+00 51 28.91	1.09550	0.00080	1	23.72	0.83	[O II] 3727
37	02 25 59.22	+00 51 50.72	0.56748	0.00012	1	19.86	0.69	[O II] 3727, Ca II H, Ca II K
38	02 25 51.90	+00 51 36.72	0.39817	0.00009	1	18.81	0.64	[O II] 3727, Ca II H, Ca II K, H_δ, H_β
39	02 25 50.75	+00 52 26.76	0.42031	0.00017	1	19.84	0.85	[O II] 3727, Ca II H, Ca II K, *G* band
40	02 25 53.79	+00 51 57.49	0.56961	0.00014	1	20.67	1.02	[O II] 3727, Ca II H, Ca II K
41	02 25 52.54	+00 52 59.84	0.46596	0.00005	2	21.20	0.69	[O II] 3727, Ca II K
42	02 25 53.04	+00 52 51.92	0.75386	0.00029	2	20.84	1.33	[O II] 3727, Ca II H, Ca II K
43	02 25 54.32	+00 52 16.68	0.39518	0.00013	1	18.50	0.54	[O II] 3727, Ca II H, Ca II K, H_γ, H_β, [O III] 4959, [O III] 5007
44	02 25 54.08	+00 52 32.38	0.39510	0.00010	1	19.81	0.76	Ca II H, Ca II K
45	02 25 54.54	+00 53 38.54	0.39550	0.00047	2	20.75	0.50	[O II] 3727, Ca II H, Ca II K
46	02 25 56.98	+00 53 36.60	0.41939	0.00002	1	20.19	0.48	H_β, [O III] 5007
47	02 25 47.15	+00 53 30.19	0.40621	0.00004	1	19.29	0.68	[O II] 3727, Ca II H, H_β, [O III] 4959, [O III] 5007
48	02 25 47.49	+00 53 17.84	0.56936	0.00046	2	20.17	1.20	Ca II H, Ca II K, *G* band

Notes. Whenever information could not be obtained for a specific target, a "..." symbol is used. Stars found in our data have zero redshift.
[a] Redshift reliability classifier.

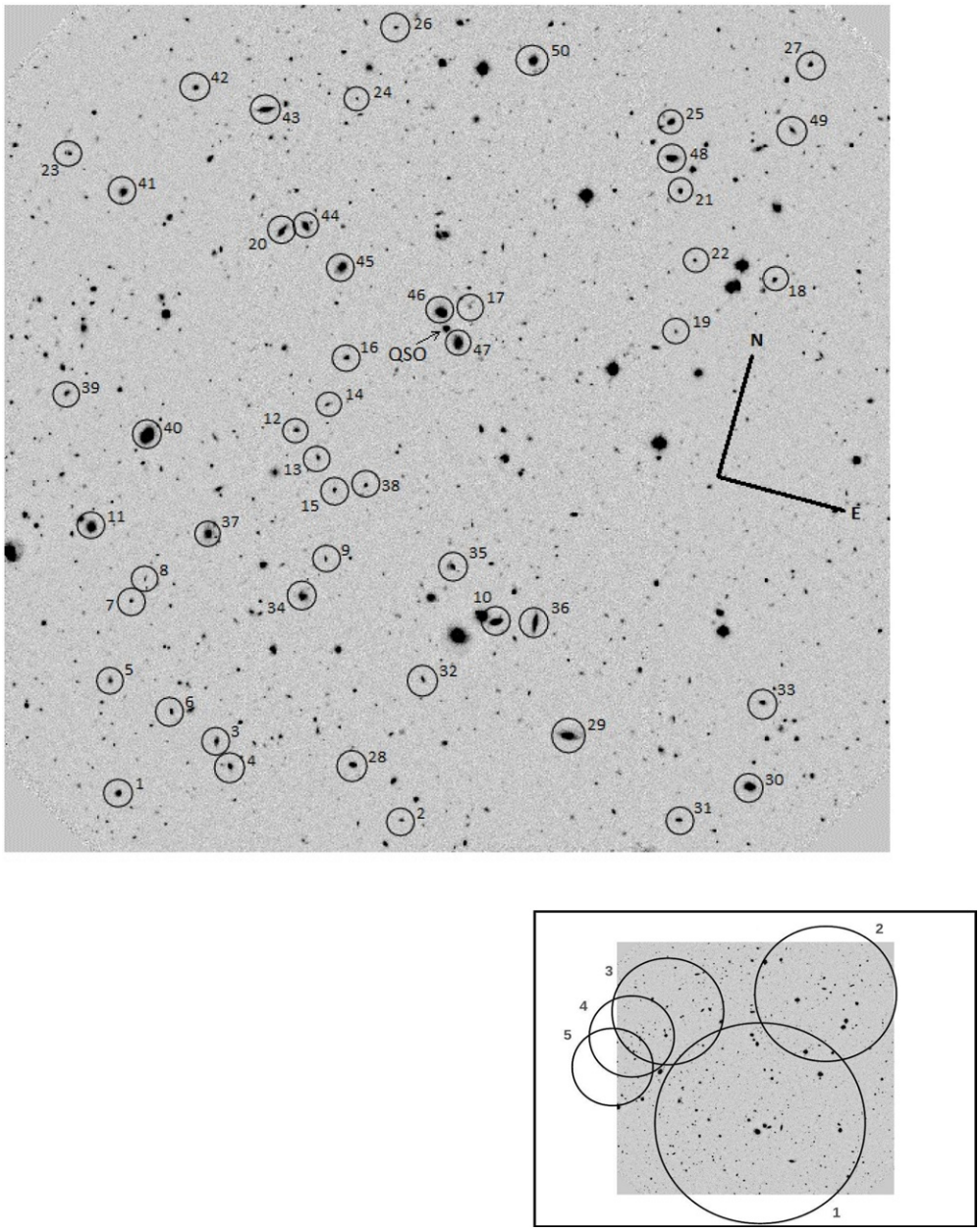

Figure 7. Top: 5′.5 × 5′.5 image of the field centered on the SDSS quasar 022839.32 + 004623.0. Galaxies are labeled according to the identification number given in Table 6. Bottom: a zoom-out of the image shown at the top. Center coordinates of each RCS1 cluster/group candidate are shown in circles. Each cluster is labeled according to their identification numbers given in the redshift histogram of Figure 8.

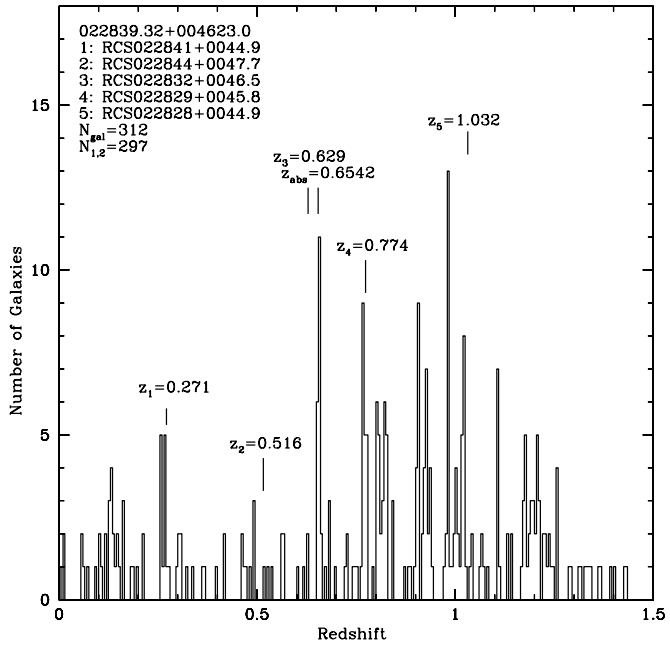

Figure 8. Redshift histogram of the field centered on the SDSS quasar 022839.32 + 004623.0. The bin size is of 0.005 in redshift space, which translates into $\Delta v \sim 1000$ km s^{-1} at $z = 0.5$. The total number of redshifts available for this field is given by $N_{\rm gal}$, from which $N_{1,2}$ is the number of redshifts classified with reliability flag 1 or 2.

groups of galaxies at a mean redshift $\bar{z} = 0.55$. This corresponds to a success rate of 71% in confirming spectroscopically photometric hits associated with clusters/groups of galaxies. Two additional Mg II absorbers have been associated with new groups identified in this study.

We also confirmed Mg II absorbing galaxies from which four appear to belong to clusters of galaxies, three to our newly defined groups of galaxies, and three to the field (i.e., isolated Mg II absorbing galaxies unconnected to groups of galaxies nearby).

While the definition of absorbing galaxies we adopt is usually used in surveys searching for absorbing galaxies (e.g., Steidel et al. 1994), some caveats must be stated about the reliability of our considerations.

The absorbing galaxies we report here may not be the only ones at $z_{\rm abs}$ and $\rho < 150\,h_{71}^{-1}$ kpc from the quasar sight lines, and as such some of them may be misidentifications. In such cases, we would be dealing with at least a pair or a group of galaxies near the LOS in the foreground of the respective quasar. This would add more candidates to our sample of Mg II–group pairs.

Instead of absorbers residing in galaxies, some may have been expelled from the galactic halo, thus exhibiting relatively large impact parameters ($\rho > 100\,h_{71}^{-1}$ kpc). In these cases, we would be tracing warm–cold gas reservoirs in the intergalactic medium or intracluster medium should the absorber reside in a cluster/group of galaxies. Despite this, we are not particularly interested in studying specifically where the absorption takes place within a galaxy. We merely state the assignment of the absorber to a specific overdensity in order to build a sample of confirmed cluster/group absorbers.

The results of our survey also have some redshift dependence that is strong for the confirmation of galaxy hosts, but mild (if any) for the confirmation of absorber–cluster pairs. From the original 24 absorbers in the 9 LOS presented here, one third are at $z > 0.7$, while for the confirmed hosts only 1 of 10 is at $z > 0.7$. On the other hand, 2 out of 12 confirmed cluster–absorber pairs are at $z > 0.7$, while we had 3 out of 14 candidates in the same redshift regime. This difference is not surprising since it is easier to confirm a cluster of galaxies using spectra from their bright members than to identify one fainter galaxy responsible for the Mg II absorption.

4.1. Are The Absorbing Galaxies Typical Cluster/Group/Field Galaxies?

When comparing the rest-frame $(B-R)$ color of our identified absorbing galaxies to those given in Fukugita et al. (1995), out of the four we confirmed we found one with a color consistent with an S_{bc} galaxy ($z_{\rm abs} = 0.6013$, $W_0^{2796} = 0.109$ Å). Another has a color consistent with an irregular/star-forming galaxy, and is also associated with a weak absorption system ($z_{\rm gal} = 0.5058$, $W_0^{2796} = 0.063$ Å). Since the field where the latter is located shows a clear overdensity of galaxies at its redshift, it could be an infalling galaxy that has yet to lose a large amount of gas. Finally, for the remaining two confirmed absorbing galaxies (near the LOS to HE2149−2745A) we do not have photometry, yet their spectra characteristics (see our Figure 19 and see Figure 12 in Eigenbrod et al. 2007) are consistent with relatively early-type galaxies, with both hosting weak absorbers ($W_0^{2796} = 0.015$ and 0.175 Å).

Thus, in general, all of these galaxies host weak absorbers; they appear as cluster galaxies undergoing some level of ongoing star formation at $z \sim 0.60$ (as shown by the presence of the [O II] λ3727 emission feature in their spectra) and lie at projected distances lower than $250\,h_{71}^{-1}$ kpc from the cluster center coordinates, with the exception of the absorbing galaxy associated with the cluster RCS231755−0011.3, where the projected distance is $\sim 1.6\,h_{71}^{-1}$ Mpc.

On the other hand, two of our absorbing group members appear disk like and irregular, respectively, producing absorptions of $W_0^{2796} = 1.181$ Å and 0.181 Å (see Table 12); unlike absorbing galaxies in clusters, they do not appear deficient in gas. Unfortunately, we lack B-band photometry to secure magnitudes for the other absorbing galaxy found in a group of galaxies (at $z_{\rm gal} = 0.4092$), though this target similarly shows properties consistent with those of a star-forming galaxy (see Figure 19).

Moreover, our small sample of isolated absorbing galaxies is bright and has a color consistent with disk galaxies. They all produce strong absorptions between $W_0^{2796} = 0.732$ Å and 1.758 Å, and appear as typical Mg II absorbing galaxies found in the field, as supported by previous works (Zibetti et al. 2007; Steidel et al. 1994; Lindner et al. 1996; Churchill et al. 2005; Kacprzak et al. 2005, 2007; Chen et al. 2010; Kacprzak et al. 2010).

The fact that absorbing group galaxies and field galaxies are indistinguishable from those found in RCS1 clusters may reflect the inclusion of small groups in our field sample. This potential cross-contamination must be investigated once further analysis is performed on those systems.

For now, we can conclude that independent of the environment which absorbing galaxies reside in, our catalog heterogeneously samples the population of absorbing galaxies and is consistent with past findings. However, in considering environmental effects, we find a dichotomy between our absorbing cluster galaxies and those confirmed in the field. While the former show generally weak ($W_0^{2796} < 0.3$ Å) absorptions and are consistent with early-type galaxies, the latter produce strong

Table 6
Spectroscopic Targets of Field Centered on 022839.32 + 004623.0

No.	R.A. (J2000)	Decl. (J2000)	z_{gal}	$\sigma_{z_{gal}}$	Flag[a]	z'	$R_c - z'$	Comments
1	02 28 34.14	+00 43 00.59	0.68320	0.00020	2	21.41	0.49	[O II] 3727, Ca II H, Ca II K
2	02 28 41.27	+00 43 16.68	0.41586	0.00004	1	22.45	0.02	[O II] 3727, H_γ, H_β, [O III] 4959, [O III] 5007
3	02 28 36.23	+00 43 28.96	0.65169	0.00002	3	20.97	0.92	[O II] 3727, Ca II H
4	02 28 36.72	+00 43 21.00	0.46362	0.00010	1	20.47	0.96	Ca II H, Ca II K
5	02 28 33.25	+00 43 41.48	...	...	0	21.54	1.49	...
6	02 28 34.94	+00 43 35.80	0.56726	0.00015	1	21.14	0.50	[O II] 3727, H_γ
7	02 28 33.28	+00 44 12.91	0.66299	0.00025	3	21.60	1.33	Ca II H, Ca II K
8	02 28 33.49	+00 44 22.42	0.80617	0.00080	2	22.19	0.53	[O II] 3727
9	02 28 37.79	+00 44 46.28	0.56164	0.00005	3	21.88	0.43	[O II] 3727, [O III] 5007
10	02 28 42.37	+00 44 38.69	0.26592	0.00003	1	18.86	0.71	Ca II H, Ca II K, *G* band
11	02 28 31.84	+00 44 36.49	0.32159	0.00008	1	19.09	0.68	[O II] 3727, Ca II H, Ca II K, *G* band, H_β, [O III] 4959, [O III] 5007
12	02 28 36.29	+00 45 31.03	0.13341	0.00005	1	21.76	0.27	H_β, [O III] 4959, [O III] 5007, H_α
13	02 28 36.98	+00 45 23.04	0.65660	0.00080	3	21.10	1.12	Ca3933
14	02 28 36.90	+00 45 43.34	0.67060	0.00080	3	22.52	0.20	[O II] 3727
15	02 28 37.60	+00 45 12.49	...	...	0	21.40	0.85	...
16	02 28 37.08	+00 46 02.39	0.65371	0.00017	1	20.88	0.77	[O II] 3727, Ca II H, Ca II K
17	02 28 39.79	+00 46 32.41	0.36409	0.00006	1	23.80	−1.07	[O II] 3727, [O III] 4959, [O III] 5007
18	02 28 47.11	+00 47 10.18	0.77262	0.00045	3	20.63	1.28	Ca II H, Ca II K
19	02 28 45.00	+00 46 42.20	0.76862	0.00080	3	22.78	0.36	[O II] 3727
20	02 28 34.72	+00 46 43.28	0.25626	0.00006	1	19.95	0.42	[O II] 3727, Ca II K, H_β, [O III] 4959, [O III] 5007
21	02 28 44.25	+00 47 34.58	0.46480	0.00030	3	20.37	0.87	Ca II H, Ca II K
22	02 28 45.04	+00 47 10.10	0.77258	0.00080	3	22.00	0.68	[O II] 3727
23	02 28 29.02	+00 46 52.28	...	...	0	20.81	1.79	...
24	02 28 35.75	+00 47 38.94	0.65156	0.00027	3	22.22	0.24	[O II] 3727, Ca II H, Ca II K
25	02 28 43.61	+00 47 59.21	0.30259	0.00003	1	20.40	0.42	H_β, [O III] 4959, [O III] 5007
26	02 28 36.26	+00 48 08.75	...	...	0	21.68	0.74	...
27	02 28 46.67	+00 48 33.19	0.91790	0.00080	3	21.31	0.95	[O II] 3727
28	02 28 39.72	+00 43 32.74	0.26685	0.00008	1	20.40	0.44	[O II] 3727, Ca II H, Ca II K, H_β
29	02 28 44.84	+00 44 03.26	0.30669	0.00007	1	18.71	0.66	Ca II H, Ca II K, *G* band, H_γ
30	02 28 49.61	+00 44 00.96	0.21074	0.00015	1	19.32	0.39	H_β, [O III] 4959, [O III] 5007
31	02 28 48.07	+00 43 42.17	0.12718	0.00005	1	20.78	0.22	H_β, [O III] 4959, [O III] 5007, H_α, [N II] 6583, [S II] 6716, [S II] 6730
32	02 28 40.92	+00 44 10.57	0.65726	0.00015	2	21.25	1.27	Ca II H, Ca II K
33	02 28 49.42	+00 44 33.22	0.49164	0.00031	3	21.13	0.29	HeII3781, [O III] 4959, [O III] 5007
34	02 28 37.46	+00 44 30.26	0.25637	0.00006	1	19.95	0.32	[O II] 3727, H_δ, H_γ, H_β, [O III] 4959, [O III] 5007
35	02 28 40.95	+00 44 55.14	0.77796	0.00080	2	24.59	−0.49	[O II] 3727
36	02 28 43.33	+00 44 42.11	0.26799	0.00015	3	19.03	0.92	Ca II H, Ca II K
37	02 28 34.75	+00 44 44.77	0.65924	0.00025	2	19.78	1.23	[O II] 3727, Ca II H
38	02 28 38.33	+00 45 17.06	0.25622	0.00006	1	24.22	0.55	[O II] 3727, H_γ, H_β, [O III] 4959, [O III] 5007
39	02 28 30.42	+00 45 23.80	0.62621	0.00080	2	21.79	0.10	[O II] 3727
40	02 28 32.65	+00 45 15.59	0.18719	0.00006	1	17.80	0.52	[O II] 3727, Ca II H, Ca II K, H_β, [O III] 5007, [N II] 6548, H_α, [N II] 6583
41	02 28 30.57	+00 46 43.18	0.65553	0.00055	1	20.26	1.02	[O II] 3727, Ca II H, Ca II K
42	02 28 31.72	+00 47 28.10	0.65552	0.00080	2	21.25	0.80	[O II] 3727
43	02 28 33.58	+00 47 26.56	0.16356	0.00007	3	19.77	0.50	[O III] 5007, H_α
44	02 28 35.27	+00 46 47.14	0.16276	0.00006	1	19.49	0.42	[O II] 3727, H_γ, H_β, [O III] 4959, [O III] 5007
45	02 28 36.41	+00 46 35.18	0.30340	0.00011	1	19.67	0.43	[O II] 3727, Ca II H, Ca II K, H_β, [O III] 5007
46	02 28 39.08	+00 46 27.91	0.15198	0.00008	1	18.14	0.62	H_β, [N II] 6548, H_α, [N II] 6583
47	02 28 39.72	+00 46 17.94	...	...	0	19.62	0.43	...
48	02 28 43.85	+00 47 45.67	0.46858	0.00019	1	19.19	0.90	[O II] 3727, Ca II H, Ca II K, *G* band
49	02 28 46.64	+00 48 07.16	...	...	0	21.16	1.38	...
50	02 28 39.84	+00 48 09.32	0.25590	0.00028	3	19.79	0.38	Ca II K, *G* band

Notes. Whenever information could not be obtained for a specific target, a "..." symbol is used. Stars found in our data have zero redshift.
[a] Redshift reliability classifier.

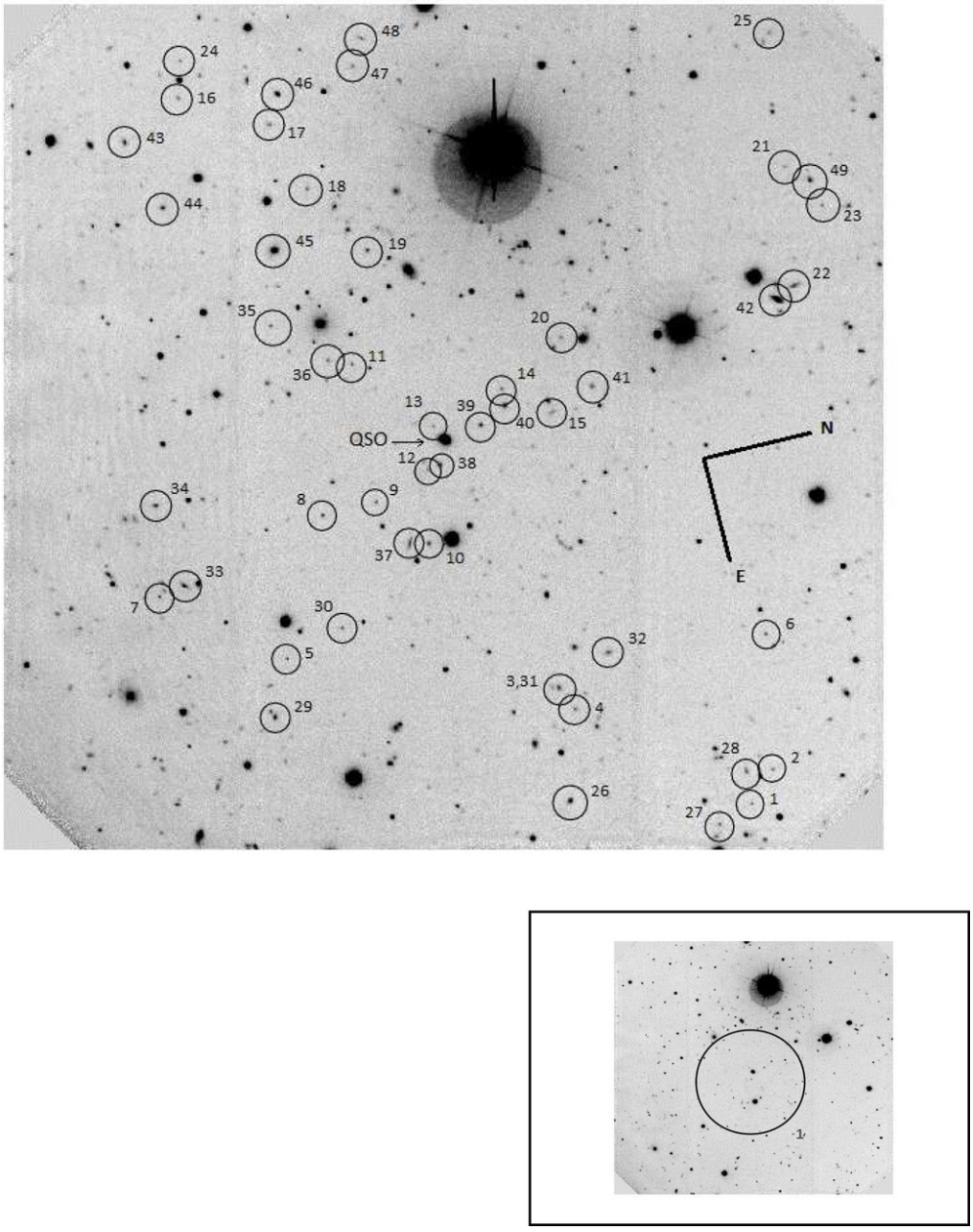

Figure 9. Top: 5.′5 × 5.′5 image of the field centered on the SDSS quasar HE2149−2745A. Galaxies are labeled according to the identification number given in Table 7. Bottom: a zoom-out of the image shown at the top. Center coordinates of each RCS1 cluster/group candidate are shown in circles. Each cluster is labeled according to their identification numbers given in the redshift histogram of Figure 10.

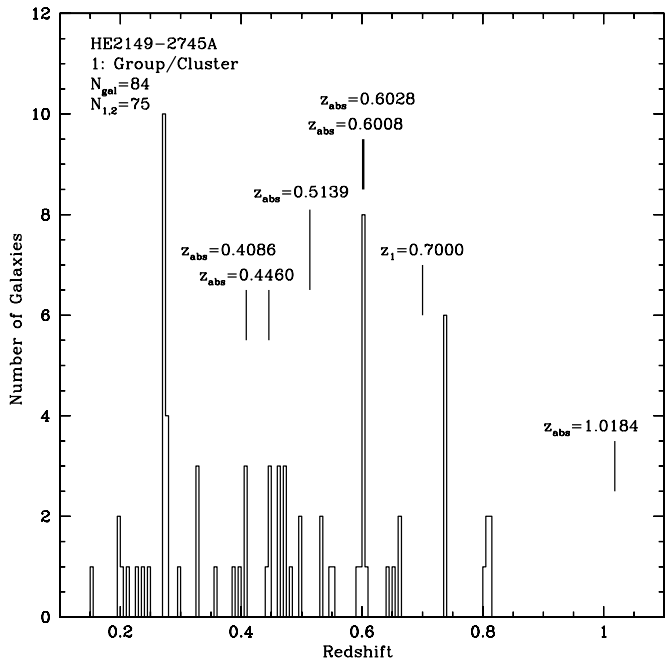

Figure 10. Redshift histogram of the field centered on the SDSS quasar HE2149−2745A. The bin size is of 0.005 in redshift space, which translates into $\Delta v \sim 1000$ km s^{-1} at $z = 0.5$. The total number of redshifts available for this field is given by $N_{\rm gal}$, from which $N_{1,2}$ is the number of redshifts classified with reliability flag 1 or 2.

absorptions and are consistent with bright star-forming galaxies typically encountered in the field.

Although relations between Mg II absorption strength and galactic halo masses (Bouché et al. 2006; Gauthier et al. 2009) or galaxy type (Zibetti et al. 2007) have already been studied, these works do not probe rest-frame equivalent widths as weak as those found in Paper I and used in this work.

4.2. Implications For Papers I and II

The sample originally presented in Paper I and studied here includes a total of 11 photometric hits, so defined at $z < 0.9$ with absorption systems having rest-frame equivalent widths $W_0^{2796} > 0.05$ Å. Table 14 shows that we recovered eight of these as spectroscopic hits, suggesting a 73% efficiency in the program. A closer look at these results finds that of three strong photometric hits ($W_0^{2796} > 1.0$ Å), two are recovered as spectroscopic hits, i.e., 2/3 of the strong Mg II system cluster member candidates genuinely reside in clusters.

In Paper I, we defined the weak systems as those having $W_0^{2796} < 1.0$ Å, and these show a dN/dz in clusters consistent with what is expected for the field. Now, in order to deal with the small number statistics, we classify weak systems as those having $W_0^{2796} < 0.3$ Å and strong systems for $W_0^{2796} > 0.3$ Å. We see that of the six photometric hits for strong systems, we recover only three as spectroscopic hits, whereas for the weak systems we recover five out of five.

Although the overall numbers are consistent with expectations from Paper I, their proposed interpretation is not supported by these new data. Here, we find that all weak absorbers are associated with clusters while this is true only for a fraction of the strong systems. The interpretation of the statistics in Paper I is that galaxies falling into the potential wells of clusters/groups lose their external shells where most of the weak systems are produced, and only the strong systems survive the interaction with the cluster. Here we see that all the weak systems are associated with clusters and only some of the strong systems. Despite dealing with small sample sizes, the results are at odds.

Regarding the analysis of halo sizes performed in Paper II, our sample of photometric hits confirmed in clusters of galaxies (for which field and group absorbers should be considered contaminants) shows that in general, Paper II accounts for field contamination (their Table 1) in a manner consistent with our findings here (28%), particularly when considering clustercentric impact parameters between [0.5, 1.0] h_{71}^{-1} Mpc. In this regime, their field absorber fraction agrees with our findings when we also include photometric hits that could not be confirmed in the field or were unclassified. Therefore, the results of Paper II on baryonic halo sizes of gas in RCS1 clusters remain valid.

All these numbers can be increased by including additional systems identified within this study. For instance, a new analysis of the LOS to the quasar HE2149−2745A indicates that we should have included the absorption system at $z_{\rm abs} = 0.4464$ as a photometric hit, since M06 and W06 detected a red sequence at a photometric redshift of $z_{\rm clus}^{\rm phot} = 0.40$, later confirmed spectroscopically as $z_{\rm clus}^{\rm spec} = 0.4465$. By including this system, the statistics remain similar.

5. SUMMARY OF RESULTS

We have performed Gemini multi-object spectroscopy of fields around nine distant background quasars, in whose spectra Mg II absorptions had previously been detected with rest-frame equivalent widths between $0.015 \leqslant W_0^{2796} \leqslant 2.028$ Å. Our project sought to build a sample of Mg II absorbers in dense environments such as clusters or groups of galaxies. To achieve this, we use our spectroscopic survey to search for absorbing galaxies near the LOS and confirm RCS1 cluster/group candidates within the nine fields ($d < 2\ h_{71}^{-1}$ Mpc from the LOS) in order to analyze the environment where the Mg II absorbers and their galactic counterparts are located. In this study, we include the analysis of spectra for 846 galaxies, 43 obtained from the SDSS database, 420 from NED, and 383 from our own GMOS observations. The highest priority for our spectroscopic observations was to detect the absorbing galaxies and then to detect the cluster galaxies. A total of 39 slits were devoted to identify the absorbing galaxies.

The main results of this work are summarized as follows.

Regarding our primary objective of identifying the absorbing galaxy, we obtained the following resutls.

1. We identified of 10 out of 24 absorbing galaxies with redshifts between $0.2509 \leqslant z_{\rm gal} \leqslant 1.0955$, up to an impact parameter of 142 h_{71}^{-1} kpc and a maximum velocity difference of 280 km s^{-1}.
2. Our small sample of isolated absorbing galaxies appears as bright disk galaxies, exhibiting strong absorptions, consistent with typical Mg II absorbing galaxies in the field, as stated by previous works.
3. Regardless of the environment, we have found a heterogeneous sample of absorbing galaxies, in agreement with previous searches published in the literature.

Regarding our objective of confirming the galaxy clusters at a maximum impact parameter of 2 Mpc from the QSO LOS, we obtained the following resutls.

Table 7
Spectroscopic Targets of Field Centered on HE2149−2745A

No.	R.A. (J2000)	Decl. (J2000)	$z_{\rm gal}$	$\sigma_{z_{\rm gal}}$	Flag[a]	z'	$R_c - z'$	Comments
1	21 52 19.30	−27 30 19.29	2.59530	0.00474	3	...	...	C IV 1550, C III 1909
2	21 52 18.44	−27 30 09.25	0.00000	0.00000	0	...	...	...
3	21 52 15.07	−27 31 23.88	0.73932	0.00012	2	...	...	[O II] 3727, Ca II K, *G* band
4	21 52 15.74	−27 31 19.20	0.73952	0.00040	2	...	...	Ca II H, Ca II K, *G* band
5	21 52 12.88	−27 33 03.71	0.00000	0.00000	0	...	...	...
6	21 52 14.57	−27 30 02.92	0.00000	0.00000	0	...	...	...
7	21 52 10.51	−27 33 47.38	...	...	0	...	...	...
8	21 52 09.02	−27 32 40.88	0.49600	0.00006	2	...	...	[O II] 3727, Ca II H, Ca II K
9	21 52 08.91	−27 32 20.11	0.00000	0.00000	0	...	...	...
10	21 52 10.34	−27 32 02.94	0.81198	0.00006	1	...	...	[O II] 3727, Ca II H, Ca II K
11	21 52 04.90	−27 32 19.93	0.59416	0.00021	1	...	...	[O II] 3727, H_γ
12	21 52 08.23	−27 31 58.62	...	...	0	...	...	...
13	21 52 07.05	−27 31 53.58	...	...	0	...	...	...
14	21 52 06.33	−27 31 25.36	0.60271	0.00006	2	...	...	[O II] 3727, Ca II H, Ca II K
15	21 52 07.24	−27 31 08.01	0.80307	0.00021	2	...	...	[O II] 3727, [O III] 5007
16	21 51 56.50	−27 33 07.38	0.60998	0.00010	1	...	...	[O II] 3727, Ca II H, Ca II K, H_γ
17	21 51 57.70	−27 32 35.09	0.48246	0.00005	1	...	...	[O II] 3727, H_γ, H_β, [O III] 5007
18	21 51 59.70	−27 32 25.05	0.73870	0.00012	1	...	...	[O II] 3727, Ca II H, Ca II K
19	21 52 01.74	−27 32 06.72	0.60433	0.00015	1	...	...	[O II] 3727, Ca II K, H_γ, H_β
20	21 52 05.17	−27 30 59.90	0.46006	0.00010	1	...	...	[O II] 3727, H_β, [O III] 4959, [O III] 5007
21	21 52 01.46	−27 29 25.12	0.47426	0.00007	3	...	...	H_β, [O III] 5007
22	21 52 04.87	−27 29 29.26	0.60338	0.00012	3	...	...	H_β, [O III] 4959, [O III] 5007
23	21 52 02.73	−27 29 13.27	...	...	0	...	...	...
24	21 51 55.45	−27 33 04.18	...	...	0	...	...	...
25	21 51 57.60	−27 29 21.88	0.81260	0.00040	2	...	...	[O II] 3727, Ca II H, Ca II K
26	21 52 18.32	−27 31 27.19	0.65148	0.00012	1	...	...	Ca II H, Ca II K, [O II] 3727
27	21 52 19.74	−27 30 32.79	0.80710	0.00078	3	...	...	Ca II H, Ca II K
28	21 52 18.36	−27 30 19.18	0.53370	0.00014	3	...	...	[O II] 3727, Ca II K
29	21 52 14.48	−27 33 12.13	0.27426	0.00009	1	...	...	[O II] 3727, Ca II H, Ca II K, H_β, [O III] 5007
30	21 52 12.30	−27 32 40.99	...	...	0	...	...	...
31	21 52 15.07	−27 31 23.88	0.73889	0.00012	2	...	...	[O II] 3727, Ca II K, *G* band
32	21 52 14.30	−27 31 02.97	0.73953	0.00046	2	...	...	[O II] 3727, Ca II H, Ca II K
33	21 52 10.31	−27 33 37.44	0.35786	0.00006	1	...	...	[O II] 3727, H_β, [O III] 5007
34	21 52 07.91	−27 33 42.95	0.27272	0.00010	1	...	...	[O II] 3727, Ca II H, Ca II K, H_β
35	21 52 03.40	−27 32 47.87	0.32849	0.00004	1	...	...	[O II] 3727, H_γ, H_β, [O III] 4959, [O III] 5007
36	21 52 04.66	−27 32 28.68	0.47360	0.00007	3	...	...	Ca II H, Ca II K
37	21 52 10.22	−27 32 10.14	0.19677	0.00006	1	...	...	H_β, [O III] 4959, [O III] 5007
38	21 52 08.18	−27 31 53.62	0.60045	0.00023	1	...	...	[O II] 3727, Ca II K, *G* band
39	21 52 07.25	−27 31 35.79	0.27610	0.00035	3	...	...	Ca II H, Ca II K
40	21 52 06.81	−27 31 25.47	0.40924	0.00012	1	...	...	[O II] 3727, Ca II H, Ca II K
41	21 52 06.70	−27 30 51.48	0.59591	0.00022	1	...	...	[O II] 3727, Ca II H, Ca II K, *G* band, H_γ
42	21 52 05.17	−27 29 36.45	0.29960	0.00007	2	...	...	H_β, [O III] 5007
43	21 51 57.49	−27 33 30.46	0.40688	0.00009	1	...	...	[O II] 3727, Ca II H, H_γ, H_β, [O III] 5007
44	21 51 59.52	−27 33 20.49	2.55150	0.00757	3	...	...	C IV 1550, C III 1909
45	21 52 01.28	−27 32 41.57	0.27412	0.00012	1	...	...	Ca II H, Ca II K, *G* band
46	21 51 56.86	−27 32 29.94	0.49543	0.00017	3	...	...	[O II] 3727, Ca II H, Ca II K
47	21 51 56.46	−27 31 59.85	0.27373	0.00012	1	...	...	[O II] 3727, H_β, [O III] 5007
48	21 51 55.71	−27 31 54.91	0.38975	0.00010	1	...	...	[O II] 3727, H_γ, H_β, [O III] 5007
49	21 52 01.98	−27 29 16.12	0.54816	0.00005	1	...	...	[O II] 3727, H_γ, H_β, [O III] 4959

Notes. Whenever information could not be obtained for a specific target, a "..." symbol is used. Stars found in our data have zero redshift.
[a] Redshift reliability classifier.

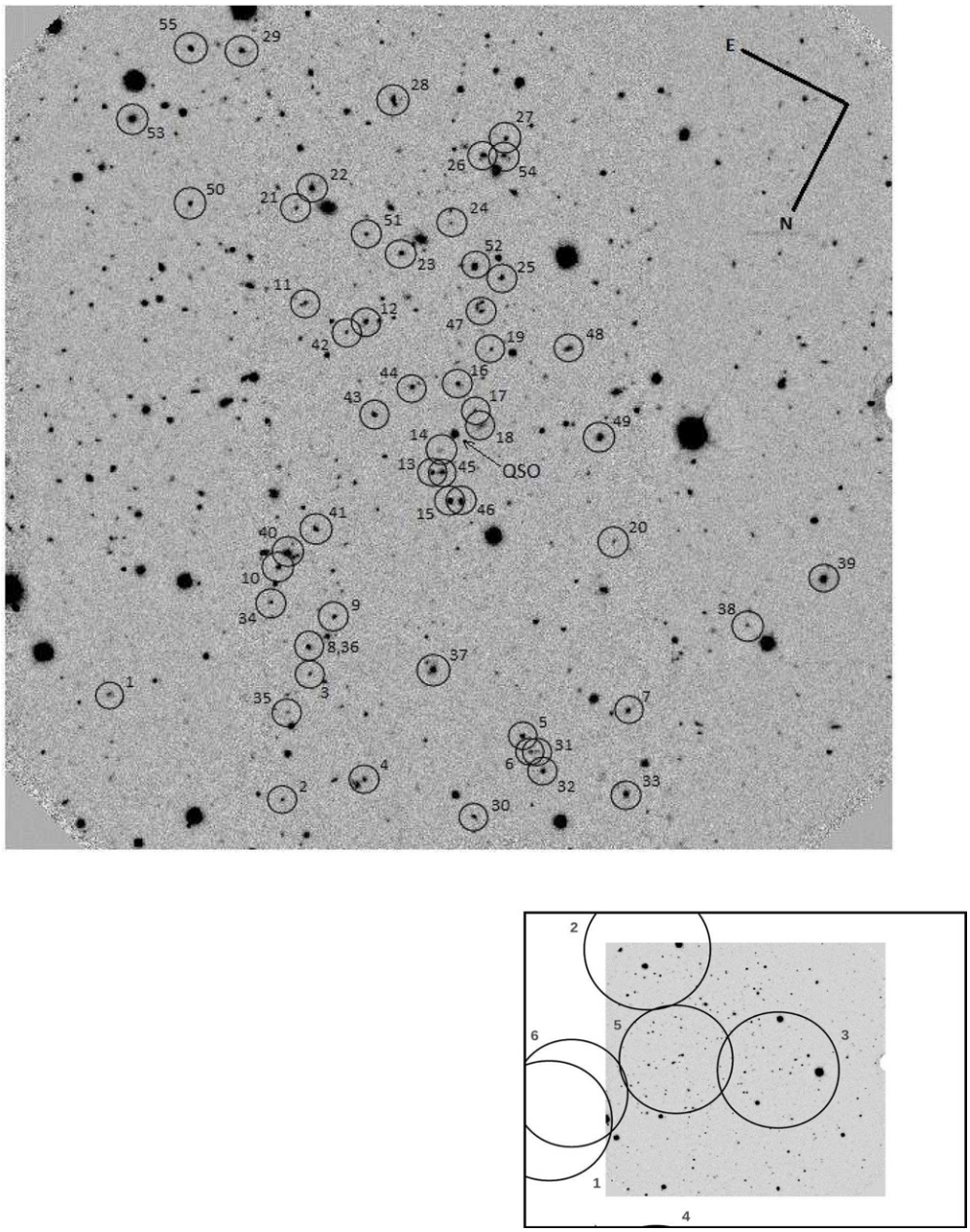

Figure 11. Top: 5′.5 × 5′.5 image of the field centered on the SDSS quasar 231500.81−001831.2. Galaxies are labeled according to the identification number given in Table 8. Bottom: a zoom-out of the image shown at the top. Center coordinates of each RCS1 cluster/group candidate are shown in circles. Each cluster is labeled according to their identification numbers given in the redshift histogram of Figure 12.

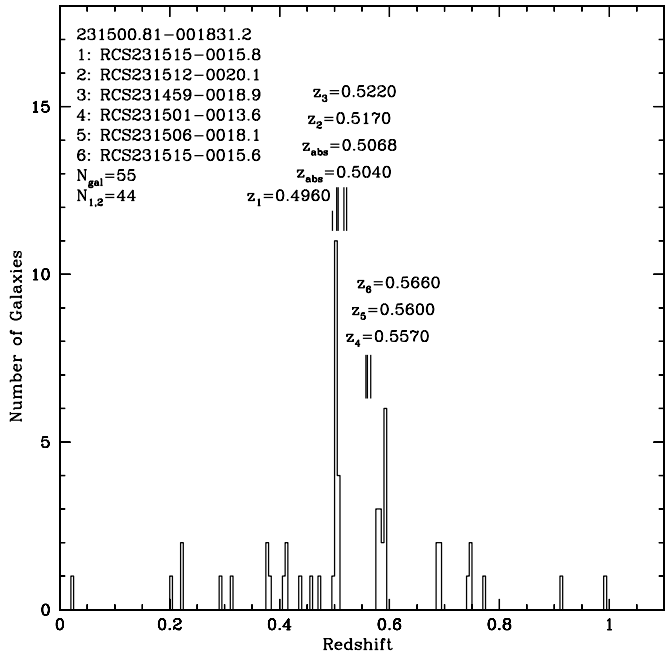

Figure 12. Redshift histogram of the field centered on the SDSS quasar 231500.81−001831.2. The bin size is of 0.005 in redshift space, which translates into $\Delta v \sim 1000$ km s^{-1} at $z = 0.5$. The total number of redshifts available for this field is given by $N_{\rm gal}$, from which $N_{1,2}$ is the number of redshifts classified with reliability flag 1 or 2.

1. From a sample of 31 cluster/group candidates, we confirmed 20 spanning a redshift range $0.2659 \leqslant z_{\rm spec} \leqslant 1.0152$ with a mean mass consistent with $\overline{B_{gc}}$ typical of low-intermediate mass clusters. Non-confirmations of galaxy clusters/groups occurred mainly because we prioritized the detection of absorbing galaxies over the confirmation of galaxy cluster candidates.

Regarding the confirmation of our photometric hits and therefore confirming that the absorber galaxy belongs to the galaxy cluster, we obtained the following resutls.

1. We successfully determined the environment within which 12 of the absorbers reside: 8 inhabit clusters of galaxies, and 4 appear in galaxy groups. Absorbers in this bound system appear to lie between +468.16 and −656.25 km s^{-1} away from their cluster/group spectroscopic redshifts. This high success rate lends support to the results of Paper I.
2. We applied our results to determine the degree of contamination due to field absorbers within the sample of Mg II absorbers matched to galaxy cluster/group environments. After spectroscopically confirming the systems, we found a contamination fraction of ∼17%–29% due to field absorbers, increasing to 33%–46% if we also classify group absorbers as contaminants.
3. We did not confirm any cluster of galaxies in fields where no candidate at the absorber redshift was expected to be present.
4. We found two group absorbers where no cluster of galaxies had been previously detected within the RCS1 survey. Hence, including these absorbers adds two more non-isolated absorbers to our sample.

To conclude, we prove that the sample of photometric hits from Paper I is robust. Even though field absorbers may contaminate the sample (mostly due to misidentification of low-redshift clusters, and instances where two absorptions fall within the photometric redshift uncertainty of the same cluster), they have a minimal impact on the sample of photometric hits in Paper I. However, for future work they should be taken into account.

We thank Franz Bauer, Cédric Ledoux, and David Murphy for important suggestions included in the manuscript. S.L., L.F.B., P.L., and N.P. were partly supported by the Chilean Centro de Astrofísica FONDAP No. 15010003. H.A. was supported by Proyecto CONICYT-ALMA 31070001 and Beca Magíster CONICYT. S.L. was supported by FONDECYT grant No. 1100214. L.F.B. was supported by FONDECYT grant Nos. 1085286 and 1120676. N.D.P. was also supported by a FONDECYT grant No. 1110328. I.L. was supported by MECESUP. The RCS project is supported by grants to H.Y. from the National Science and Engineering Research Council of Canada and the Canada Research Chair Program. This research has made use of the NASA/IPAC Extragalactic Database (NED), which is operated by the Jet Propulsion Laboratory, California Institute of Technology, under contract with the National Aeronautics and Space Administration. Funding for the SDSS and SDSS-II has been provided by the Alfred P. Sloan Foundation, the Participating Institutions, the National Science Foundation, the US Department of Energy, the National Aeronautics and Space Administration, the Japanese Monbukagakusho, the Max-Planck Society, and the Higher Education Funding Council for England. The SDSS Web site is http://www.sdss.org/.

APPENDIX

SPECIAL REMARKS

A.1. On Individual Clusters

LOS 231500.81−001831.2. As seen in Table 13, the field around the LOS 231500.81−001831.2 presents six RCS1 cluster/group candidates that are spectroscopically confirmed by two cluster redshifts, one at $z_{\rm clus}^{\rm spec} = 0.5040$ and the other at $z_{\rm clus}^{\rm spec} = 0.5870$. All these RCS1 cluster/group candidates present low richness values ($B_{gc} < 600$) and low detection significance ($<3.3\sigma_{\rm RCS}$; except for RCS231506−0018.1 and RCS231515−0015.8) indicating that these candidates are much less likely to be confirmed with limited follow-up spectroscopy per se. Also, since this survey is constrained by the number of slits we can observe, and our first priority was to find the absorbing galaxies, it was not possible to put slits near all the cluster centers (see Figure 11). Moreover, all candidates appear superimposed in redshift (as seen in Figure 12), color, and angular space (see Table 8 and Figure 11), which did not allow us to distinguish them individually. We observe a concentration of galaxies between redshifts $z \sim 0.502$ and 0.507, centered on a notorious peak at $z \sim 0.504$ (see Figure 12). These galaxies have $(R_c - z')$ colors between 0.6 and 1.0, and occupy similar locations in the color–magnitude diagrams built from considering objects at a projected distance $d_{\rm clus} < 0.5\ h_{71}^{-1}$ Mpc from each cluster center. Therefore, it is not easy to discriminate between the different candidates. This, however, is not a major issue since we are mostly interested in determining the velocity difference between the cluster redshift estimate and the absorption redshift, in order to establish whether the absorber resides in a cluster environment or not, and here the presence of a galaxy cluster in terms of redshift overdensity, color, and angular coverage is clear.

Table 8
Spectroscopic Targets of Field Centered on 231500.81−001831.2

No.	R.A. (J2000)	Decl. (J2000)	$z_{\rm gal}$	$\sigma_{z_{\rm gal}}$	Flag[a]	z'	$R_c - z'$	Comments
1	23 15 05.95	−00 16 06.92	...	...	0	20.94	1.48	...
2	23 15 00.86	−00 15 58.32	0.22311	0.00006	1	21.98	0.11	H_β, [O III] 4959, [O III] 5007
3	23 15 01.58	−00 16 46.02	0.99420	0.00080	3	22.16	0.83	[O II] 3727
4	23 14 59.20	−00 16 18.37	...	...	0	21.02	1.65	...
5	23 14 56.03	−00 16 58.80	0.58952	0.00007	3	21.06	0.52	[O II] 3727, Ca II H
6	23 14 55.68	−00 16 54.52	0.74977	0.00080	2	22.33	0.81	[O II] 3727
7	23 14 53.88	−00 17 24.40	0.74160	0.00007	3	20.96	0.67	[O II] 3727, Ca II K
8	23 15 01.89	−00 16 55.20	0.59264	0.00017	1	21.16	0.70	[O II] 3727, Ca II H, Ca II K
9	23 15 01.63	−00 17 09.53	0.74944	0.00012	1	21.73	1.16	[O II] 3727, Ca II H, Ca II K
10	23 15 03.43	−00 17 17.74	0.50683	0.00012	2	21.08	0.84	Ca II H, Ca II K, *G* band
11	23 15 05.64	−00 18 53.28	0.50470	0.00025	1	20.75	0.94	[O II] 3727, Ca II H, Ca II K, *G* band
12	23 15 04.06	−00 18 56.59	0.31196	0.00005	1	21.10	0.22	[O II] 3727, H_β, [O III] 4959, [O III] 5007
13	23 15 00.92	−00 18 14.98	0.29255	0.00005	1	20.99	0.45	[O II] 3727, H_β, [O III] 4959, [O III] 5007
14	23 15 00.96	−00 18 24.52	0.41367	0.00003	1	22.47	−0.03	[O II] 3727, [O III] 4959, [O III] 5007
15	23 15 00.21	−00 18 08.06	0.41360	0.00004	1	20.23	0.39	[O II] 3727, H_δ, H_γ, H_β, [O III] 4959, [O III] 5007
16	23 15 01.29	−00 18 49.86	0.58493	0.00080	3	20.65	1.16	[O II] 3727
17	23 15 00.62	−00 18 43.42	0.50576	0.00080	1	22.07	0.42	[O II] 3727
18	23 15 00.31	−00 18 38.92	0.49888	0.00042	2	21.27	0.07	[O II] 3727, Ca II H
19	23 15 00.90	−00 19 06.82	0.57703	0.00007	3	22.02	0.55	[O II] 3727, Ca II K
20	23 14 56.02	−00 18 20.38	...	...	0	22.37	0.74	...
21	23 15 06.88	−00 19 24.53	0.68810	0.00014	2	21.52	0.72	[O II] 3727, Ca II K
22	23 15 06.73	−00 19 33.85	0.68793	0.00028	2	20.05	1.33	Ca II H, Ca II K
23	23 15 03.98	−00 19 25.72	0.59259	0.00029	2	20.58	0.94	[O II] 3727, Ca II H, Ca II K
24	23 15 03.17	−00 19 44.40	0.50138	0.00080	3	22.00	0.57	[O II] 3727
25	23 15 01.42	−00 19 33.10	...	...	0	20.17	1.63	...
26	23 15 03.15	−00 20 12.73	0.22222	0.00012	1	20.13	0.70	H_β, [O III] 4959, [O III] 5007
27	23 15 02.82	−00 20 22.13	0.69295	0.00029	1	21.72	0.60	[O II] 3727, Ca II H, Ca II K
28	23 15 05.81	−00 20 17.59	0.59108	0.00021	2	20.13	0.84	[O II] 3727, Ca II K
29	23 15 09.82	−00 20 10.07	0.58384	0.00007	1	20.19	1.17	Ca II H, Ca II K
30	23 14 56.27	−00 16 22.91	0.37639	0.00012	1	21.34	0.46	[O II] 3727, H_β, [O III] 5007
31	23 14 55.54	−00 16 55.56	...	...	0	22.33	0.81	...
32	23 14 55.19	−00 16 49.98	0.38087	0.00007	2	21.06	0.54	[O II] 3727, H_β
33	23 14 53.03	−00 16 55.34	...	...	0	20.29	1.70	...
34	23 15 03.22	−00 17 04.52	0.91013	0.00080	1	21.74	0.66	[O II] 3727
35	23 15 01.68	−00 16 29.32	0.77120	0.00080	3	22.52	0.76	[O II] 3727
36	23 15 01.89	−00 16 55.20	0.59352	0.00021	1	21.16	0.70	[O II] 3727, Ca II K
37	23 14 58.80	−00 17 07.40	0.50386	0.00012	2	19.50	1.03	[O II] 3727, Ca II K, *G* band
38	23 14 52.06	−00 18 12.74	0.69403	0.00080	3	22.24	0.85	[O II] 3727
39	23 14 50.80	−00 18 40.97	0.50149	0.00014	1	19.43	0.96	Ca II H, Ca II K
40	23 15 03.39	−00 17 24.00	0.50529	0.00007	1	23.12	0.05	Ca II H, Ca II K
41	23 15 02.99	−00 17 37.07	0.50416	0.00007	2	21.15	0.47	[O II] 3727, Ca II K
42	23 15 04.39	−00 18 49.82	...	...	0	21.94	0.70	...
43	23 15 02.88	−00 18 25.85	0.50343	0.00080	3	21.11	0.77	[O II] 3727
44	23 15 02.31	−00 18 41.51	0.50527	0.00007	1	20.21	0.87	Ca II K, *G* band
45	23 15 00.69	−00 18 16.78	...	...	0	20.32	1.71	...
46	23 15 01.53	−00 19 18.66	0.50250	0.00035	3	20.82	0.80	Ca II H, Ca II K, H_δ, *G* band
47	23 14 59.97	−00 18 09.72	0.50278	0.00080	1	20.15	0.88	[O II] 3727
48	23 14 59.14	−00 19 19.49	0.57724	0.00080	3	20.76	0.46	[O II] 3727
49	23 14 57.46	−00 18 53.93	0.50294	0.00006	1	19.61	0.93	Ca II H, Ca II K, *G* band
50	23 15 09.36	−00 19 09.23	...	...	0	20.63	1.16	...
51	23 15 04.99	−00 19 26.80	0.43890	0.00012	1	21.88	0.68	[O II] 3727, H_β, [O III] 5007
52	23 15 02.17	−00 19 33.46	0.59303	0.00007	1	19.87	1.19	Ca II H, Ca II K
53	23 15 11.60	−00 19 29.17	0.47277	0.00042	1	19.45	0.89	Ca II H, Ca II K
54	23 15 02.67	−00 20 15.86	0.57669	0.00021	2	20.71	0.86	Ca II H, Ca II K
55	23 15 11.01	−00 20 02.76	0.58508	0.00007	1	20.19	1.05	Ca II H, Ca II K

Notes. Whenever information could not be obtained for a specific target, a "..." symbol is used. Stars found in our data have zero redshift.
[a] Redshift reliability classifier.

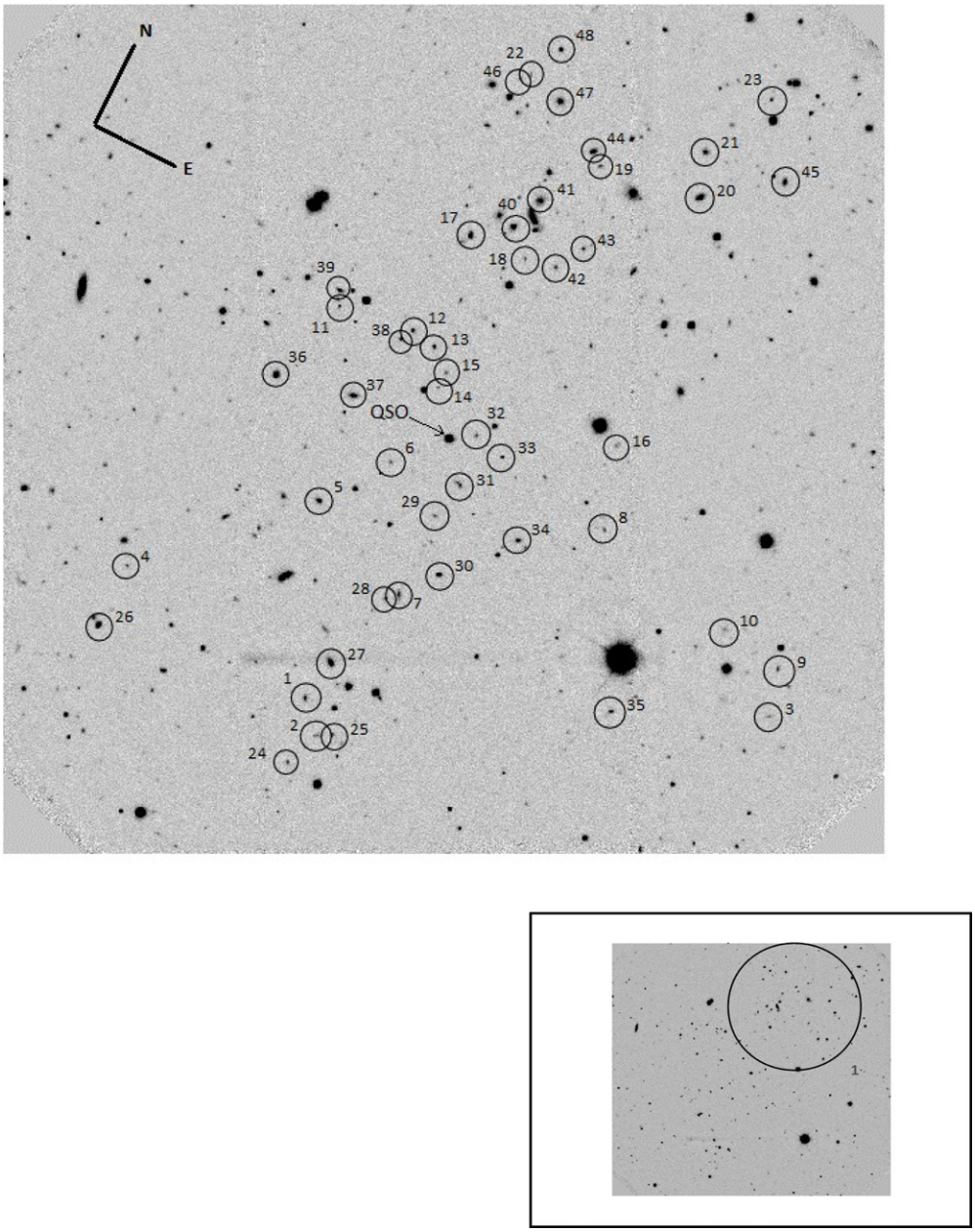

Figure 13. Top: 5.′5 × 5.′5 image of the field centered on the SDSS quasar 231509.34 + 001026.2. Galaxies are labeled according to the identification number given in Table 9. Bottom: a zoom-out of the image shown at the top. Center coordinates of each RCS1 cluster/group candidate are shown in circles. Each cluster is labeled according to their identification numbers given in the redshift histogram of Figure 14.

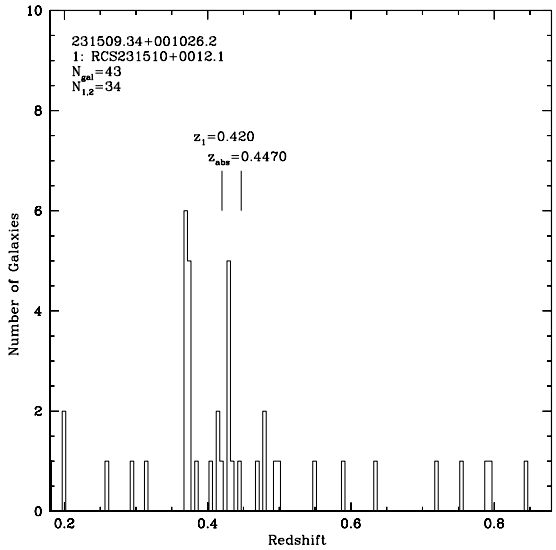

Figure 14. Redshift histogram of the field centered on the SDSS quasar 231509.34 + 001026.2. The bin size is of 0.005 in redshift space, which translates into $\Delta v \sim 1000$ km s^{-1} at $z = 0.5$. The total number of redshifts available for this field is given by $N_{\rm gal}$, from which $N_{1,2}$ is the number of redshifts classified with reliability flag 1 or 2.

LOS 022441.09 + 001547.9. Among the three low-z cluster/group candidates that were not confirmed, one is at $z_{\rm clus}^{\rm phot} = 0.173$ near the LOS 022441.09 + 001547.9. This galaxy cluster candidate may be a false positive detection as suggested by its low richness value $B_{gc} = 167$ ($3.25\sigma_{\rm RCS}$), and the fact that no redshift overdensity is observed in Figure 4 and a color–magnitude relation is barely detected (and heavily polluted by galaxies at $z \sim 0.3$–0.4) considering all extended sources within $d_{\rm clus} < 500\ h_{71}^{-1}$ kpc from the cluster center (near object No. 14; see Figure 3). A possible explanation for such misidentification relies on the fact that the RCS1 red-sequence finding algorithm works as long as the R_c (6500 Å) and z' (9100 Å) bands sample the 4000 Å break, being more effective at isolating the red sequence at $z \gtrsim 0.4$ (Gladders & Yee 2000, 2005), where the 4000 Å break is entering the R_c band (∼5600 Å).

LOS to 022441.09 + 001547.9 and LOS to 231958.70−002449.3. For the other two unconfirmed low-z cluster/group candidates ($z_{\rm clus}^{\rm phot} = 0.511$, LOS to 022441.09 + 001547.9; $z_{\rm clus}^{\rm phot} = 0.651$, LOS to 231958.70−002449.3), though their richness (B_{gc} ∼400) and detection significance values ($>3.6\sigma_{\rm RCS}$) support their presence, the number of redshifts available for those fields did not allow a proper confirmation of the systems. This is mainly because we prioritized observing the objects near the LOS, instead of observing the objects near the cluster center positions.

LOS to 022839.32 + 004623.0. Among the 10 cluster/group candidates at $z_{\rm clus}^{\rm phot} \gtrsim 0.7$, only 2 were confirmed (the two high-z cluster/group candidates near the LOS to 022839.32 + 004623.0; see Table 13) and this was only possible due to the redshifts taken from the NED database.

LOS 022441.09 + 001547.9. The problem encountered with the low-z cluster candidate in the field around 022441.09+001547.9 is also found when looking at the redshift histogram of the field 022300.41+005250.0. In this field, we can see a redshift overdensity at $z \sim 0.19$ (see Figure 2), which is considered as a galaxy cluster at a photometric redshift $z_{\rm clus}^{\rm phot} = 0.1973$ by Goto et al. (2002). The RCS1 did not detect the presence of a significant red sequence at such redshift, probably because of its finding algorithm. However, it does not matter for the purpose of this work, since the photometric hits we expect to confirm are at $z > 0.2$.

RCS022829 + 0045.8. Gerke et al. (2005) found a group of galaxies at a spectroscopic redshift $z_{\rm clus}^{\rm spec} = 0.7700$ that we detected at $z_{\rm clus}^{\rm spec} = 0.7702$ as the cluster redshift of RCS022829 + 0045.8. Though center positions differ (∼1.5 h_{71}^{-1} Mpc), the population of galaxies at such redshift is seen throughout the entire GMOS pre-image field of view.

A.2. On Confirmed Photometric Hits

LOS 231500.81−001831.2. There are two photometric hits confirmed with the same cluster environment in the field around the LOS 231500.81−001831.2 (see Tables 13 and 14). As mentioned in Section 3.2, not being able to confirm individually superimposed galaxy cluster/group candidates in a single field is not a relevant problem in this case, because we are interested in highlighting that the environment where the absorption process took place was not that of an isolated galaxy, but a galaxy subjected to extreme events happening in clusters or groups of galaxies.

It should be noted that even if the RCS1 detected different color–magnitude relations, the overlap in color and angular space of several galaxies could be due to the presence of merging events or a filamentary structure just along the LOS where warm gas produced the absorption. If this were the case, then the Mg II absorptions would be related to a dense environment too.

LOS 231958.70−002449.3. One of the photometric hits detected in a group of galaxies is observed in the field centered on the LOS 231958.70−002449.3. There are five cluster/group candidates that could not be distinguished individually based on redshift information only. This field is crowded with high-z galaxies ($z \sim 0.7$–0.8) quite red in color ($(R_c - z') > 1.0$) and sufficiently faint ($z' > 20.5$), so that these galaxies may have been overlooked in the target selection algorithm or were observed but the S/N were not enough to retrieve a redshift from their spectra. Since the RCS1 cluster finding method has proven to work quite well at $z \sim 0.7$–0.8 (Gilbank et al. 2007), the pair of galaxies at $z_{\rm clus}^{\rm spec} = 0.8486$ (Nos. 10 and 11; see Table 11 and Figure 17) could be tracing the external regions of the cluster candidate RCS231944−0026.8 at $z_{\rm clus}^{\rm phot} = 0.8440$ ($d = 1.9$–$2\ h_{71}^{-1}$ Mpc). This galaxy cluster candidate happens to be near the Mg II absorption redshift at $z_{\rm abs} = 0.8463$. Therefore, this system is now classified as a spectroscopic hit that is most probably associated with a group of galaxies. The unidentified Mg II absorbing galaxy could be located at the outskirts of this cluster/group of galaxies.

LOS 022441.09 + 001547.9. The other spectroscopic hit in a group of galaxies was detected in the field 022441.09 + 001547.9 at $z_{\rm clus}^{\rm spec} = 0.3813$ (see Table 14). Here the RCS1 cluster/group candidate near the absorption redshift $z_{\rm abs} = 0.3791$ was the cluster RCS022443 + 0017.6. This one was finally confirmed based on color, redshift, and angular space information at $z_{\rm clus}^{\rm spec} = 0.3518$ with 17 members (see the redshift histogram in Figure 4 and Table 13). The absorbing galaxy in this case appears to have a companion at a similar redshift (see Fgiure 3). However, both galaxies are in the background of the confirmed RCS galaxy cluster (>5000 km s^{-1}). Thus, this absorbing galaxy is considered to belong to a group, and not to the expected RCS galaxy.

A.3. On Unconfirmed Photometric Hits

Out of the four unconfirmed photometric hits, one is at a high redshift ($z_{\rm abs} > 0.9$) and we were unable to classify it, mostly

Table 9
Spectroscopic Targets of Field Centered on 231509.34 + 001026.2

No.	R.A. (J2000)	Decl. (J2000)	$z_{\rm gal}$	$\sigma_{z_{\rm gal}}$	Flag[a]	z'	$R_c - z'$	Comments
1	23 15 09.52	+00 08 32.89	...	...	0	20.97	0.30	...
2	23 15 10.24	+00 08 22.74	0.20110	0.00003	1	21.59	0.21	H_β, [O III] 4959, [O III] 5007
3	23 15 19.93	+00 09 54.97	0.38483	0.00015	3	21.54	0.58	H_β, [O III] 5007
4	23 15 03.91	+00 08 42.72	0.37344	0.00005	2	21.59	0.42	[O II] 3727, H_β
5	23 15 07.31	+00 09 40.68	0.47830	0.00001	1	19.89	0.69	[O II] 3727, Ca II H, Ca II K
6	23 15 08.39	+00 10 06.96	0.49733	0.00015	2	22.23	0.41	[O II] 3727, [O III] 5007
7	23 15 10.24	+00 09 24.91	0.29651	0.00009	1	20.76	0.36	[O II] 3727, H_β, [O III] 4959, [O III] 5007
8	23 15 13.93	+00 10 25.36	0.37115	0.00005	1	22.17	0.08	[O II] 3727, H_β, [O III] 4959, [O III] 5007
9	23 15 19.53	+00 10 12.18	...	...	0	21.18	0.64	...
10	23 15 17.87	+00 10 15.13	...	...	0	21.75	0.27	...
11	23 15 05.30	+00 10 48.86	0.43027	0.00007	1	22.08	−0.05	[O II] 3727, [O III] 5007, H_β, [O III] 4959
12	23 15 07.22	+00 10 54.62	0.41790	0.00005	2	20.65	1.39	H_β, [O III] 4959
13	23 15 07.88	+00 10 53.36	0.37240	0.00023	2	20.79	0.63	Ca II H, Ca II K, H_γ
14	23 15 08.50	+00 10 40.76	0.59149	0.00080	3	22.85	−0.13	[O II] 3727
15	23 15 08.47	+00 10 47.06	...	...	0	21.71	1.05	...
16	23 15 13.16	+00 10 55.34	0.79466	0.00080	3	21.92	0.33	[O II] 3727
17	23 15 07.26	+00 11 36.96	0.37010	0.00005	3	20.05	0.50	H_β, [O III] 5007
17	23 15 07.26	+00 11 36.96	0.72158	0.00080	3	21.39	0.39	[O II] 3727
18	23 15 08.77	+00 11 39.70	0.75464	0.00080	3	21.64	1.44	[O II] 3727
19	23 15 09.24	+00 12 24.52	...	...	0	21.40	1.12	...
20	23 15 11.83	+00 12 33.26	0.43011	0.00001	1	19.30	0.80	Ca II H, Ca II K, *G* band
21	23 15 11.36	+00 12 49.18	0.37113	0.00006	1	20.51	0.26	H_β, [O III] 4959, [O III] 5007, H_γ
22	23 15 06.56	+00 12 41.69	0.40355	0.00012	2	22.60	0.26	[O II] 3727, O III4363, H_β, [O III] 5007
23	23 15 12.16	+00 13 19.02	...	...	0	21.83	0.50	...
24	23 15 09.92	+00 08 08.38	0.42953	0.00075	3	24.19	0.10	H_β, [O III] 5007
25	23 15 10.57	+00 08 26.02	0.20009	0.00003	1	22.67	0.25	[O II] 3727, H_β, [O III] 4959, [O III] 5007
26	23 15 04.04	+00 08 17.81	0.41585	0.00012	2	19.87	0.78	[O II] 3727, Ca II H, Ca II K
27	23 15 09.61	+00 08 49.52	0.37335	0.00011	1	18.81	0.87	Ca II H, Ca II K, *G* band, Mg I 5176
28	23 15 10.01	+00 09 20.81	...	...	0	21.86	0.34	...
29	23 15 10.04	+00 09 57.64	0.36937	0.00011	1	21.39	0.48	[O II] 3727, Ca II K, *G* band, H_β, [O III] 5007
30	23 15 10.88	+00 09 39.02	0.31363	0.00006	1	20.25	0.70	H_β, [O III] 4959, [O III] 5007, [O II] 3727, H_γ
31	23 15 10.21	+00 10 12.43	0.84680	0.00080	3	20.09	1.56	[O II] 3727
32	23 15 09.95	+00 10 32.27	0.44652	0.00008	1	21.69	0.01	[O III] 5007, [O III] 4959, H_β, H_γ, H_δ, [O II] 3727
33	23 15 10.78	+00 10 30.00	...	...	0	21.23	0.84	...
34	23 15 12.18	+00 10 05.38	0.49620	0.00012	1	22.38	−0.22	Ca II H, Ca II K, H_δ, H_γ
35	23 15 16.39	+00 09 26.57	0.63448	0.00010	1	20.97	0.37	[O II] 3727, [O III] 5007, [O III] 4959
36	23 15 04.75	+00 10 14.16	0.47947	0.00008	1	19.69	0.64	[O II] 3727, Ca II H, Ca II K, *G* band
37	23 15 06.72	+00 10 22.01	0.26136	0.00006	1	19.50	0.54	H_α, [O III] 5007, H_β, H_γ, [O II] 3727
38	23 15 07.05	+00 10 49.58	0.37117	0.00012	2	21.13	0.60	Ca II H, Ca II K, *G* band
39	23 15 05.09	+00 10 54.05	0.47045	0.00017	1	20.54	0.53	Ca II H, Ca II K, [O II] 3727, H_β, [O III] 5007
40	23 15 08.10	+00 11 48.26	0.37283	0.00013	1	19.56	0.71	Ca II H, Ca II K, *G* band
41	23 15 08.35	+00 12 01.80	0.43074	0.00001	1	19.52	0.55	Ca II H, Ca II K
42	23 15 09.54	+00 11 42.65	0.37023	0.00006	1	21.50	0.60	[O II] 3727, H_β, Fe II 5284
43	23 15 09.91	+00 11 54.06	0.37290	0.00050	3	20.85	0.60	Ca II H, Ca II K
44	23 15 08.90	+00 12 28.15	0.42986	0.00025	2	19.62	0.82	Ca II H, Ca II K
45	23 15 13.50	+00 12 54.32	0.79003	0.00089	2	19.72	0.63	[O II] 3727, Ca II H, Ca II K
46	23 15 06.37	+00 12 38.45	0.54693	0.00031	2	22.01	0.33	[O II] 3727, [O III] 4959, H_β, [O III] 5007
47	23 15 07.53	+00 12 38.30	0.43340	0.00012	2	19.29	0.74	Ca II H, Ca II K, *G* band
48	23 15 06.89	+00 12 55.58	...	...	0	20.30	1.24	...

Notes. Whenever information could not be obtained for a specific target, a "..." symbol is used. Stars found in our data have zero redshift.
[a] Redshift reliability classifier.

Table 10
Spectroscopic Targets of Field Centered on 231759.63−000733.2

No.	R.A. (J2000)	Decl. (J2000)	z_{gal}	$\sigma_{z_{gal}}$	Flag[a]	z'	$R_c - z'$	Comments
1	23 18 06.15	−00 05 27.64	0.69533	0.00029	1	22.40	0.24	[O II] 3727, Ca II H, Ca II K
2	23 17 50.90	−00 05 16.98	0.70286	0.00009	1	21.43	0.30	[O II] 3727, [Ne III] 3868, He I 3888, H_δ, H_γ
3	23 17 59.34	−00 05 43.69	0.46756	0.00010	1	22.49	0.29	[O II] 3727, H_β, [O III] 4959, [O III] 5007
4	23 17 57.61	−00 06 04.93	0.46890	0.00006	2	21.52	0.95	[O II] 3727, Ca II H, Ca II K
5	23 17 57.33	−00 05 54.60	0.31495	0.00005	1	21.82	0.35	[O II] 3727, H_β, [O III] 4959, [O III] 5007
6	23 18 02.59	−00 07 39.32	1.41520	0.00028	1	22.50	0.30	Fe II 2344, Fe II 2374, Fe II 2382, Fe II 2586, Fe II 2600, Mn II 2594, Mg II 2796, Mg II 2803
7	23 18 01.39	−00 06 30.17	0.50117	0.00023	2	21.36	0.69	[O II] 3727, Ca II H, Ca II K
8	23 18 01.20	−00 07 13.08	0.59330	0.00007	1	22.46	0.30	[O II] 3727, H_γ
9	23 18 01.04	−00 07 22.08	...	...	0	22.33	1.57	...
10	23 18 00.65	−00 06 49.72	...	...	0	22.65	0.58	...
11	23 18 00.65	−00 06 59.22	0.59770	0.00030	3	23.07	0.38	[O II] 3727, Ca II H, Ca II K, *G* band
12	23 18 00.17	−00 06 42.16	...	...	0	22.23	1.98	...
13	23 17 56.81	−00 07 28.60	...	...	0	22.42	0.94	...
14	23 18 02.34	−00 08 05.60	0.47300	0.00012	1	21.57	0.35	[O II] 3727, Ca II H, Ca II K, H_γ, H_β, [O III] 5007
15	23 18 02.26	−00 07 52.10	...	...	0	21.72	2.00	...
16	23 17 56.41	−00 08 45.13	...	...	0	21.99	1.64	...
17	23 17 52.75	−00 08 58.88	0.38222	0.00006	1	22.36	0.25	H_β, [O III] 4959, [O III] 5007
18	23 17 52.97	−00 08 30.59	0.56368	0.00035	2	20.97	0.39	[O II] 3727, Ca II H, Ca II K
19	23 17 53.25	−00 08 24.04	0.59975	0.00012	1	19.72	1.20	Ca II H, Ca II K, *G* band
20	23 17 52.53	−00 09 10.48	...	...	0	21.89	1.03	...
21	23 18 04.23	−00 09 27.40	...	...	0	21.96	3.25	...
22	23 17 54.16	−00 09 35.50	0.66210	0.00049	3	22.53	1.25	[O II] 3727, Ca II K
23	23 17 52.03	−00 09 43.99	0.91214	0.00080	2	22.42	0.53	[O II] 3727
24	23 17 55.54	−00 09 55.19	0.38519	0.00004	1	22.50	0.13	[O II] 3727, H_γ, H_β, [O III] 4959, [O III] 5007
25	23 17 54.92	−00 10 06.64	0.60990	0.00052	2	21.51	0.51	[O II] 3727, Ca II H, Ca II K
26	23 18 02.61	−00 05 01.25	0.56462	0.00014	2	21.31	0.54	[O II] 3727, Ca II K
27	23 17 55.64	−00 05 12.37	0.47181	0.00035	2	20.05	0.78	[O II] 3727, Ca II H, H_β
28	23 18 00.96	−00 05 37.10	0.47310	0.00014	2	21.53	0.61	[O II] 3727, H_β
29	23 17 59.80	−00 06 02.66	0.40260	0.00006	2	20.63	0.74	[O II] 3727, H_β, [O III] 5007
30	23 17 58.01	−00 05 52.12	0.75690	0.00085	3	21.68	1.46	Ca II H, Ca II K
31	23 18 01.95	−00 08 07.40	0.46606	0.00021	3	22.01	0.67	[O II] 3727, H_β
32	23 18 01.71	−00 07 43.64	0.38053	0.00006	1	21.33	0.31	[O II] 3727, H_β, [O III] 5007
33	23 17 59.78	−00 06 49.28	...	...	0	21.64	1.63	...
34	23 17 59.62	−00 07 54.73	0.16752	0.00023	1	20.52	0.37	H_β, [O III] 4959, [O III] 5007
35	23 17 59.54	−00 07 20.42	0.60088	0.00015	1	20.59	1.17	[O II] 3727, Ca II H, Ca II K, H_γ
36	23 17 59.27	−00 07 08.94	0.59913	0.00020	1	20.61	0.78	[O II] 3727, Ca II H, Ca II K, H_δ
37	23 17 57.80	−00 06 59.51	0.59569	0.00028	2	21.18	1.17	[O II] 3727, Ca II K
38	23 17 56.68	−00 07 33.67	0.64769	0.00023	2	20.56	1.22	Ca II H, Ca II K, *G* band
39	23 17 52.49	−00 06 28.44	0.40436	0.00012	1	22.33	0.23	H_γ, [O III] 4959, [O III] 5007
40	23 17 50.95	−00 06 38.23	0.61876	0.00001	2	21.48	0.58	[O II] 3727, Ca II H
41	23 18 06.78	−00 08 54.24	0.28994	0.00012	2	20.94	0.38	[O II] 3727, H_β, [O III] 5007
42	23 18 06.58	−00 09 12.49	0.28360	0.00007	1	22.12	0.32	H_β, [O III] 5007
43	23 17 58.64	−00 08 25.40	0.58640	0.00069	3	21.57	0.84	[O II] 3727, Ca II H, Ca II K
44	23 17 55.44	−00 09 04.72	0.71340	0.00023	1	21.05	0.76	[O II] 3727, Ca II H, Ca II K
45	23 17 55.14	−00 08 39.34	0.56384	0.00006	1	21.30	0.26	[O II] 3727, Ca II H, Ca II K
46	23 17 56.00	−00 09 36.04	...	...	0	21.31	1.50	...
47	23 17 51.31	−00 09 24.59	0.75810	0.00021	2	21.04	0.70	[O II] 3727, Ca II H
48	23 17 49.98	−00 09 46.66	0.32390	0.00012	1	21.18	0.30	H_β, [O III] 4959, [O III] 5007
49	23 18 06.66	−00 10 02.93	0.59449	0.00080	3	21.75	0.49	[O II] 3727

Notes. Whenever information could not be obtained for a specific target, a "..." symbol is used. Stars found in our data have zero redshift.
[a] Redshift reliability classifier.

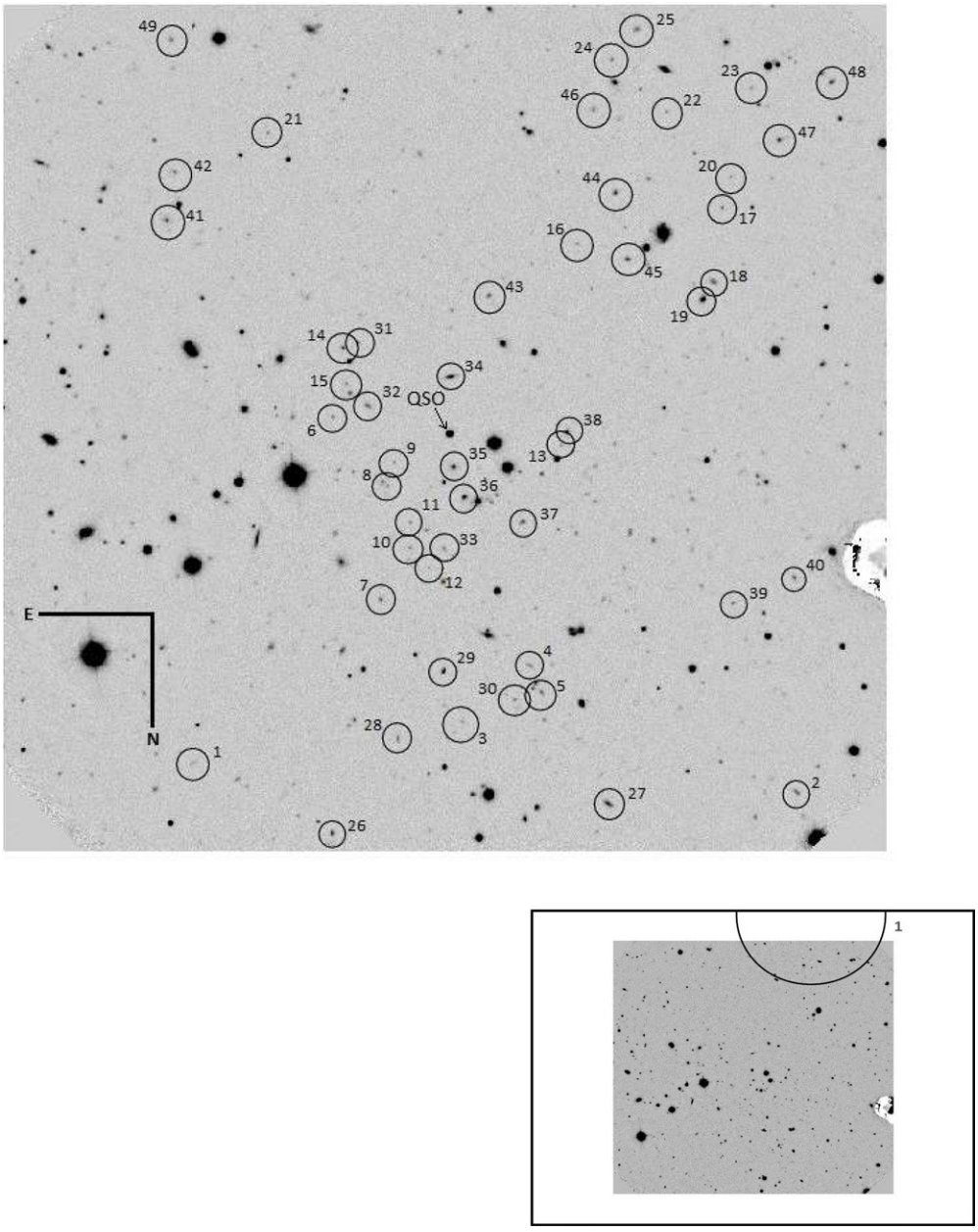

Figure 15. Top: 5′.5 × 5′.5 image of the field centered on the SDSS quasar 231759.63−000733.2. Galaxies are labeled according to the identification number given in Table 10. Bottom: a zoom-out of the image shown at the top. Center coordinates of each RCS1 cluster/group candidate are shown in circles. Each cluster is labeled according to their identification numbers given in the redshift histogram of Figure 16.

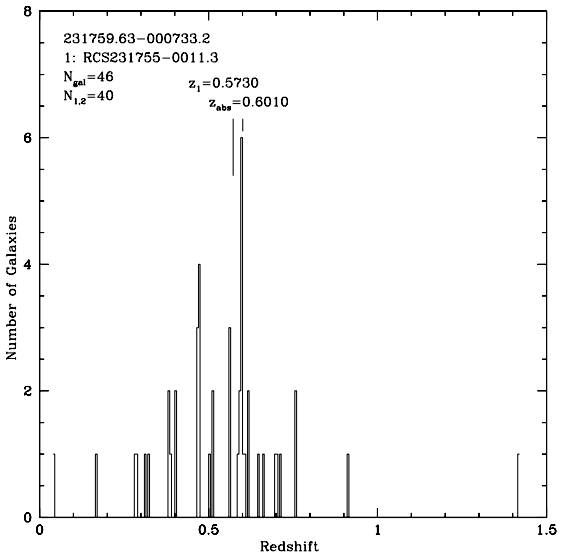

Figure 16. Redshift histogram of the field centered on the SDSS quasar 231759.63−000733.2. The bin size is of 0.005 in redshift space, which translates into $\Delta v \sim 1000$ km s^{-1} at $z = 0.5$. The total number of redshifts available for this field is given by $N_{\rm gal}$, from which $N_{1,2}$ is the number of redshifts classified with reliability flag 1 or 2.

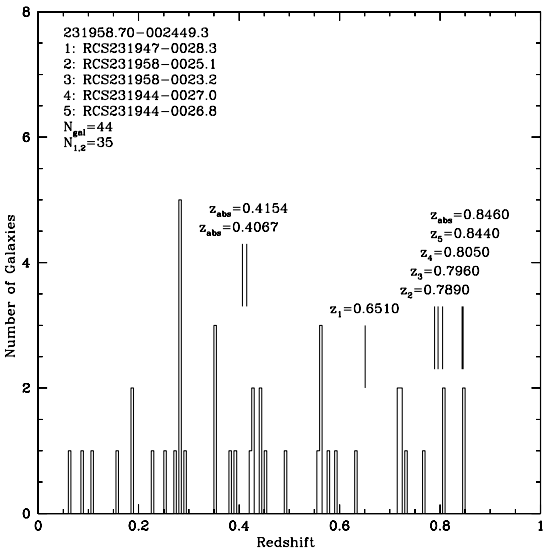

Figure 18. Redshift histogram of the field centered on the SDSS quasar 231958.70−002449.3. The bin size is of 0.005 in redshift space, which translates into $\Delta v \sim 1000$ km s^{-1} at $z = 0.5$. The total number of redshifts available for this field is given by $N_{\rm gal}$, from which $N_{1,2}$ is the number of redshifts classified with reliability flag 1 or 2.

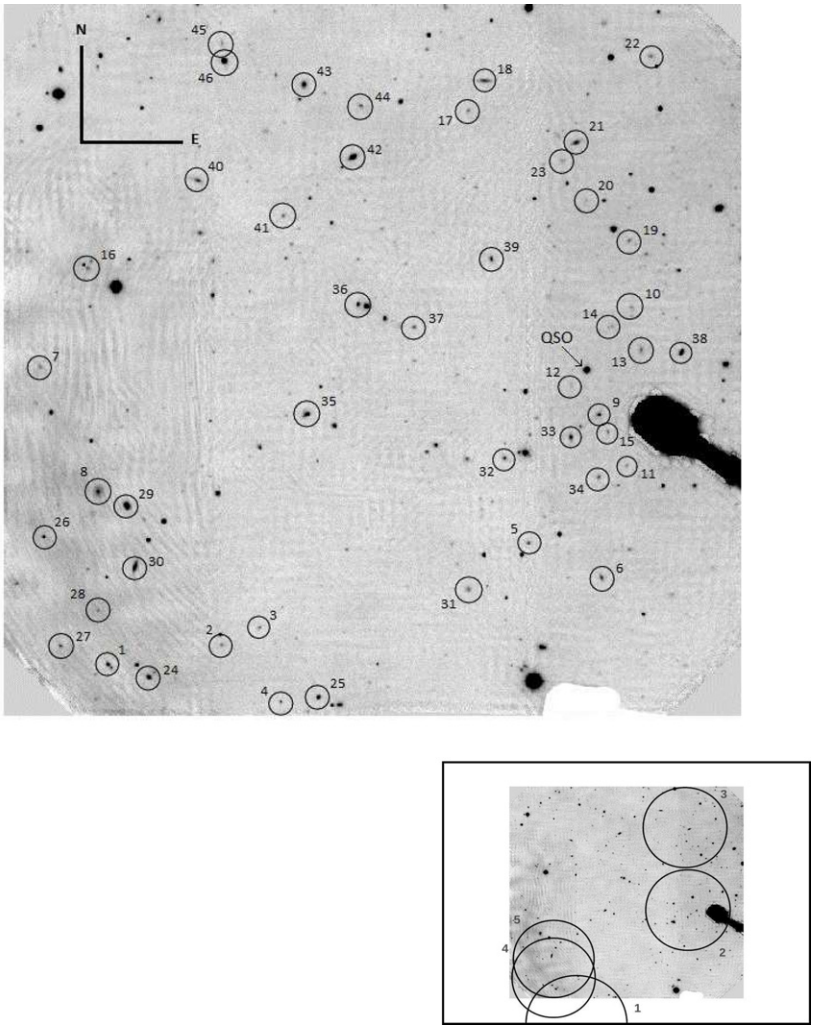

Figure 17. Top: 5′.5 × 5′.5 image of the field centered on the SDSS quasar 231958.70−002449.3. Galaxies are labeled according to the identification number given in Table 11. Bottom: a zoom-out of the image shown at the top. Center coordinates of each RCS1 cluster/group candidate are shown in circles. Each cluster is labeled according to their identification numbers given in the redshift histogram of Figure 18.

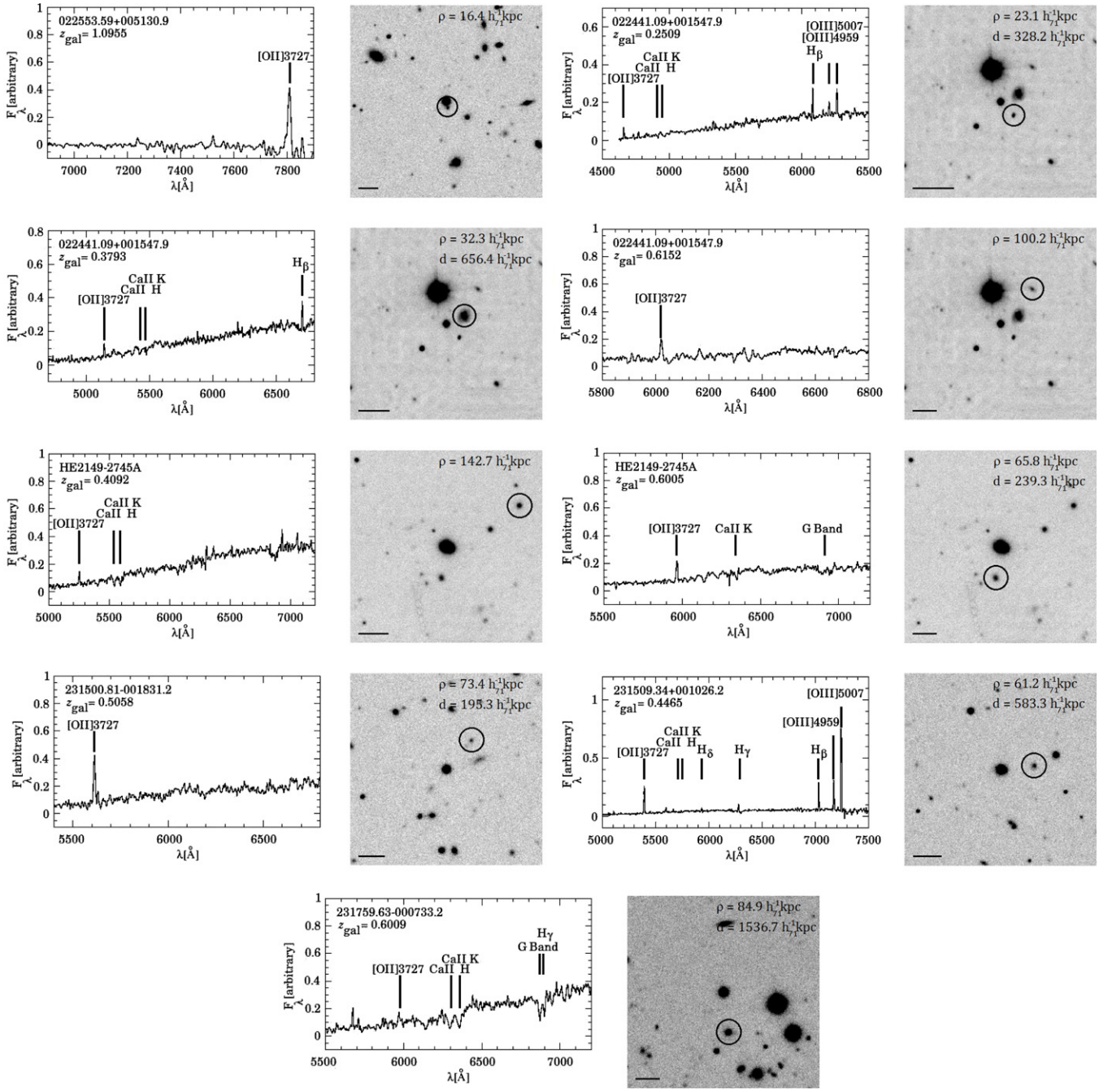

Figure 19. Spectra of nine absorbing galaxies confirmed in our sample together with a snapshot of the field centered on the respective quasar in a window 60″ wide. All spectra have been smoothed with a boxcar of 5 pixels. In each image, the black line represents a physical distance of 50 h_{71}^{-1} kpc at z_{gal}. Each absorbing galaxy is enclosed in a circle, and their impact parameters to the LOS ρ (h_{71}^{-1} kpc) are given in the upper right corner of the image. In those fields where the absorption is classified as a photometric hit by Paper I, the projected distance between the cluster/group candidate center and the LOS d (h_{71}^{-1} kpc) is also specified. In the case of the LOS to the quasar 231500.81−001831.2, only the impact parameter to the closest cluster/group candidate is shown.

because our spectroscopic survey turned out to be much more effective in detecting galaxies at $z \lesssim 0.7$, and not to such high redshifts.

Among the other three photometric hits reported in Paper I, one remains unconfirmed and two are no longer valid according to our spectroscopic survey of the fields.

LOS 022553.59+005130.9. This field presents two Mg II absorption systems ($z_{abs} = 0.6821$ and 0.7500) that were associated with the same cluster/group candidate RCS022558+0051.8 at $z_{clus}^{phot} = 0.701 \pm 0.1$ (see Table 13). This degeneracy is now broken because the galaxy cluster candidate was confirmed at $z_{clus}^{spec} = 0.7489$, becoming a spectroscopic hit with absorption at $z_{abs} = 0.7500$. Since no other RCS1 galaxy cluster candidate is expected to be found near $z_{abs} = 0.6821$ and no overdensity of galaxies is seen in redshift or angular space at that absorption redshift, we conclude that its designation as a photometric hit no longer applies. However, the existence of a group of galaxies cannot be ruled out considering the spectroscopic depth of this survey. Thus, this photometric hit remains unconfirmed.

Table 11
Spectroscopic Targets of Field Centered on 231958.70−002449.3

No.	R.A. (J2000)	Decl. (J2000)	$z_{\rm gal}$	$\sigma_{z_{\rm gal}}$	Flag[a]	z'	$R_c - z'$	Comments
1	23 19 44.07	−00 27 04.54	0.73498	0.00055	1	21.08	1.31	Ca II H, Ca II K
2	23 19 47.51	−00 26 55.72	0.55650	0.00080	3	21.37	0.67	[O II] 3727
3	23 19 48.68	−00 26 47.76	0.57801	0.00003	1	21.18	0.54	[O II] 3727, Ca II H, Ca II K
4	23 19 49.31	−00 27 21.82	0.56133	0.00008	1	21.64	0.43	[O II] 3727, Ca II H, Ca II K, H_δ, H_γ
5	23 19 56.85	−00 26 09.20	0.72041	0.00060	3	20.87	1.29	Ca II H, Ca II K
6	23 19 59.07	−00 26 25.01	0.35052	0.00032	3	20.25	0.58	*G* band, H_β, [O III] 5007
7	23 19 42.02	−00 24 49.00	0.80880	0.00080	3	21.97	0.79	[O II] 3727
8	23 19 43.77	−00 25 46.02	0.29361	0.00007	1	19.36	0.48	[O II] 3727, Ca II H, Ca II K
9	23 19 59.00	−00 25 10.81	0.71750	0.00023	2	20.44	1.32	[O II] 3727, Ca II H, Ca II K
10	23 19 59.97	−00 24 21.60	0.84995	0.00080	3	22.94	0.28	[O II] 3727
11	23 19 59.83	−00 25 34.03	0.84727	0.00080	2	22.10	0.58	[O II] 3727
12	23 19 58.14	−00 24 57.49	...	...	0	23.30	0.64	...
13	23 20 00.28	−00 24 41.29	0.10786	0.00003	2	25.82	−0.84	H_α, [S II] 6716, [S II] 6730
14	23 19 59.27	−00 24 30.78	0.56299	0.00005	1	22.96	0.14	[O II] 3727, [Ne III] 3868, He I 3888, [Ne III] 3967, H_δ, H_γ, H_β
15	23 19 59.26	−00 25 18.70	0.72096	0.00010	2	21.27	1.28	Ca II H, Ca II K
16	23 19 43.45	−00 24 03.74	0.80923	0.00080	2	21.73	0.56	[O II] 3727
17	23 19 55.00	−00 22 52.10	0.44211	0.00006	1	21.53	0.33	[O II] 3727, H_γ, H_β, [O III] 4959, [O III] 5007
18	23 19 55.53	−00 22 38.24	...	...	0	20.11	0.47	...
19	23 19 59.91	−00 23 51.22	...	...	0	21.24	0.79	...
20	23 19 58.61	−00 23 32.96	...	...	0	22.37	0.79	...
21	23 19 58.30	−00 23 06.43	0.59366	0.00017	1	21.76	0.75	[O II] 3727, Ca II H, Ca II K, *G* band
22	23 20 00.58	−00 22 26.94	...	...	0	20.43	1.60	...
23	23 19 57.89	−00 23 14.75	...	...	0	21.21	1.31	...
24	23 19 45.31	−00 27 10.40	...	...	0	19.86	1.50	...
25	23 19 50.46	−00 27 19.58	0.27483	0.00004	1	20.48	0.31	[O II] 3727, H_γ, H_β, [O III] 4959, [O III] 5007
26	23 19 42.12	−00 26 06.29	0.42579	0.00010	1	20.96	0.36	[O II] 3727, H_β, [O III] 4959, [O III] 5007
27	23 19 42.64	−00 26 56.15	0.39177	0.00007	1	21.17	0.74	[O II] 3727, H_β
28	23 19 43.76	−00 26 39.95	...	...	0	21.50	1.41	...
29	23 19 44.64	−00 25 52.28	0.25271	0.00005	1	18.56	0.62	Ca II H, Ca II K, H_β, [O III] 5007
30	23 19 44.89	−00 26 20.04	0.18640	0.00014	2	19.44	0.57	[O II] 3727, H_β, H_α
31	23 19 55.02	−00 26 30.37	0.38420	0.00005	1	20.99	0.31	[O II] 3727, H_β, [O III] 4959, [O III] 5007
32	23 19 56.12	−00 25 30.72	0.35157	0.00035	3	20.56	0.43	Ca II K, H_β
33	23 19 58.13	−00 25 21.00	0.49035	0.00006	1	20.19	0.70	[O II] 3727, Ca II H, Ca II K
34	23 19 58.97	−00 25 39.29	...	...	0	20.82	0.70	...
35	23 19 50.11	−00 25 10.74	0.15560	0.00002	1	19.50	0.30	H_γ, H_β, [O III] 4959, [O III] 5007, H_α
36	23 19 51.67	−00 24 20.30	0.45332	0.00037	2	20.28	0.73	Ca II H, Ca II K, *G* band
37	23 19 53.37	−00 24 30.82	0.63093	0.00010	1	21.46	0.12	[O II] 3727, H_γ, [O III] 5007
38	23 20 01.50	−00 24 42.37	0.08539	0.00008	1	19.35	0.49	H_α, [N II] 6583, [S II] 6716, [S II] 6730
39	23 19 55.72	−00 23 59.71	0.18561	0.00003	1	20.40	0.21	H_β, [O III] 4959, [O III] 5007, H_α
40	23 19 46.78	−00 23 23.68	0.42541	0.00040	3	20.29	0.25	H_β, [O III] 5007
41	23 19 49.40	−00 23 39.95	0.76568	0.00020	3	21.54	0.63	[O II] 3727, H_γ
42	23 19 51.50	−00 23 13.06	0.28258	0.00005	1	19.00	0.60	Ca II H, Ca II K
43	23 19 50.03	−00 22 39.90	0.42397	0.00015	1	19.37	0.50	[O II] 3727, Ca II H, Ca II K, H_β
44	23 19 51.76	−00 22 49.69	0.71920	0.00018	3	20.83	1.05	[O II] 3727, Ca II H, Ca II K
45	23 19 47.54	−00 22 21.18	0.22817	0.00012	1	22.16	−0.12	[O II] 3727, [O III] 4959, [O III] 5007
46	23 19 47.60	−00 22 29.03	0.44134	0.00023	1	19.16	0.69	[O II] 3727, Ca II H, *G* band

Notes. Whenever information could not be obtained for a specific target, a "..." symbol is used. Stars found in our data have zero redshift.
[a] Redshift reliability classifier.

Table 12
Confirmation of Absorbing Galaxies

The Sample										
LOS	z_{abs}	W_0^{2796} (Å)	$\sigma_{W_0^{2796}}$ (Å)	z_{gal}[a]	$\sigma_{z_{gal}}$	δv (km s^{-1})	ρ[b] (h_{71}^{-1} kpc)	Photo-hit	Spectral Lines	M_{R_c}
022300.41+005250.0	0.9500	0.043	0.010	...	...	...	...	Yes	...	...
022441.09+001547.9	0.2507	0.732	0.037	0.2509	0.0001	−48	23.13	Yes	[O II] 3727, Ca II K, Ca II H, H_γ, H_β, [O III] 4959, [O III] 5007, [N II] 6548–6583, H_α, [S II] 6716–6730	−18.78
	0.3791	1.181	0.043	0.3793	0.0001	−44	32.31	Yes	[O II] 3727, Ca II K, Ca II H, H_δ, H_β	−22.07
	0.6152	0.181	0.016	0.6152	0.0008	0	100.17	No	[O II] 3727, Ca II K, Ca II H	−20.82
	0.9402	0.080	0.020	...	...	...	...	No	...	...
	1.0560	0.881	0.036	...	...	...	...	No	...	...
022553.59+005130.9	0.6821	0.333	0.019	...	...	...	...	Yes	...	...
	0.7500	0.159	0.015	...	...	...	...	Yes	...	...
	1.0951	1.685	0.065	1.0955	0.0008	−57	16.38	No	[O II] 3727	−20.21
	1.2258	0.177	0.032	...	...	...	...	No	...	...
022839.32+004623.0	0.6548	0.597	0.016	...	...	...	...	Yes	...	...
HE2149−2745A	0.4090	0.228	0.008	0.4092	0.0001	−43	142.71	No	[O II] 3727, Ca II K, Ca II H, *G* band	...
	0.4464	0.016	0.005	...	...	...	...	Yes	...	...
	0.5144	0.028	0.003	...	...	...	...	No	...	...
	0.6012	0.175	0.006	0.6005	0.0002	131	65.78	Yes	[O II] 3727, Ca II K, Ca II H, *G* band	...
	0.6032	0.015	0.004	0.6030	0.0010	37	5.72	Yes	Ca II K, Ca II H, *G* band	...
	1.0189	0.219	0.013	...	...	...	...	No	...	...
231500.81−001831.2	0.5043	0.148	0.009	...	...	...	...	Yes	...	...
	0.5072	0.063	0.009	0.5058	0.0008	279	73.36	Yes	[O II] 3727, Ca II K, Ca II H	−19.72
231509.34+001026.2	0.4473	1.758	0.009	0.4465	0.0008	166	61.19	Yes	[O II] 3727, H_δ, H_γ, H_β, [O III] 4959, [O III] 5007	−20.17
231759.63−000733.2	0.6013	0.109	0.016	0.6009	0.0002	75	84.92	Yes	[O II] 3727, Ca II K, Ca II H, *G* band	−21.49
231958.70−002449.3	0.4071	0.151	0.017	...	...	...	...	No	...	...
	0.4158	0.192	0.021	...	...	...	...	No	...	...
	0.8463	2.028	0.024	...	...	...	...	Yes	...	...

Notes. The LOS to the QSO 022553.59+005130.9 also presents a high-redshift absorption at $z_{abs} = 1.2258$ as shown in Table 1. However, at such high redshift, no absorbing galaxy could have been detected due to problems encountered with our observations. Therefore, in the following it is removed from our sample (see Section 3.1).

[a] Redshift of the absorbing galaxy.

[b] Galaxy impact parameter to the LOS.

Table 13
Confirmation of RCS1 Cluster/Group Candidates

The Sample						
Field	Cluster/Group	$z_{\rm clus}^{\rm phot}$	$z_{\rm clus}^{\rm spec}$	σ_v (km s^{-1})	$N^{\rm a}$	Comments
022300.41+005250.0	RCS022302+0052.9	0.509	0.4386	300 ± 90	8	Central galaxies. There is a group at $z \sim 0.4740$ but do not follow a red sequence.
	RCS022253+0055.1	0.939	...	...	...	...
022441.09+001547.9	RCS022436+0014.2	0.173	...	...	...	Possible false positive detection.
	RCS022443+0017.6	0.431	0.3518	646 ± 93	17	Central galaxies.
	RCS022431+0018.0	0.480	0.4338	234 ± 73	8	Central galaxies. Confirmation possible because of SDSS data.
	RCS022454+0013.3	0.511	...	...	...	...
	RCS022449+0016.2	0.818	...	...	...	There is one early-type galaxy at $\sim z_{\rm clus}^{\rm phot}$ at $d_{\rm clus} \sim 1\ h_{71}^{-1}$ Mpc from the cluster center.
022553.59+005130.9	RCS022602+0055.5	0.352	0.3974	606 ± 40	31	Center outside field of view. Galaxies are at $d_{\rm clus} > 1\ h_{71}^{-1}$ Mpc from the cluster center.
	RCS022553+0052.5	0.423	0.4172	965 ± 38	25	Central galaxies. Immersed in the background of galaxies at $z \sim 0.3956$.
	RCS022558+0051.8	0.701	0.7489	833 ± 48	5	Central galaxies. Galaxies follow a red sequence.
	RCS022546+0050.0	0.873	...	...	...	...
	RCS022556+0052.7	0.928	...	...	...	...
022839.32+004623.0	RCS022841+0044.9	0.271	0.2659	944 ± 80	6	Central galaxies. Confirmation possible because of SDSS data.
	RCS022844+0047.7	0.516	0.4934	314 ± 49	5	Central galaxies.
	RCS022832+0046.5	0.629	0.6559	319 ± 67	19	We found one galaxy at the cluster center.
	RCS022829+0045.8	0.774	0.7702	560 ± 86	23	Center outside field of view. These are at 1.5–2 h_{71}^{-1} Mpc from the cluster center.
	RCS022828+0044.9	1.032	1.0152	742 ± 57	22	Confirmation possible because of NED data.
HE2149−2745A	Group/Cluster	0.603	0.6030	287 ± 69	9	Central galaxies. In agreement with M06. According to W06, these galaxies follow a red sequence.
231500.81−001831.2	RCS231515−0015.8	0.496	0.5040	214 ± 58	16	Center outside field of view.
	RCS231512−0020.1	0.517	0.5040	214 ± 58	16	Center outside field of view.
	RCS231459−0018.9	0.522	0.5040	214 ± 58	16	This is a preliminary result.
	RCS231501−0013.6	0.557	0.5870	699 ± 42	14	The groups at $z \sim 0.5040$ and 0.5925 also could confirm this cluster.
	RCS231506−0018.1	0.560	0.5040	214 ± 58	16	We may have detected the central galaxy at $z = 0.5046$.
	RCS231515−0015.6	0.566	0.5870	699 ± 42	14	The groups at $z \sim 0.5040$ and 0.5925 also could confirm this cluster.
231509.34+001028.2	RCS231510+0012.1	0.420	0.4282	735 ± 46	10	Central Galaxies. There is a group of galaxies with $z = 0.3726$ and 0.2 mag bluer in color.
231759.63−000733.2	RCS231755−0011.3	0.573	0.5974	631 ± 25	12	Center outside field of view. There is a group of galaxies at $z \sim 0.4730$ but do not follow a red sequence.
231958.70−002449.3	RCS231947−0028.3	0.651	...	...	...	There is a group of galaxies at $z \sim 0.5614$ near the cluster center.
	RCS231958−0025.1	0.789	...	...	...	There are two galaxies at $z \sim 0.7196$. We may have observed central galaxies.
	RCS231958−0023.2	0.796	...	...	...	The groups at $z \sim 0.8092$ or 0.7194 may also confirm it.
	RCS231944−0027.0	0.805	...	...	...	There are two galaxies at $z \sim 0.8090$.
	RCS231944−0026.8	0.844	...	...	...	Center outside field of view. There are two galaxies at $z \sim 0.8486$ and $> 1.5\ h_{71}^{-1}$ Mpc from the LOS.

Notes. The field centered on HE2149−2745A could not be studied photometrically. However, according to M06 and W06, there appear to be photometrically and spectroscopically two clusters of galaxies at $z = 0.6030$ and $z = 0.4465$.

[a] The number of galaxy cluster members.

Table 14
Detection of Spectroscopic Hits

Field	z_{abs}	W_0^{2796} (Å)	$\sigma_{W_0^{2796}}$ (Å)	z_{gal}	$\sigma_{z_{gal}}$	δv_{gal} (km s^{-1})	ρ (h_{71}^{-1} kpc)	Photo-hit	Photo-hit I	z_{clus}^{spec}	σ_v (km s^{-1})	N	δv_{clus} (km s^{-1})
022300.41 + 005250.0	0.9500	0.043	0.010	...	...	...	...	Yes	No	...	...	...	...
022441.09 + 001547.9	0.2507[a]	0.732	0.037	0.2509	0.0001	−48	23.13	Yes	Yes	...	...	...	...
	0.3791	1.181	0.043	0.3793	0.0001	−44	32.31	Yes	Yes	0.3791*	... [c]	2	−43.50
	0.6152	0.181	0.016	0.6152	0.0008	0	100.17	No	No	0.6127*	... [c]	3	−473.36
	0.9402	0.080	0.020	...	...	...	...	No	No	...	...	...	...
	1.0560	0.881	0.036	...	...	...	...	No	No	...	...	...	...
022553.59 + 005130.9	0.6821	0.333	0.019	...	...	...	...	Yes	Yes	...	...	...	...
	0.7500	0.159	0.015	...	...	...	...	Yes	Yes	0.7489	833 ± 48	5	−188.63
	1.0951	1.685	0.065	1.0955	0.0008	−57	16.38	No	No	...	...	...	...
	1.2258	0.177	0.032	...	...	...	...	No	No	...	...	...	...
022839.32 + 004623.0	0.6548	0.597	0.016	...	...	...	...	Yes	Yes	0.6559	319 ± 67	19	+199.35
HE2149−2745A	0.4090	0.228	0.008	0.4092	0.0001	−43	142.71	No	No	0.4095*	... [c]	2	+59.60
	0.4464	0.016	0.005	...	...	...	...	Yes[b]	No	0.4482	292 ± 32	5	+373.11
	0.5144	0.028	0.003	...	...	...	...	No	No	...	...	...	...
	0.6012	0.175	0.006	0.6005	0.0002	131	65.78	Yes	Yes	0.6030	287 ± 69	9	+468.24
	0.6032	0.015	0.004	0.6030	0.0010	37	5.72	Yes	No	0.6030	287 ± 69	9	+37.43
	1.0189	0.219	0.013	...	...	...	...	No	No	...	...	...	...
231500.81−001831.2	0.5043	0.148	0.009	...	...	...	...	Yes	Yes	0.5040	214 ± 58	16	−59.83
	0.5072	0.063	0.009	0.5058	0.0008	279	73.36	Yes	Yes	0.5040	214 ± 58	16	−358.83
231509.34 + 001026.2	0.4473	1.758	0.009	0.4465	0.0008	166	61.19	Yes	Yes	...	...	...	...
231759.63−000733.2	0.6013	0.109	0.016	0.6009	0.0002	75	84.92	Yes	Yes	0.5974	631 ± 25	12	−656.60
231958.70−002449.3	0.4071	0.151	0.017	...	...	...	...	No	No	...	...	...	...
	0.4158	0.192	0.021	...	...	...	...	No	No	...	...	...	...
	0.8463	2.028	0.024	...	...	...	...	Yes	Yes	0.8486*	... [c]	2	+373.49

Notes. All spectroscopic hits most probably associated with a galaxy group are denoted by ∗ symbols.

[a] As mentioned in Section 3.2, the galaxy cluster at $z_{clus}^{phot} = 0.173$ in the field 022441.09 + 001547.9 (Table 13) seems to be a misidentification and as such its association with the absorption at $z_{abs} = 0.2507$ as a photometric hit is no longer valid. Only three galaxies were detected within the cluster candidate photometric redshift uncertainty ($z_{min} = 0.2240$ and $z_{max} = 0.2730$; see Paper I) at $\bar{z} \sim 0.2377$ at a rest-frame velocity > 3 000 km s^{-1} from the absorber redshift.

[b] A red sequence at $z_{clus}^{phot} = 0.40$ was detected by W06 and later spectroscopically confirmed in M06 at $z_{clus}^{spec} = 0.4465$. Here we consider it as a spectroscopic hit associated with a cluster of galaxies, even though we did not detect a considerable overdensity expected at that redshift.

[c] No velocity dispersion estimate is given in this case as there are only two to three group members.

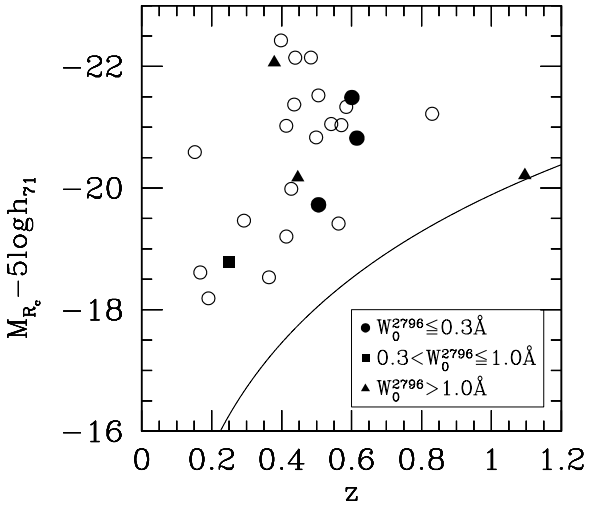

Figure 20. R_c-band absolute magnitude distribution with redshift. Galaxies responsible for weak Mg II absorptions ($W_0^{2796} \leqslant 0.3$ Å) are shown as filled circles; those producing absorptions of intermediate strength ($0.3 < W_0^{2796} \leqslant 1.0$ Å) are shown as filled squares; and the ones related to stronger absorptions with $W_0^{2796} > 1.0$ Å are shown as filled triangles. Interlopers found in our fields are shown in open circles. These are galaxies observed near the LOS that do not produce any Mg II absorption detected in the spectra of the quasars. Absorbing galaxies in the field centered on HE2149−2745A do not appear in this plot since there is no available SDSS nor RCS1 photometry for them. The solid line shows a magnitude limit of $R_c = 23.5$.

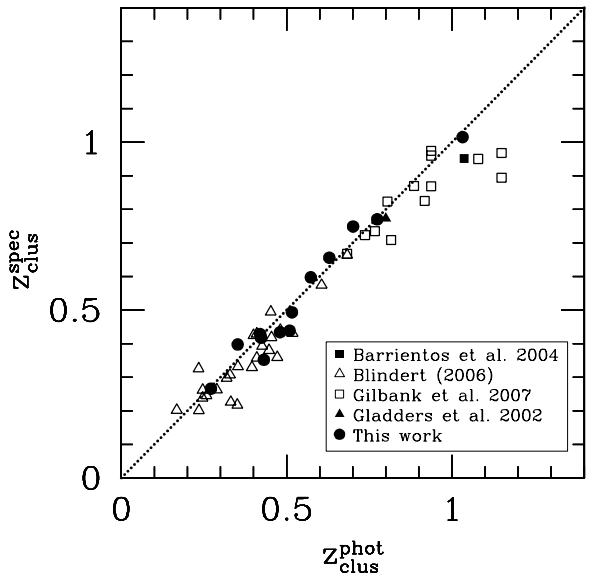

Figure 21. Comparison of RCS1 cluster photometric redshifts and the spectroscopic redshifts we obtained in this work (filled circles), together with the data of Barrientos et al. (2004; filled squares), Blindert (2006; open triangles), Gilbank et al. (2007; open squares), and Gladders et al. (2002; filled triangles). The dotted line represents the one-to-one relation. Our absolute redshift differences span the range $\delta z \leqslant 0.08$, with a mean value of $\overline{\delta z} = 0.03$.

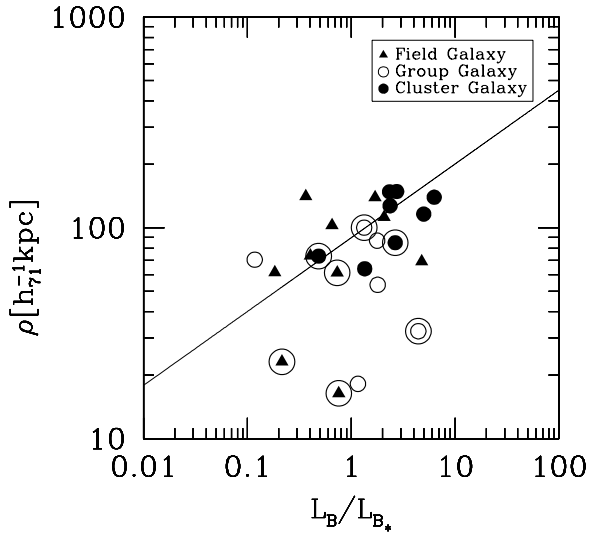

Figure 22. Observed impact parameter vs. B-band luminosity for our absorbing galaxies (enclosed in a larger open circle) and interlopers (not enclosed in a larger open circle), associated with the field (filled triangles), galaxy groups (open circles), and galaxy clusters (closed circles). The line plotted is the Holmberg relation determined by Chen & Tinker (2008) with $R^* \sim 89\ h_{71}^{-1}$ kpc and $\beta = 0.35$.

LOS to 022441.09+001547.9. The photometric hit of the cluster RCS022436+0014.2 at $z_{clus}^{phot} = 0.173$ with the absorption system at $z_{abs} = 0.2507$ in the LOS to 022441.09+001547.9 is now considered to be a (confirmed) field absorber since this cluster/group candidate is most likely a false detection. Only three galaxies were detected within the cluster candidate photometric redshift uncertainty ($z_{min} = 0.2240$ and $z_{max} = 0.2730$; see Paper I) at $\overline{z} \sim 0.2377$, more than 3000 km s^{-1} from the absorber redshift.

LOS to 231509.34+001026.2. The last unconfirmed photometric hit is now classified as a (confirmed) field absorber in the LOS to 231509.34+001026.2. Here we confirmed the (only) RCS1 cluster/group candidate near the LOS at $z_{clus}^{spec} = 0.4282$, >3000 km s^{-1} away from the absorbing galaxy (at $z_{gal} = 0.4465$). No overdensity of galaxies was found at the absorber redshift.

A.4. On Absorption Systems Not Classified As Photometric Hits

From a total of nine absorption systems that are not classified as photometric hits in Paper I, we found two related to groups of galaxies and none associated with clusters of galaxies, which is consistent with their classification as "not photometric hits."

One Mg II absorber found at a redshift consistent with that of a group of galaxies is in the LOS HE2149−2745A at $z_{abs} = 0.4090$. Although no notorious redshift peak is found at this redshift (see Figure 10), the fact that it has a companion may induce some modification in its halo size.

The other spectroscopic hit related to a group of galaxies is in the field around the LOS 022441.09+001547.9 at $z_{clus}^{spec} = 0.6127$. Even though this group of galaxies is undetected by the RCS1 color-based cluster finding algorithm, it does not mean that such a group does not exist, recalling that the common definition of a group of galaxies primarily involves a high number density contrast with respect to the field; meanwhile, the usual definition of a cluster admits the presence of a color–magnitude relation for the brightest cluster members due to their coeval evolution since early times.

Among the other seven absorption systems, we did not find clusters or groups of galaxies at the absorption redshifts. Four of these absorption systems are at high redshift $z_{abs} > 0.9$ and, as mentioned before, galaxies at these redshifts were difficult to observe with our spectroscopic survey. The other three systems are at redshifts $z_{abs} < 0.6$, where our survey would have been able to detect galaxy overdensities. In fact, in some cases, we detected groups of galaxies, but all of them were quite far from the absorber redshifts.

Therefore, it is quite likely that these seven systems are actually field absorbers consistent with their classification given

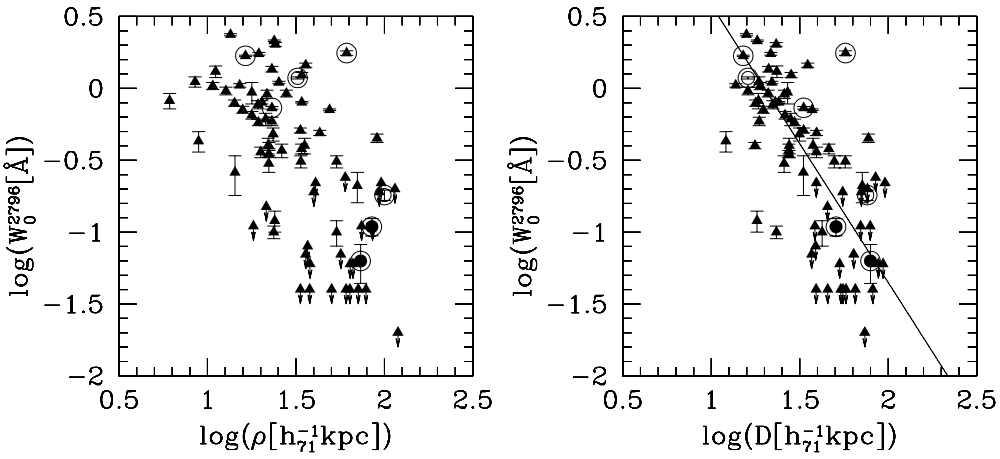

Figure 23. Left: absorption rest-frame equivalent width W_0^{2796} (Å) vs. the observed galaxy impact parameter to the LOS of our absorbing galaxies (enclosed in a larger open circle) associated with the field (filled triangles), galaxy groups (open circles), and galaxy clusters (closed circles). Also the absorbing field galaxies published in the work of Chen et al. (2010) are shown as a reference (filled triangles). Right: absorption rest-frame equivalent width W_0^{2796} (Å) vs. the impact parameter weighted by the B-band luminosity of the galaxies $D \equiv \rho \times (L_B/L_{B^*})^{-0.35}$ (h_{71}^{-1} kpc). The plot shows our data (enclosed by a larger open circle) together with the absorbing field galaxies of Chen et al. (2010). Again the symbols are the same as shown in the left panel. We include the anti-correlation found by Chen et al. (2010) for absorbing field galaxies (solid line).

in Paper I. In other words, this small sample is not contaminated by cluster absorbers. Nevertheless, there are two spectroscopic hits in groups that require further spectroscopy.

REFERENCES

Barrientos, L. F., Gladders, M. D., Yee, H. K. C., et al. 2004, ApJL, 617, L17
Bechtold, J., & Ellingson, E. 1992, ApJ, 396, 20
Beers, T. C., Flynn, K., & Gebhardt, K. 1990, AJ, 100, 32
Blanton, M. R., Dalcanton, J., Eisenstein, D., et al. 2001, AJ, 121, 2358
Blindert, K. 2006, PhD thesis, Univ. Toronto, Canada
Bouché, N., Murphy, M. T., Péroux, C., Csabai, I., & Wild, V. 2006, MNRAS, 371, 495
Bowen, D. V., Blades, J. C., & Pettini, M. 1995, ApJ, 448, 634
Carlberg, R. G., Yee, H. K. C., & Ellingson, E. 1997, ApJ, 478, 462
Chen, H.-W., Helsby, J. E., Gauthier, J.-R., et al. 2010, ApJ, 714, 1521
Chen, H.-W., & Tinker, J. L. 2008, ApJ, 687, 745
Churchill, C., Steidel, C., & Kacprzak, G. 2005, in ASP Conf. Ser. 331, Workshop on Extraplanar Gas, ed. R. Braun (San Francisco, CA: ASP), 387
Churchill, C. W., & Charlton, J. C. 1998, in ASP Conf. Ser. 136, Galactic Halos: A UC Santa Cruz Workshop, ed. D. Zaritsky (San Francisco, CA: ASP), 187C
Churchill, C. W., Steidel, C. C., & Kacprzak, G. G. 2005, in ASP Conf. Ser. 331, Extra-Planar Gas, ed. R. Braun (San Francisco, CA: ASP), 387
Dressler, A. 1980, ApJS, 42, 565
Eigenbrod, A., Courbin, F., & Meylan, G. 2007, A&A, 465, 51
Fadda, D., Girardi, M., Giuricin, G., et al. 1996, ApJ, 473, 670
Fukugita, M., Shimasaku, K., & Ichikawa, T. 1995, PASP, 107, 945
Gauthier, J.-R. 2013, MNRAS, 432, 1444
Gauthier, J.-R., Chen, H.-W., & Tinker, J. L. 2009, ApJ, 702, 50
Gerke, B. F., Newman, J. A., Davis, M., et al. 2005, ApJ, 625, 6
Gilbank, D. G., Yee, H. K. C., Ellingson, E., et al. 2007, AJ, 134, 282
Gilbank, D. G., Yee, H. K. C., Ellingson, E., et al. 2008, ApJ, 673, 742
Gladders, M. D., & Yee, H. K. C. 2000, AJ, 120, 2148
Gladders, M. D., & Yee, H. K. C. 2005, ApJS, 157, 1
Gladders, M. D., Yee, H. K. C., & Ellingson, E. 2002, AJ, 123, 1
Goto, T., Sekiguchi, M., Nichol, R. C., et al. 2002, AJ, 123, 1807
Kacprzak, G. G., Churchill, C. W., & Steidel, C. C. 2005, in IAU Colloq. 199, Probing Galaxies through Quasar Absorption Lines, ed. P. R. Williams, C. Shu, & B. Ménard (Cambridge: Cambridge Univ. Press), 80
Kacprzak, G. G., Churchill, C. W., Steidel, C. C., Murphy, M. T., & Evans, J. L. 2007, ApJ, 662, 909
Kacprzak, G. G., Murphy, M. T., & Churchill, C. W. 2010, MNRAS, 406, 445
Le Brun, V., Bergeron, J., & Deharveng, J. M. 1997, A&A, 321, 733
Lin, W.-P., & Zou, Z.-L. 2001, ChJAA, 1, 21
Lindner, U., Alvensleben, U., & Fricke, K. J. 1996, A&A, 316, 123
López, S., Barrientos, L. F., Lira, P., et al. 2008, ApJ, 679, 1144 (Paper I)
Ménard, B., Wild, V., Nestor, D., et al. 2011, MNRAS, 417, 801
Momcheva, I., Williams, K. A., Keeton, C. R., et al. 2006, ApJ, 641, 169
Padilla, N., Lacerna, I., López, S., et al. 2009, MNRAS, 395, 1135
Rubin, K. H. R., Prochaska, J. X., Koo, D. C., Phillips, A. C., & Weiner, B. J. 2010, ApJ, 712, 574
Schlegel, D. J., Finkbeiner, D. P., & Davis, M. 1998, ApJ, 500, 525
Steidel, C. C. 1995, in Proc. ESO Workshop on QSO Absorption Lines, Garching, Germany, 1994 November 21–24, ed. G. Meylan (Berlin: Springer), 139
Steidel, C. C., & Dickinson, M. 1992, ApJ, 394, 81
Steidel, C. C., Dickinson, M., & Persson, S. E. 1994, ApJL, 437, L75
Steidel, C. C., Kollmeier, J. A., Shapley, A. E., et al. 2002, ApJ, 570, 526
Williams, K. A., Momcheva, I., Keeton, C. R., et al. 2006, ApJ, 646, 85
Windhorst, R. A., Burstein, D., Mathis, D. F., et al. 1991, ApJ, 380, 362
Wisotzki, L., Koehler, T., López, S., & Reimers, D. 1996, A&A, 315, L405
Wittman, D., Tyson, J. A., Margoniner, V. E., Cohen, J. G., & DellAntonio, I. P. 2001, ApJL, 557, L89
Yee, H. K. C. 1991, PASP, 103, 396
Yee, H. K. C., & Ellingson, E. 2003, ApJ, 585, 215
Yee, H. K. C., & López-Cruz, O. 1999, AJ, 117, 1985
Zibetti, S., Ménard, B., Nestor, D. B., et al. 2007, ApJ, 658, 161